https://doi.org/10.15388/vu.thesis.227
https://orcid.org/0000-0002-4015-275X

VILNIUS UNIVERSITY
FACULTY OF CHEMISTRY AND GEOSCIENCES

Inga
GABRIŪNAITĖ

Formation and Characterisation of Phospholipid Bilayers on Metal Oxide Surfaces

DOCTORAL DISSERTATION

Natural sciences,
Chemistry (N 003)

VILNIUS 2021

This dissertation was written between 2017 and 2021 in Vilnius University, Faculty of Chemistry and Geosciences. The research was supported by Research Council of Lithuania.

Academic supervisor:
Assoc. Prof. Dr. Aušra Valiūnienė (Vilnius University, Natural sciences, chemistry – N 003).
Academic consultant:
Prof. Dr. Gintaras Valinčius (Vilnius University, Natural sciences, biochemistry – N 004).

This doctoral dissertation will be defended in a public meeting of the Dissertation Defence Panel:
Chairman – **Prof. Habil. Dr. Audrius Padarauskas** (Vilnius University, Natural Sciences, chemistry – N 003).
Members:
Dr. Rima Budvytytė Vilnius University, Natural Sciences, biochemistry – N 004).
Prof. Habil. dr. Aivaras Kareiva (Vilnius University, Natural Sciences, chemistry – N 003).
Prof. Habil. Dr. Albertas Malinauskas (Center for Physical Sciences and Technology, Natural Sciences, chemistry – N 003).
Prof. Dr. Vida Vičkačkaitė (Vilnius University, Natural Sciences, chemistry – N 003).

The dissertation shall be defended at a public meeting of the Dissertation Defence Panel at 12:00 on 1 October 2021 at the Applied Chemistry Auditorium (117) of the Faculty of Chemistry and Geosciences, Vilnius University.
Address: Naugarduko str. 24, LT-03225, Vilnius, Lithuania, tel. (8 5) 219 3108; e-mail: info@chgf.vu.lt

The text of this dissertation can be accessed at the libraries of (name of the institutions granted the right to conduct doctoral studies in alphabetical order), as well as on the website of Vilnius University: www.vu.lt/lt/naujienos/ivykiu-kalendorius

https://doi.org/10.15388/vu.thesis.227
https://orcid.org/0000-0002-4015-275X

VILNIAUS UNIVERSITETAS
CHEMIJOS IR GEOMOKSLŲ FAKULTETAS

Inga
GABRIŪNAITĖ

Fosfolipidinių dvisluoksnių formavimas ant metalų oksidinių elektrodų ir jų savybių tyrimas

DAKTARO DISERTACIJA

Gamtos mokslai,
Chemija (N 003)

VILNIUS 2021

Disertacija rengta 2017– 2020 metais Vilniaus universiteto Chemijos ir Geomokslų fakultete.
Mokslinius tyrimus rėmė Lietuvos mokslo taryba.

Mokslinė vadovė:
Doc. dr. Aušra Valiūnienė (Vilniaus universitetas, gamtos mokslai, chemija – N 003).
Mokslinis konsultantas:
Prof. dr. Gintaras Valinčius (Vilniaus universitetas, gamtos mokslai, biochemija – N 004).

Gynimo taryba:
Pirmininkas – **prof. habil. dr. Audrius Padarauskas** (Vilniaus universitetas, gamtos mokslai, chemija – N 003)
Nariai:
dr. Rima Budvytytė (Vilniaus universitetas, gamtos mokslai, biochemija – N 004).
prof. habil. dr. Aivaras Kareiva (Vilniaus universitetas, gamtos mokslai, chemija – N 003).
prof. habil. dr. Albertas Malinauskas (Fizinių ir technologijos mokslų centras, gamtos mokslai, chemija – N 003).
prof. dr. Vida Vičkačkaitė (Vilniaus universitetas, gamtos mokslai, chemija – N 003).

Disertacija ginama viešame Gynimo tarybos posėdyje 2021 m. spalio mėn. 1 d. 12 val. Chemijos ir geomokslų fakulteto Taikomosios chemijos auditorijoje. Adresas: Naugarduko g. 24, LT03225, Vilnius, Lietuva, tel. (8 5) 219 3108; el. paštas: info@chgf.vu.lt

Disertaciją galima peržiūrėti Vilniaus universiteto, FTMC Chemijos instituto bibliotekose ir VU interneto svetainėje adresu: https://www.vu.lt/naujienos/ivykiu-kalendorius

LIST OF ORIGINAL PAPERS

Paper 1 Aušra Valiūnienė, Žana Margarian, **Inga Gabriūnaitė**, Vaida Matulevičiūtė, Tomas Murauskas and Gintaras Valinčius, Cadmium Stannate Films for Immobilization of Phospholipid Bilayers, J. Electrochem. Soc. 2016, 163, H762-H767. https://doi.org/10.1149/2.0331609jes

Paper 2 **Inga Gabriunaite**, Aušra Valiūnienė, Gintaras Valincius, Formation and properties of phospholipid bilayers on fluorine doped tin oxide electrodes, Electrochimica Acta, 2018, 283 1351-1358. https://doi.org/10.1016/j.electacta.2018.04.160

Paper 3 **Inga Gabriunaite**, Aušra Valiūnienė, Margarita Poderyte, Arunas Ramanavicius, Silane-based self-assembled monolayer deposited on fluorine doped tin oxide as model system for pharmaceutical and biomedical analysis, Journal of Pharmaceutical and Biomedical Analysis, 2020, 177, 112832. https://doi.org/10.1016/j.jpba.2019.112832

Paper 4 **Inga Gabriunaite**, Aušra Valiūnienė, Tomas Sabirovas, Gintaras Valincius, Mixed Silane-based Self assembled Monolayers Deposited on Fluorine Doped Tin Oxide as Model System for Development of Biosensors for Toxin Detection, Electroanalysis, 2021, 33, 1315. https://doi.org/10.1002/elan.202060578

AUTHOR‘S CONTRUBUTION TO ORIGINAL PAPERS

Paper 1 Carried out cadmium tin oxide thin films deposition and functionalisation with self-assembled monolayers, recorded electrochemical impedance spectra, analysed acquired data, prepared literature review, contributed to the preparation of the manuscript.

Paper 2 Planned and carried out all the experiments, analysed acquired data, prepared literature review, contributed to the preparation of the manuscript.

Paper 3 Prepared fluorine doped tin oxide samples and modified them with self-assembled monolayers, analysed acquired data, prepared literature review, contributed to the preparation of the manuscript.

Paper 4 Planned and carried out all the experiments, analysed acquired data, prepared literature review, contributed to the preparation of the manuscript.

TABLE OF CONTENTS

LIST OF ABBREVIATIONS

AC	altering current
αHL	α-hemolysin
ATS	allyltrichlorosilane
CA	contact angle
Chol	cholesterol
CPE	constant phase element
CTO	cadmium tin oxide
CV	cyclic voltammetry
DOPC	1,2-dioleoyl-sn-glycero-3-phosphocholine
DMPA	2,2-dimethoxy-2-phenylacetophenone
EIS	electrochemical impedance spectroscopy
FFT-EIS	fast Fourier-transform electrochemical impedance spectroscopy
FTIR	Fourier-transform infrared spectroscopy
FTO	fluorine doped tin oxide
FWHM	full width at half maximum
hBLM	hybrid bilayer lipid membrane
IR	infrared
ITO	indium tin oxide
Mel	melittin
mhBLM	mixed hybrid bilayer lipid membrane
MTS	methyltrichlorosilane
NMR	nuclear magnetic resonance spectroscopy
ODT	octadecanthiol
OLED	organic light emitting diode
OTS	octadecyltrichlorosilane
PBS	phosphate buffer saline
PC	phosphocholine
PE	phosphatidylethanolamine
PEG	polyethyleneglycol
PI	phosphatidylinositol
PL	phospholipid layer
PLA2	phospholipase A_2
PS	phosphatidylserine
RAIRS	reflection adsorption infrared spectroscopy
R	resistance
SAM	self-assembled monolayer
SECM	scanning electrochemical microscopy
sPLA2	secreted phospholipase A_2
tBLM	tethered bilayer lipid membrane
TOPS	trichloro(3-(octadecylthio)propyl)silane

UME	ultramicroelectrode
UV-Vis	ultraviolet-visible spectroscopy
VLY	vaginolysin
XRD	X-ray diffraction

INTRODUCTION

Every living cell is surrounded by plasma membrane. It protects and separates the inside of the cell from the outside. Membrane consists mainly of phospholipids arranged in two-layer structure where the hydrophilic heads are directed outward and the hydrophobic tails are directed inwardly of the bilayer. Plasma membrane has the property to accommodate different proteins: integral (such as ion channels) [1] and peripheral (such as electron carriers, enzymes or peptides) [2] membrane proteins. Therefore membrane models were developed as a platform for protein studies [3].

The first lipid membrane model was called black lipid membrane [3]. Membrane was freely suspended in an aperture (diameter was usually between tens and hundreds of micrometers) of hydrophobic material [3],[4]. However main drawback of black lipid membranes was lack of stability, thus solid supported [5] and tethered [6] bilayer lipid membranes were developed. The addition of solid support for membrane models enabled to apply surface sensitive methods: atomic force microscopy, surface plasmon resonance or electrochemical impedance spectroscopy. Tethered bilayer lipid membrane (tBLM), which was anchored to solid surface by a self-assembled monolayer [7] or a polymer layer [8], appeared to be the more favourable membrane model due to higher stability.

The key point of membrane applicability for protein studies is the existence of thin ionic reservoir between solid support and phospholipid bilayer [9]. It acts as a cytosol and ensures incorporation of transmembrane proteins inside lipid membrane without the loss of protein biological activity. Hence, anchoring self-assembled monolayers have been developed that ensures ionic reservoir formation during phospholipid bilayer formation [6][7][9]. Most studies of phosholipid bilayer formation have been done on gold-thiol systems [6][7][9][10][11]. The strong covalent bond between gold and thiols (Au-SR) ensures the stability of formed layers and such systems proved to be applicable for protein studies [12] or for the development of biosensors [13][14]. However, due to expensive preparation and the lack of optical transparency of gold surfaces other substrates could be considered for tethered bilayer membrane formation. One of the examples include metal oxides and their functionalisation with silane based self-assembled monolayers have been showed on different oxide surfaces: indium tin oxide [15], sputtered Ti/TiO_2 [16], metallurgical Ti [17] and Al [18]. The commercial availability and ease of preparation are some of the beneficial properties of the metal oxides. These properties enhance the applicability of oxide surfaces as substrates for the phospholipid bilayer formation. However, the lack of commercially available silane based molecular anchors prevents from developing tethered bilayer membranes on metal oxide surfaces with thin ionic reservoir. Nevertheless, phospholipid bilayer formation on metal oxide surfaces could improve the known gold-thiol system by decreasing the effective cost of membrane related investigations or possible application as biosensing devices.

The aim of this study was to design and characterise phospholipid bilayers on metal oxides, particularly on cadmium tin oxide and fluorine doped tin oxide surfaces as well as to demonstrate the application of phospholipid bilayers for the development of biosensors for membrane damaging/pore forming toxins detection.

The objectives of this study:

1. To establish optimal conditions of cadmium tin oxide thin film deposition for the formation of OTS self-assembled monolayer and phospholipid bilayer membrane. To characterise SAM and bilayer with CA, CV and EIS methods.

2. To establish optimal conditions of OTS SAM formation on fluorine doped tin oxide. To investigate phospholipid bilayer membrane formation and test the functionality of the membrane with vaginolysin and phospholipase A_2 toxins. To apply SECM method for the characterization of modified FTO surface along with EIS, CV and CA methods.

3. To investigate phospholipid bilayer membrane formation on fluorine doped tin oxide surface functionalised with mixed SAM consisting of OTS and MTS and test the functionality of the membrane with melittin toxin. To investigate surface hydration effect on SAM and bilayer membrane properties. To characterise formed SAM and bilayer with CA, CV and EIS methods.

4. To functionalize FTO surface with synthesized trichloro(3-(octadecylthio)propyl)silane (TOPS) molecular anchor for tethering bilayer lipid membrane formation containing water reservoir between the solid surface and the membrane. To investigate biological relevance of the membranes with pore-forming toxin α-hemolysin. To characterise formed SAM and bilayer with CA and EIS methods.

5. To test the reusability of silane-based self-assembled monolayers on FTO surface for the formation of phospholipid bilayer.

SCIENTIFIC NOVELTY

Artificial membrane models were designed as a platform to study membrane/protein related processes. Most studies of artificial membrane systems have been done on gold surfaces modified with alkylthiol self-assembled monolayers. However, these systems display several drawbacks. First, anchoring molecules exhibit surface mobility on gold surfaces resulting in cluster formation, that lipid bilayer would not form after vesicle fusion on the same sample, therefore gold substrates are disposable after single use. Second, atomically flat Au surface is usually prepared by magnetron sputtering device and the overall expenses of buying the material itself make the preparation of the potential biosensing device expensive. Additionally, gold surfaces are not transparent and could not be investigated by optical methods. Meanwhile, metal oxides are cheaper, do not require expensive devices for preparation, oxides as thin films are transparent and silane based self-assembled monolayers, exhibiting the chemical stability of siloxane bonds could be potentially reused for lipid bilayer formation. Thus, metal oxides functionalized with silane-based SAM are promising platform for artificial lipid membrane formation. However the lack of research in this particular scientific area as well as essential materials for the development of tethered bilayers on metal oxide surfaces are major challenges for developing tBLMs. With respect to the aforementioned problems, the major contributions of this thesis are:

1. Optically transparent, low-cost in preparation and/or commercially available thin films of cadmium tin oxide and fluorine doped tin oxide functionalized with OTS monolayers were proposed to use for DOPC/Chol phospholipid bilayer formation.
2. It was demonstrated that in contrast to similar tBLMs on gold, phospholipid bilayers on silanized FTO surface can be easily regenerated several times without losing their functionality.
3. It was determined that depending on FTO surface hydration phospholipid bilayers can be formed on SAMs with even sparsely populated OTS molecular anchors (containing up to 80% of MTS back-filler).
4. Simplified procedure for the tethered bilayer membrane formation on FTO surface functionalised with synthesised silane based molecular anchor was proposed, and biological relevance of formed membranes with pore forming toxins melittin and α-hemolysin was shown.

To sum up, metal oxides, such as cadmium tin oxide and fluorine doped tin oxide can be successfully applied for phospholipid bilayer formation, reducing the expenses for the development of biosensors for toxin detection.

STATEMENTS FOR DEFENCE:

1. Cadmium tin oxide and fluorine doped tin oxide functionalised with OTS can be used for the hybrid bilayer membrane formation.

2. Scanning electrochemical microscopy along with CA, CV and EIS can be used for self-assembled monolayer characterisation.

3. Fluorine doped tin oxide functionalised with a mix of OTS molecular anchor and short-chain MTS can be used for the formation of mixed hybrid bilayer membrane suitable for reconstitution of melittin toxin.

4. Synthesised trichloro(3-(octadecylthio)propyl)silane molecular anchor can be used for fluorine doped tin oxide functionalisation and formation of the tethered bilayer membrane containing submembrane water reservoir that is needed for functional reconstitution of α-hemolysin pores.

5. Surface of fluorine doped tin oxide functionalised with silane based self-assembled monolayer can be used multiple times for the formation of phospholipid bilayer membrane exhibiting the same electrochemical properties.

1. LITERATURE REVIEW

1.1. Phospholipid bilayer membrane

Cell is the smallest structural unit of every living organism. It is surrounded by plasma membrane, which separates interior of the cell from the outside. Plasma membrane is two dimensional bilayer that consists mainly of phospholipids, but also includes sphingolipids, sterols, proteins [19]. Phospholipids have hydrophilic phosphate heads and hydrophobic tails of two fatty acid chains. Due to amphiphilic structure of phospholipids, hydrophobic tails are facing inwards and hydrophilic heads are facings outwards in the bilayer membrane. The hydrophobic interior and hydrophilic exterior of the membrane, makes it a convenient platform for immobilization of different types of proteins [20].

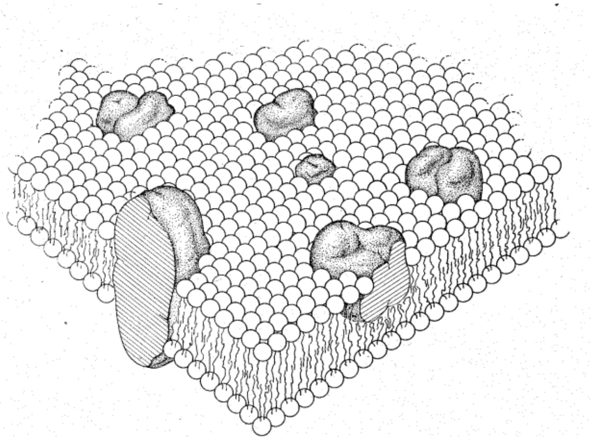

Fig. 1. Fluid mosaic membrane model, where proteins are embbeded in lipid matrix [21].

The composition of the lipids in the membrane influences physicochemical properties of the membrane. There are four types of phospholipids that are predominant in cell membrane: phosphatidylcholine (PC), phosphatidylethanolamine (PE), phosphatidylinositol (PI) phosphatidylserine (PS). Electrically neutral PC, PE, PI and negatively charged PS are important for membrane fusion, disassembly, apoptosis, membrane-mediated cell signalling [22]. The saturation and length of fatty acids in phospholipids plays an important role in phase transition of the membrane. Lipids with longer chains and fully saturated have tendency to interact decreasing mobility of the lipids in the membrane, thus membrane transitions to gel (solid phase) [23]. To avoid it, membranes in nature contains a mixture of lipids with saturated and unsaturated, shorter and longer hydrocarbon chains, increasing membrane fluidity [19]. Sterols, such as cholesterol, increase packing of the phospholipids in the membrane, prevent from hydrocarbon chains coming together and impede phase transition into gel maintaining membrane fluidity [24]. The diversity of lipids allows to form functional phospholipid membranes for different types of cells in eukaryotes (neurons, blood cells, etc), prokaryotes (bacteria, etc.) and for organelles of the cell [19]. In 1972 fluid mosaic membrane model was presented where proteins are embedded in lipid matrix by random distribution (Fig. 1) [21]. In general, lipid membrane is a complex structure that requires considerable amount of research. Therefore model membrane systems were developed to investigate the properties of phospholipid membranes [6][9][25][26][27][28]. The artificial bilayer provides milieu for reconstitution of biomaterials such as proteins [29][30], DNA chains [31], pore-forming toxins [32], etc. to study their functionality under conditions closely mimicking those in natural organisms.

1.2. Model membrane systems

1.2.1. Liposomes

Liposomes are phospholipid bilayer membranes in spherical shape. They were first described by Bangham et al. in 1960s [33][34]. Liposomes are readily formed by exposing dehydrated phospholipids to aqueous solution [33]. Liposomes are classified as unilamellar vesicles or multilamellar vesicles (MLV). Freshly prepared liposomes usually are MLV, where each vesicle contains several concentric bilayers. Meanwhile unilamellar vesicles has only one bilayer and can be small (SUV, diameter 20-100 nm), large (LUV, diameter more than 100 nm), and giant (GUV, more then 1 µm). Liposomes are mostly applied for drug delivery. It enhances the effectiveness of the drug while reducing the toxicity of the drug.

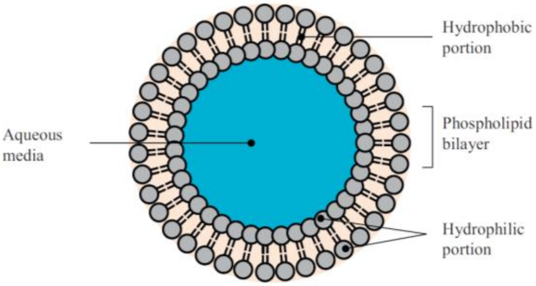

Fig. 2. Structure of liposome [35].

1.2.2. Hybrid bilayer lipid membranes

Immobilization of the phospholipid membranes on the solid support allows applications of surface sensitive techniques such as reflection-absorption infrared spectroscopy (RAIRS) [36], surface plasmon resonance (SPR) [37], quartz crystal microbalance [38] and others. If artificial bilayer membrane systems are formed on solid conducting surfaces, then electrochemical methods can be applied for experimentation [39][40].

To obtain stable, nearly defect free surface supported membranes, typically, the self-assembled monolayer (SAM) serving as a molecular anchor of phospholipid bilayer is formed. Subsequently, the bilayer can be deposited atop SAM via solvent exchange [9][41], unilamellar [42] or multilamellar [43] vesicle fusion processes. Monolayer composition and structure influence the solid supported membrane properties. If monolayer consists of one type of molecules, for example, long-chain alkylthiol, such as octadecylthiol, a hybrid bilayer membrane (hBLM) is accomplished (Fig. 4) [44]. hBLMs are characterized as stable and they can be successfully used for biotin binding protein study [45] or for membrane sensitivity characterization using lipids hydrolysing proteins such as phospholipase A_2 [46].

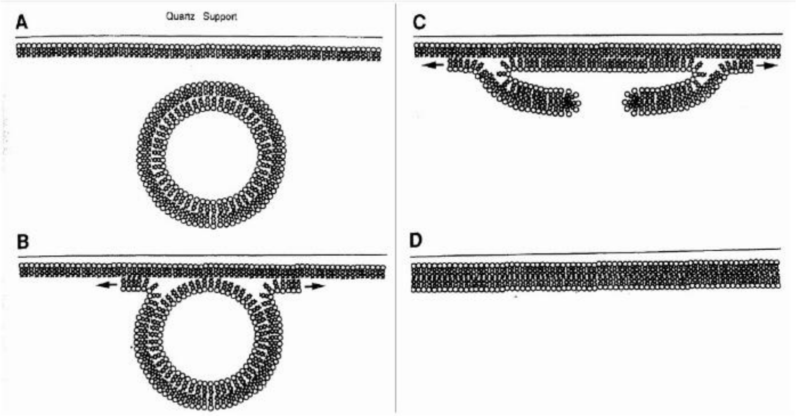

Fig. 3. Vesicle fusion process on solid surface: A - vesicle approaches surface; B – defects in monolayer lead to close contact between SAM and vesicle; C – vesicle ruptures as lipid layer spreads out on SAM; D – completed bilayer lipid membrane [47].

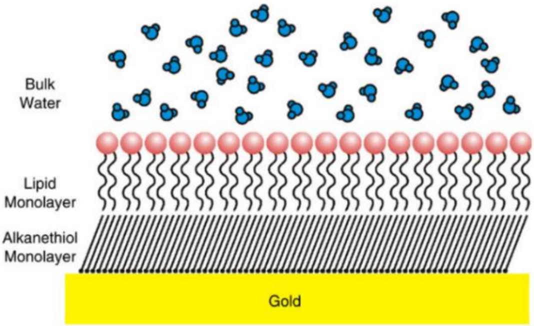

Fig. 4. Structure of hybrid bilayer lipid membrane [48].

1.2.3. Tethered bilayer lipid membrane

Although hBLM can be used for protein-membrane studies as showed earlier [45][46], however it does not possess sufficient biological relevance due to the absence of water reservoir between the solid support and bilayer, as well as the rigidity of proximal to a surface layer, therefore reconstitution of integral transmembrane proteins into hBLM is being impeded [49]. To address such issues monolayers of mixed molecular anchors of different lengths were suggested to assemble sparsely tethered phospholipid membranes (Fig. 5) [7][9]. Short molecular backfillers along with the long-chain anchors create enough void to accommodate 1-2 nm thick water ionic reservoir between the membrane and the surface [25]. This makes tethered bilayers similar to phospholipid membranes in living cells [7][50], which are bathed by water phase from both sides [9][25][30].

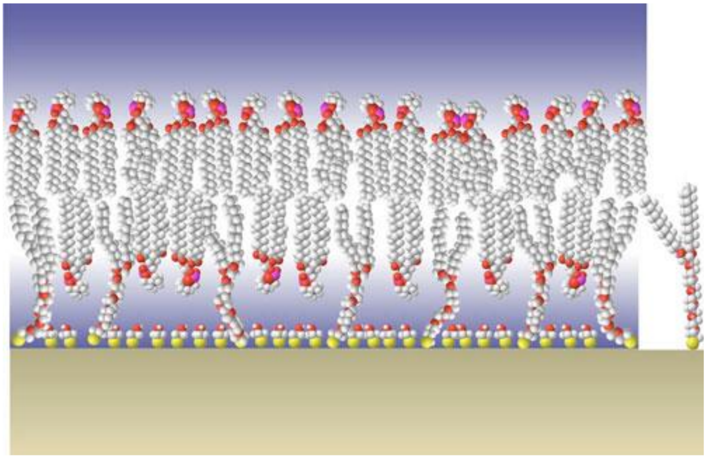

Fig. 5. Structure of tethered bilayer lipid membrane [7].

1.3. Self-assembled monolayer

Modification of electrode surfaces by self-assembled monolayers (SAMs) is widely used by many researchers [51][52][53]. Molecular adlayers of SAMs are usually deposited spontaneously on substrate surfaces by immersing the substrate into a surfactant solution [54][55]. Preparation of SAMs does not require expensive equipment [54], moreover, the obtained monolayers improve chemical and physical surface properties such as hydrophilicity [56][57] and electric charge [58]. Therefore, the method of modification of surfaces by SAMs is applied for studies in nanoscience and technology. The most versatile systems for designing SAMs are monolayers of alkanethiols on gold substrate [59][60][61].

In addition to self-assembled monolayers of alkanethiols, the method of surfaces silanization is widely used, particularly when silica and metal oxides are applied as substrates [52][58][62]. The process of silanization of the oxide surfaces is well developed [55][58][62]. Deposited silane monolayers are stable because of a strong attachment to the surface through covalent bonding [52][57]. Fig. 6 depicts schematic representation of surface silanization reaction. First, oxide surface is enriched with hydroxy groups (Fig. 6 A), then surface is immersed in trichloro or trimethoxy silane solution (Fig. 6 B) and reactive silanol groups are formed (Fig. 6 C). After hydrolysis reaction (Fig. 6 D and E), strong covalent bonds are formed with oxide surface. These kinds of systems like silica or metal oxides modified by silanization reaction have been used to investigate proteins for new drug delivery methods [63], cell growth [64].

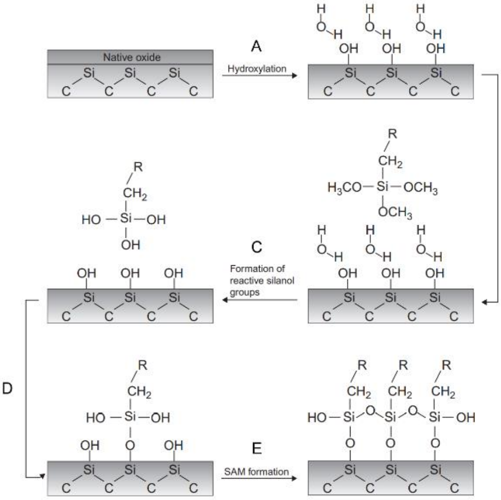

Fig. 6. Scheme showing the mechanism of silanization reaction [65].

1.4. Metal oxides

Most of the silane SAMs studies are carried out on Si/SiO_2 surface [66][67][68][69]. Although low electrical conductivity and increasing cost of silica caused different metal oxides to become more attractive for surface silanization and phospholipid bilayer membrane formation [70]. Tin oxide is convenient to use in biological systems [71] because of its good electrical and optical properties, absence of toxicity and, most importantly, biocompatibility [72][73]. In consequence, when investigating the electrical properties of biomembranes, it is convenient to use indium tin oxide (ITO) as a substrate [74][75][76].

It should be noted that there are plenty of research papers around the use of ITO, however slightly different variation of the substrate – fluorine doped tin oxide (FTO), is applied scarcely and mostly investigating its optical and electrical properties [77][78][79], also in the field of solar cells and photovoltaic devices [80][81]. Min-Jung Song et al. has proposed that modified FTO electrode can be applied for use in the enzyme-free, direct electrochemical detection of serotonin [82]. The advantage by comparison to differently doped tin oxide (ITO) is that FTO has similar/superior properties in addition to being cheaper.

1.4.1. Cadmium tin oxide

Transparent conducting oxides have been widely studied over the last several decades. They belong to the semiconductor materials with wide energy band gap, low resistivity and high optical transparency. One of the most widely studied are the films of ternary oxides [83][84][85] due to variety of properties such as low metal-like electrical resistivity (10-6 Ω m), high transmissivity (>90%) in the visible range of the light spectrum and high reflectivity in the IR range. One of them is cadmium tin oxide (CTO), which due to relatively low cost of cadmium is considered as a potential substitute for a variety of semiconductor applications of more expensive oxides of rare elements such as indium.

For optoelectronics film materials are of great interest. One of the first studies of CTO films was carried out by Nozik in 1972 [86]. The charge carrier concentration of 5×10^{18} cm^{-3} was reported in this work. Later CTO thin films were deposited using: spray pyrolysis [87][88], magnetron sputtering [89][90][91], pulsed laser deposition [92][93], sol-gel method [94][95][96][97], chemical bath deposition [98]. These methods differ by their complexity and equipment necessary to produce oxide films. There are certain advantages using relatively simple and inexpensive sol-gel method: it does not require sophisticated vacuum devices and it is energy saving. Sol-gel film properties can be controlled by changing thin film deposition conditions. Sol-gel deposition of CTO films was first proposed by Dislich et al. [99]. Later such a technology was used in a number of studies in other groups [97][100]. CTO films can be deposited by the sol–gel dip-coating using tin isopropoxide [97] and tin tetra-t-butoxide [100][101] as tin precursors and cadmium acetate as a source of cadmium.

Because of their optical and electrical characteristics, CTO films are good candidates as transparent conductive electrodes in CdS/CdTe and CdS/CIGS type solar cells. Therefore CTO films may find applications in photovoltaic cells [89][90][95][102][103], liquid crystal displays [104] and heat mirrors [105]. Recent studies show that cadmium tin oxide thin films can be used also in development of unconventional radiation dosimeters [106].

1.4.2. Fluorine doped tin oxide

Tin oxide has been extensively studied because of its wide range of applications in different fields [107][108][109]. As thin films, it can be prepared using various methods: sol-gel method [110], spray pyrolysis [111], pulsed laser deposition [112], chemical vapor deposition [113] and others. Different properties could be obtained using various dopants, such as indium [112][114], antimony [115], fluorine [110][111][116], manganese [117]. Electrical conductance and optical transmittance was found to be increasing using various concentration of fluorine, indium or antimony dopant [112][115][118] [119][120]. Using manganese as dopant magnetic semiconducting properties were observed [117]. Tin oxide can be used in different devices such as organic light emitting diode (OLED) devices [121], solar cells [122] and photovoltaic devices [123], gas sensors [109][124].

1.5. Membrane damaging/pore forming toxins

To test the biological relevance of formed phospholipid bilayers, membrane damaging or pore forming toxins may be used. Toxins are peptides/proteins that are usually produced by bacteria or are found in the venom of insects or snakes. The effectiveness of the toxin depends on the structure and composition of phospholipid bilayer and toxin itself.

Vaginolysin (VLY). VLY is produced by *Gardnerella vaginalis* bacteria that causes bacterial vaginosis in women of reproductive age [125]. VLY belongs to cholesterol-dependant cytolysin (CDC) family but uses complement regulatory molecule CD59 as its receptor [125]. Vaginolysin damages cell membrane by forming oligomeric pore that reaches diameter of 26 nm [126]. In general, CDC pore formation can be described in several steps (Fig. 7): first, water soluble monomer bounds to receptor on the surface of the bilayer membrane. Then monomer oligomerizes and forms prepore structure. It unfolds from α-helical bundles into β-hairpins. Lastly transmembrane β-barrel forms [127].

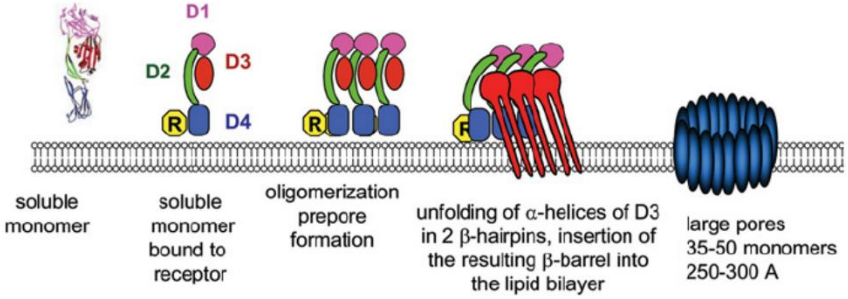

Fig. 7. Schematic representation of CDC pore formation in phospholipid bilayer [128].

Phospholipase A_2 (PLA2). Phospholipases are peripheral membrane proteins that hydrolyse phospholipibs by binding to phospholipid interface. The products of hydrolysis depend on type of phospholipase (Fig. 8). Phospholipase A_2 (PLA2) hydrolyse fatty acid at sn-2 position of phospholipids, generating corresponding fatty acids and lysophospholipids [129]. Most of phospholipids have unsaturated fatty acid at sn-2 position, which is transformed into eicosanoids. Eicosanoids are signalling molecules

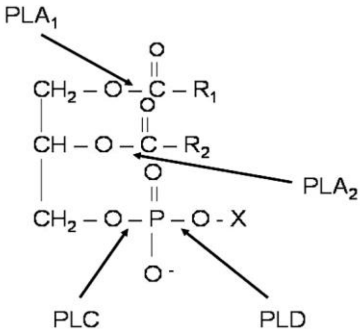

Fig. 8. Hydrolysis of phospholipids by different phospholipases: A_1, A_2, C and D [129].

that accelerate or inhibit inflammation, allergies, fever, other immune responses, affect miscarriages and normal child development, pain sensation, regulate cell growth [130].

Phospholipase A_2 is classified into 4 main groups: secreted PLA2, citosolic PLA2, calcium independent PLA2 and platelet activating factor acetyl hydrolase/oxidized lipid lipoprotein associated PLA2 [131]. Secreted PLA2 has been used in this work, thus will be discussed in more detail.

Secreted phospholipase A_2 (sPLA2) was the first type of PLA2 that was discovered. It is found in a variety of snakes, scorpion venom, pancreatic juice, synovial fluid and many other mammalian tissues[132]. sPLA2 is low molecular weight (13-15 kDa), it has histidine at the active site and requires Ca^{2+} ions for activity [131].

Melittin (Mel). Melittin is a cationic amphiphilic peptide that consists of 26 amino acids. It is found in honey bee (Apis mellifera) venom and it is the main pain producing ingredient [133]. Each peptide consists of two α-helixes that are connected at amino acid positions 10-12, which results in a bent conformation [134]. At the lipid-liquid interface melittin peptides act as surfactants because of their amphiphilic nature and lower surface tension [136]. Then peptides easily oligomerize into tetramer and form transmembrane channels inside plasma membrane which lead to lysis of the cell [137]. Usualy melittin is calssified as a carpet-like disruptor [138] Fig. 9,

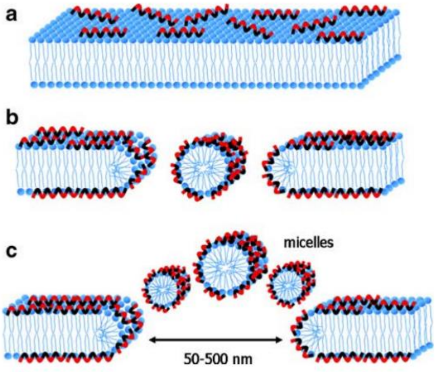

Fig. 9. Schematic representation of carpet-like mechanism for membrane disruption: a – peptides electrostaticaly binds to the surface of phospholipid bilayer; b and c – when high enough concentration of peptides on surface of membrane is reached, peptides form transient holes leading to micellization [135].

however, depending on concentration the mechanism of membrane disruption can be switch to forming of the pore [139].

α-hemolysin (αHL). α-hemolysin (33 kDa) is a toxin from Staphylococcus aureus which upon the contact with cell membranes inserts and forms hexameric/heptameric transmembrane pores Fig. 10. Such process disrupts membrane integrity, impairs ionic homeostasis and leads to cell death. Mechanism of α-hemolysin reconstitution into mammalian phospholipid membranes is well established [140]. Even though the toxin is not strictly dependent on cholesterol, the latter accelerates damage of cell membranes [141].

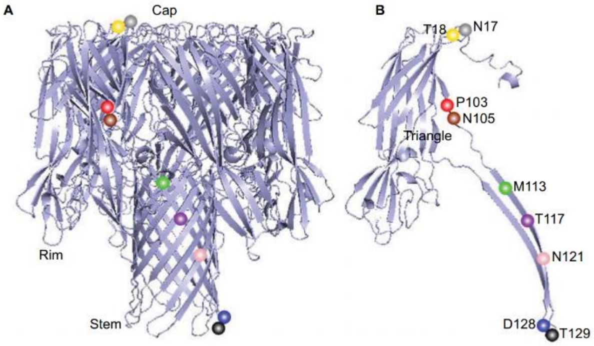

Fig. 10. Structure of α-hemolysin: A - heptamer; B – monomer [142].

1.6. Electrochemical impedance spectroscopy

Electrochemical impedance spectroscopy is often applied to investigate kinetics of electrochemical reactions by measuring impedance of a system in dependence of the altering current (AC) [143].

The potential (E) of AC can be expressed as a function of time (t):

$$E = E_0 \sin \omega t \qquad (1)$$

where, E_0 – amplitude of altering potential, ω – radial frequency (rad/s; frequency f (Hz) multiplied by 2π).

The response of altering current (I) is observed in sine function with a phase shift (φ) (Fig. 11):

$$I = I_0 \sin (\omega t + \varphi) \qquad (2)$$

where, I_0 – amplitude of altering current.

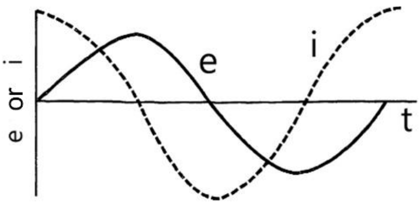

Fig. 11. The response of altering current as a sine function [143].

Considering an electrochemical system as resistance (R) and capacitor (C) in series, applied voltage must be equal:

$$\mathrm{E} = \mathrm{E_R} + \mathrm{E_C} \tag{3}$$

E_R and E_C can be expressed as:

$$E_R = I\,R \tag{4}$$
$$E_C = \frac{I}{\omega C} \tag{5}$$

Following equations will be expressed as complex notation ($j = \sqrt{-1}$). Combining (3), (4) and (5):

$$E = I\left(R - j\frac{1}{\omega C}\right) \tag{6}$$
$$Z = R - j\frac{1}{\omega C} \tag{7}$$

where, Z – impedance. It can also be expressed as:

$$Z = Z_{Re} - jZ_{Im} \tag{8}$$

Where, Z_{Re} and Z_{Im} is real and imaginary parts of the impedance. The phase shift (φ) can be expressed as:

$$\tan\varphi = \frac{Z_{Im}}{Z_{Re}} = \frac{X_C}{R} = \frac{1}{\omega RC} \tag{9}$$

One the most common ways to represent impedance data is through Nyquist plot, where displays Z_{Im} *vs* Z_{Re} for different values of ω (Fig. 12 a). Bode plot is also commonly used as it displays log Z or φ *vs* log ω (Fig. 12 b and c).

Cole – Cole plot may be also used (Fig. 13), where C_{Re} and C_{Im} are calculated from Z_{Re} and Z_{Im}:

$$\mathrm{C_{Re}} = \frac{\mathrm{Z_M}}{\omega|\mathrm{Z}|^2} \tag{10}$$
$$\mathrm{C_{Im}} = \frac{\mathrm{Z_{Re}}}{\omega|\mathrm{Z}|^2} \tag{11}$$

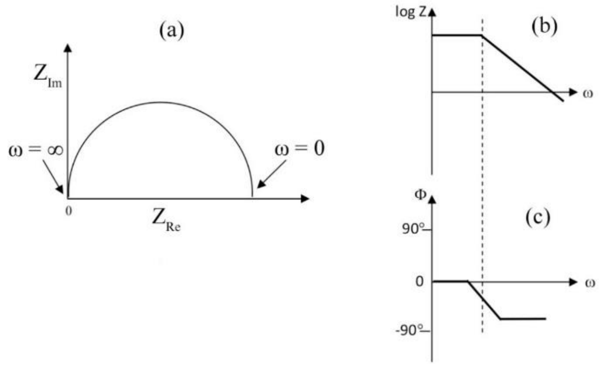

Fig. 12. Electrocemical impedance spectra in: (a) Nyquist plot; (b) and (c) Bode plot [144].

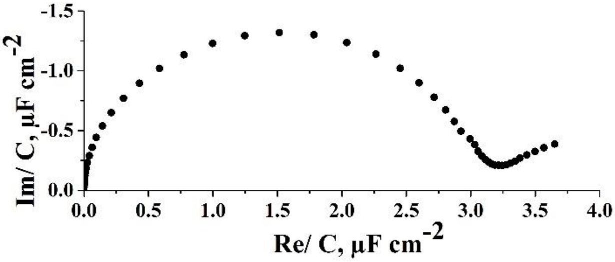

Fig. 13. Electrochemical impedance spectrum in Cole – Cole plot.

Cole – Cole plot is convenient to use to determine the complex capacitance of surface double layer. The diameter of semicircle multiplied by two gives an estimate of the complex capacitance value. Cole – Cole plot can be easily applied to investigate surface modification with self-assembled monolayers and phospholipid bilayers. Considering SAM formation on conductive surfaces as planar capacitors in series, the total capacitance can be expressed as:

$$\frac{1}{C_{meas.}} = \frac{1}{C_{SAM}} + \frac{1}{C_{surf.}} \qquad (12)$$

Where $C_{meas.}$ – is the measured capacitance of surface functionalized with SAM; C_{SAM} – is the capacitance of SAM; $C_{surf.}$ – is the capacitance of the conductive surface.

From equation (12) follows that by modifying the surface with SAM, diameter of semicircular EI spectrum should shrink and complex capacitance should decrease [7][39][145][146].

2. MATERIALS AND METHODS

2.1. Cadmium tin oxide thin film deposition

Cadmium tin oxide thin film electrodes were made by the sol-gel method. The sol-gel deposition solution was prepared as follows. 1 mL (1.02 g) of tin(IV) tert-butoxide (Alfa Aesar GmbH & Co KG, Germay) was dissolved in 13 mL of absolute methanol (Poch s.a., Poland) followed by dissolution of 1.06 g of anhydrous cadmium acetate (Roth, Germany). After full dissolution of the salts, 0.2 mL of acetylacetone (Fluka, Germany) were added to the solution. Then it was left to equilibrate overnight and stored in a desiccator filled with anhydrous $CaCl_2$ (Reachem Slovakia, Slovakia).

Microscope glass plates (2.5 cm x 2.5 cm) (Thermo scientific, Germany) were used as substrates for CTO film deposition. The substrates were cleaned by sonication in a Micro 90 (Sigma-Aldrich, Germany) detergent ethanol mixture, deionized water and 2-propanol (Roth, Germany), each time for 8 min. Film deposition procedure followed these steps:

1. 200 µL of sol-gel solution was dropped onto cleaned and dried substrates, rotating at 3000 rpm; SCS SpinCoater P6700 was used throughout the work.
2. Spin-coated samples were dried for 20 min at 200 °C on a hotplate in a hood.
3. First and second steps were repeated 2-4 times.
4. Deposited films were heated at 400 °C and 520 °C for 20 min in each temperature in an in-house designed quartz tube furnace with the automatic temperature control.

All samples were allowed to cool in air. Temperatures below 100 °C were typically reached within 2 min.

2.2. Cadmium tin oxide thin film characterisation

The sheet resistance of the CTO films was measured with APPA 201N multimeter keeping 1 cm distance between two electrodes. The phase composition of the CTO films was characterized by Rigaku MiniFlex2 diffractometer. Bragg-Brentano geometry was used for measurements of the reflection from films.

The ultraviolet-visible (UV-Vis) absorbance spectrum was acquired on Perkin Elmer Lambda 25 UV/VIS Spectrometer, in 400-700 nm wavelength range. The twin beam measurement mode was used with a glass substrate as reference.

CTO samples were probed by the Perkin-Elmer FTIR Frontier Dual-Range spectrometer. Measurements were carried out in a wavelength range from 2700 cm^{-1} to 3100 cm^{-1}, with the resolution of 2 cm^{-1}. Spectrometer was equipped with the Pike GladiATR single reflection diamond prism allowing measurements in a total internal reflection mode. As a reference a spectrum of the neat, non-silanized CTO film was used.

Dependence of the CTO film resistance on temperature was estimated using 4 probe method. The sample was placed into the in-house designed tube furnace with tungsten thermocouple. Measurement was performed using nitrogen gas flow in the temperature range 20 - 70 °C.

The thickness of CTO thin films was measured using Talystep (Taylor Hobson) profilometer. In order to measure the thickness, films were partially coated with vacuum oil. The uncoated parts of the sample were exposed to HCl (1:10) solution. After etching in acid a steep step was formed and the distance from the glass to the top of the film was measured. Reasonable number of measurements (per sample) were performed to assess statistically significant interval of thicknesses. Typically, the CTO film thickness was found in the interval form 65 to 80 nm.

2.3. Preparation of fluorine doped tin oxide

FTO covered glass sheet (300 x 300 x 2 mm) was purchased from Sigma-Aldrich, Germany and cut into smaller pieces (1 cm x 2.5 cm). Cleaning procedure of FTO samples were as follows: FTO electrodes were incubated in sonication bath for 10 min in each medium: (i) in 2% “Micro 90” cleaning solution (Sigma Aldrich, Germany), (ii) in deionized water. Then glass slides were incubated in concentrated H_2SO_4 (Reachem Slovakia, 98 %, Slovakia) for 1 h in order to remove any surfactant residues left from “Micro 90”. Afterwards, electrodes were washed with copious amount of deionized water and incubated in sonication bath for 10 min in each medium: (i) in deionized water and (ii) in 2-propanol. Electrodes were dried in a stream of nitrogen gas (Elme Messer, Lithuania) and immediately used for further experiments.

2.4. Synthesis of trichloro(3-(octadecylthio)propyl)silane

Synthesis procedure was adapted from the reference [147], where chemicals for click reaction were mixed at equimolar ratio. In this work, we used thiol- and allyl- groups containing chemicals in 1:2 molar ratio. Specifically, octadecanthiol (ODT, Fluka, Germany) and allyltrichlorosilane (ATS, Aldrich, USA) were mixed in a clear glass vial at molar ratio 1:2. Then

2 mol% of photoinitiator 2,2-dimethoxy-2-phenylacetophenone (DMPA, Acros Organics, USA) was added into the mixture and mixed until dissolved. This mixture was irradiated using 365 nm wavelength 5 W UV light for 24 hours. After this synthesis procedure, half of the ATS reacted with ODT to make TOPS and half of the ATS left in the synthesis mixture as residue. Thus, we have ready-to-use silanization mixture (TOPS:ATS 1:1) for SAM formation. The TOPS:ATS 1:1 mixture was kept wrapped in aluminium foil to avoid direct sunlight which could possibly influence chemical activity of prepared mixture. Synthesis reaction of the mixture is shown in Fig. 14.

^{1}H and ^{13}C nuclear magnetic resonance (NMR) spectra were determined with Bruker Ascend 400 spectrometer (400 MHz frequency for ^{1}H NMR and 100 MHz for ^{13}C NMR) by using residual solvent ($CDCl_3$) signals. Chemical shift are given in the δ scale (ppm). In descriptions of the spectrum ^{1}H NMR the following abbreviations are used: d – doublet; t – triplet and m – multiplet.

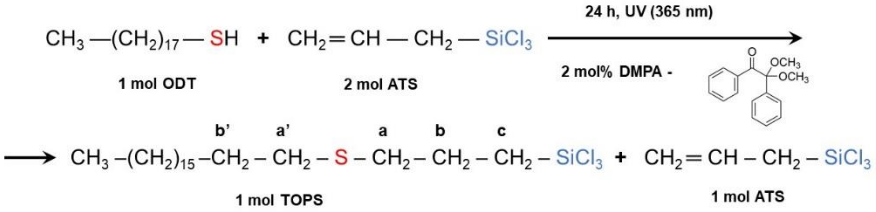

Fig. 14. Synthesis reaction of TOPS via click reaction between ODT and ATS. Atoms marked with the letters a, b, c, a' and b' showed characteristic signals in the 1H and 13C NMR spectrums of the reaction products (Fig. 49-50).

2.5. Self-assembled monolayer formation

CTO and FTO functionalisation with OTS monolayer. 50 mL of heptane (Sigma-Aldrich, Germany) was heated to 60 °C in a small beaker, then octadecyltrichlorosilane (OTS, Aldrich, USA) was added to reach, depending on needs, 0.1 – 5% (v/v) of OTS. The sample plate was fixed vertically in the solution, which was intensively mixed. Temperature was kept constant at 60 °C throughout 60 min of silanization. After that, sample plate was rinsed 3 times with pure heptane and dried using N_2 stream.

FTO functionalisation with mixed OTS:MTS monolayer. FTO were functionalised by applying two different protocols: (i) direct silanization of FTO sample by mixture of silanes (SAM-P1) and (ii) overnight incubation of FTO sample in deionized water prior to silanization procedure (SAM-P2). For P1 and P2 protocols silanization procedures were as follows: 50 mL of heptane was heated to 60°C in a 50 mL volume beaker. After that, silanization solution was prepared: OTS and methyltrichlrosilane (MTS, Alfa Aesar, Germany) was added to heptane to make the total concentration of 2.5 mM at different OTS:MTS molar ratios. The same 2.5 mM concentration was used during all experiments. FTO glass slide was immersed into stirred silanization solution in a vertical position and incubated for 60 min at 60°C. Then, silanized FTO sample was rinsed with heptane and dried in a stream of nitrogen.

FTO functionalisation with TOPS:ATS monolayer. The silanization solution was prepared by heating 20 mL of heptane to 60 ºC and adding 30 µL of synthesised TOPS:ATS mixture into heated heptane. The FTO electrode was immersed into silanization solution, fixed in a vertical position, and incubated for 1 h at 60 ºC while mixing. Afterwards, FTO electrode was washed with heptane and dried in a nitrogen gas stream. Then, the electrode was heated at 100 ºC for 1 h in air to remove adsorbed water and solvent residues.

2.6. Phospholipid bilayer membrane formation

tBLM formation was carried out using vesicles fusion method. Preparation of vesicles solution is described in detail in ref [43]. In this work, two compositions of tBLMs were formed: 1,2-dioleoyl-sn-glycero-3-phosphocholine (DOPC, Avanti Polar Lipids, inc., USA) and cholesterol (Chol, Avanti Polar Lipids, inc., USA) at molar ratio 6:4 (DOPC/Chol 6:4) and 100% DOPC. Total lipid concentration in vesicles solution was 1 mM in phosphate buffer saline (PBS) pH 4.6 (0.1 M NaCl (Reachem Slovakia), 0.01 M NaH_2PO_4 (Reachem Slovakia)). Vesicles solution was injected directly into electrochemical cell on SAM and incubated for 1 h. Then, it was rinsed out of the cell using a syringe with PBS pH 7.1. Biological relevancy of formed membranes was tested using vaginolysin (VLY was provided by dr. Milda Pleckaityte at the Institute of Biotechnology, Vilnius University), phospholipase A_2 (PLA2) from bee venom (Sigma-Aldrich, Germany), melittin (mel) from honey bee venom (Sigma-Aldrich, Germany) and α-hemolysin (aHL) from Staphylococcus aureus (Sigma-Aldrich, Germany). All toxins were dissolved in PBS pH 7.1.

2.7. Regeneration of self-assembled monolayer

Regeneration of SAM was carried out in these steps: (i) lipid bilayer was formed by vesicle fusion method (2.5 section), (ii) EI spectra was recorded. Then (iii) lipid layer was removed by rinsing the SAM with 2-propanol and deionised water mixter (1:1 v/v), followed by rinsing with deionised water. (iv) After filling the cell with PBS pH 7.1, EI spectra of SAM was recorded. Repeating (i) - (iv) steps multiple times regeneration of SAM was determined.

2.8. Contact angle measurements

Surface wetting characteristics were measured using Theta Lite optical tensiometer from Biolin Scientific (Finland). Contact angles of 5 µL deionised water droplet at 6 different spots on each sample were measured and averaged.

2.9. Electrochemical measurements

All measurements were carried out in PBS pH 7.1. Solution of the redox active probe was made of 1 mM potassium ferrocyanide trihydrate and 1 mM potassium ferricyanide in PBS pH 7.1.

Electrochemical impedance spectroscopy (EIS) measurements were recorded using either µAutolab (Type III) potentiostat/galvanostat or Zennium electrochemical workstation (Zahner GmbH, Germany), frequency range 0.1 Hz – 100 kHz. Fast Fourier transform (FFT) impedance spectrometer EIS-128/16 (University of Kiel, Germany) constructed by G. Popkirov [148][149] was used for dynamic electrochemical impedance spectroscopy (EIS) measurements. Cyclic voltammetry curves were recorded using µautolab (Type III) potentiostat/galvanostat.

Measurements were performed in 6 vial cell, which was described previously (supporting material in ref. [150]). A three-electrode cell was used for all electrochemical measurements, where the FTO glass slide (0.32 cm^2 geometric surface area) served as the working electrode, Pt wire (99.99% purity, Aldrich, Germany) as a counter electrode and Ag/AgCl, $NaCl_{sat.}$ (Microelectrode Model M-401 F, Bedford, JAV) as a reference electrode. All the potentials given in this study are *vs* Ag/AgCl, $NaCl_{sat.}$ electrode.

Approach curves were recorded using Sensolytics SECM – 030 equipment combined with Autolab PGSTAT 30 potentiostat/galvanostat. A conventional three electrode cell based on (i) $Ag/AgCl/Cl_{sat.}$ as reference electrode, (ii) platinum wire (99.99%) as counter and (iii) platinum ultra-microelectrode (UME, diameter – 20 µm) as working electrode was applied. Measurements were recorded in PBS pH 7.1 All measurements were recorded at -0.75 V vs $Ag/AgCl/Cl_{sat}$.

3. RESULTS AND DISCUSSION

3.1. Hybrid bilayer formation on cadmium tin oxide

3.1.1. Characterisation of cadmium tin oxide

Film fabrication conditions. One of the important characteristics of the metal oxide films is their conductivity. Therefore, before attempting surface functionalization, the electrical properties of the sol-gel CTO films were estimated. We found several factors determining square resistance of the CTO films. First, as follows from the data in Fig. 15A, the effect of the number of sol-gel layers is non-monotonic. Resistance minimum was observed for 3-layer films, which exhibited values of the square resistance near 0.35 ± 0.05 kΩ.

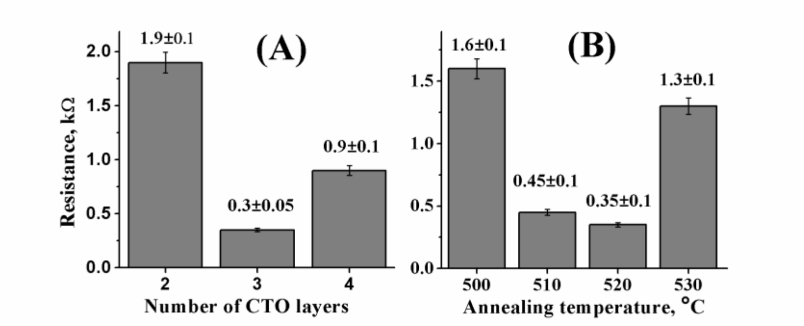

Fig. 15. The dependence of the resistance of CTO films on (A) the number of CTO layers (annealing temperature 520 °C), and (B) annealing temperature (3 layer films). Annealing time 20 min.

Two- and four-layer CTO films exhibited significantly higher resistances 1.9 ± 0.1 and 0.9 ± 0.1 kΩ correspondingly. The absence of resistance scaling with the film thickness, which is obvious from the data in Fig. 15 A, points to the role of film thickness in the solid state chemistry determining the residual conductivity of the films. This may be primarily related to the oxygen exchange between films and ambient during the annealing process. As pointed out, loss of oxygen and generation of oxygen vacancies may be responsible for increased conductivity of CTO [151][152]. An increase of film thickness limits such a process that occurs during relatively short annealing (approx. 20 min), thus, leading to increased square resistance. Therefore, for further experiments 3 layer CTO substrates were used.

Another important factor affecting the resistance of CTO films is the annealing temperature [100][152]. We observed quite significant variation of the resistance in a relatively narrow annealing temperature interval from 500 °C to 530 °C, with the clearly expressed minimum at 520 °C (Fig. 15 B), at which films attained resistance of 0.35 ± 0.05 kΩ. This value is fairly close to the one reported earlier [100]. It is important to note that in ref. [100] the global (temperature interval from 400 to 900 °C) minimum of the resistance of CTO films on Si substrates was recorded at 750-800 °C with the resistance values 15-20 Ω. In the current study, we substituted Si with glass substrates, therefore we "traded" higher CTO film conductance for less expensive glass substrates, which required lowering the annealing temperature of the films. Lower annealing temperatures yield significantly lower CTO conductance. Taking into account these factors, the optimal annealing temperature was found to be at 520 °C.

Electrical and optical properties. Fig. 16 A displays film resistance temperature dependence trace in the 20-70 °C temperature range. Sharp local drops of the resistance seen in the plot (Fig. 16A) were artefacts, most likely related to the instability of the contact resistance. However, the general temperature trend, shown in Fig. 16 B was fairly reproducible. Plotting the resistance vs. temperature curve in the Arrhenius type plot (inset Fig. 16 A) indicate the extremely shallow donor level of about 10 meV below the conduction band. This along with the high carrier concentration (vide infra) suggest that CTO film electrical properties are close to a transition from the semiconductor-type to metal-type.

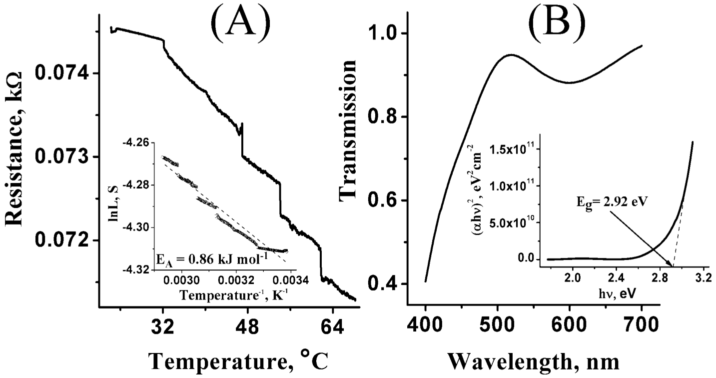

Fig. 16. CTO sol-gel film resistance and optical transmission spectra.

The sol-gel CTO films were transparent (Fig. 16 B) in the visible wavelength range. In the interval from 400 to 700 nm, the transmission was above 90%. Assuming the direct transition the optical band gap estimated from the transmission coefficient dependence from the photon energy was

2.92 eV. So, the transparent, yellowish CTO films used in this work exhibited properties of wide-band gap, conducting metal oxide semiconductors.

Crystal structure. Crystallinity of CTO films was assessed by the XRD method. The representative XRD curve is presented in Fig. 17. From Fig. 17 it follows that the samples annealed at 520 °C exhibited partial crystallinity with the large fraction of amorphous material. The major crystalline component of the films is cubic Cd_2SnO_4 with the most intense peak corresponding to a reflection from (311) crystallographic planes. Relative intensities of the XRD lines roughly correspond to a randomly oriented powder samples, so we may conclude our CTO samples were polycrystalline non-textured films. The presence of a large amorphous “bulge” in the low 2θ range is consistent with the earlier observations [100] for 600 °C CTO films. However, in our case, we consistently detected second, CdO, component with the most prominent reflections from planes (111), (200) and (220). The CdO diffraction lines exhibited noticeably narrower FWHM (Fig. 17) compared to the lines of Cd_2SnO_4. The very presence of CdO crystals points out to an incomplete solid state reaction between cadmium and tin precursors. Moreover, significantly larger CdO crystallites suggest that during the annealing process CdO forms first (or faster), thus becoming the precursor sites for further solid state transformation into Cd_2SnO_4.

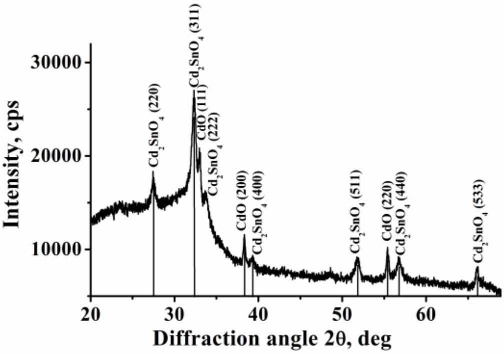

Fig. 17. Typical XRD pattern of the CTO films on glass annealed at 520 °C for 20 min.

Flat-band potential and carrier concentration. To probe type and concentration of carriers in CTO films the Mott-Schottky plots were derived from the electrochemical impedance spectroscopy (EIS) data. Fig. 18 displays typical electrochemical impedance data sets plotted in the complex capacitance plots (Fig. 18 A) and Mott-Schottky type curve estimated from the EIS data (Fig. 18 B). The complex capacitance plots exhibit typical semi-circular shape similar to ones observed earlier [100]. Such a shape is typical for ideally polarizable interphases exhibiting near ideal capacitive behaviour. The increase of the bias potential triggers significant reduction of the diameter of semicircles reflecting a decrease of the capacitance on an interphase between CTO surface and solution. This effect leads to a conclusion that CTO is an n-type semiconductor consistent with previous works [86][91][93][96][100]. EIS spectra in Fig. 18 A can be fitted as it was done in ref. [100] to a simple R(CPE, R_{rf}) model, where R is the resistance of the bulk CTO material and liquid electrolyte, and CPE is the constant phase element of the interphase, and R_{rf} is the residual resistance of interface accounting for the residual electron transfer currents due to reduction and/or oxidation of residual electroactive impurities such as dissolved oxygen and others. The experimental impedance spectra were fitted to this model, in which the CPE exponents were found to be between 0.95 and 0.98. Due to relatively insignificant deviation of the CPE exponent from 1.00 we have treated the coefficient of the CPE element as a capacitance. Thus estimated electrode capacitance vs. potential was plotted in the Mott-Schottky coordinates as shown in Fig. 18 B. The near linear relationship between the squared reciprocal of capacitance and the potential allows estimation of carrier density and flat band potential of CTO electrodes using the Mott-Schottky relationship. The mean value of the flat band potential obtained from the intersection of the Mott-Schottky line with abscissa was close to -0.1 V, while the charge carrier concentration established as described in [100] was found to be $N_d = (3.31 \pm 0.38) \cdot 10^{19}$ cm^{-3}. Together with the weak temperature dependency (Fig. 16 A, inset) high carrier concentration hints at electronic degeneracy of the fabricated CTO films.

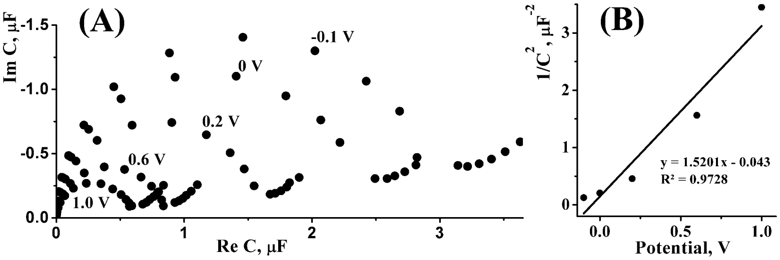

Fig. 18. Electrochemical impedance spectra obtained at various potentials by using CTO electrode annealed at 520 °C, t = 20 min, surface area 0.32 cm^2, (A) - Cole-Cole plot; (B) - Mott-Schottky plot.

3.1.2. Formation and properties of octadecyl silane self-assembled monolayer on CTO

To obtain compact and highly electrically isolating phospholipid monolayers (bilayers) solid supports need to be functionalized by the anchor molecules [10][153]. In contrast to noble metals, metal oxide surfaces are typically tailored by oxysilane chemistry. In this study, OTS was used to functionalize surface of CTO films. The progress of the silanization was monitored by several surface sensitive techniques.

The most straightforward way to detect the formation of hydrophobic organic material layer is the contact angle measurements. In Fig. 19 contact angles of differently silanized CTO are presented. Pristine CTO films are hydrophilic, they exhibited contact angles of 40 ± 6 degrees. Silanization significantly increased hydrophobicity, thus attesting for the formation of the hydrophobic overlayer on CTO surface. The degree of hydrophobicity varied depending on silanization conditions. Maximal contact angle values of 103 degrees were achieved upon silanization in 0.1% OTS solutions. Taking into account the beneficial effects of the surface hydrophobicity on phospholipid layer completeness [10] (the higher the contact angle the more complete phospholipid overlayer can be formed), the CTO samples silanized in 0.1% OTS solution were chosen for further phospholipid monolayer anchoring experiments.

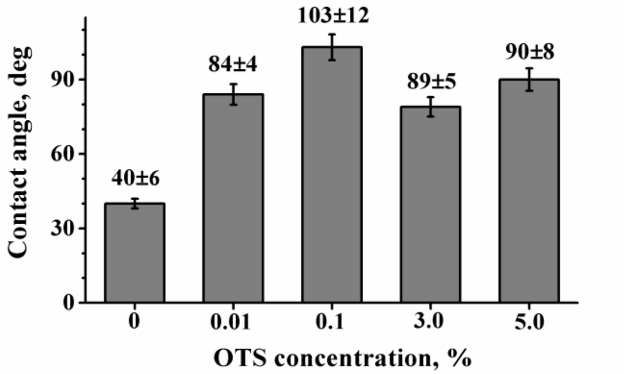

Fig. 19. Contact angles of CTO sol-gel film electrodes silanized using various OTS concentrations.

The silanized CTO films were analysed using the reflection absorption FT-IR spectroscopy. In FT-IR spectrum (Fig. 20) three vibration absorption bands are detected in the methyl and methylene C-H bond vibration spectral range. The bands at 2851 and 2922 cm^{-1} (Fig. 20) are assigned as the symmetric stretching mode ($\nu_s(CH_2)$) and asymmetric stretching mode ($\nu_{as}(CH_2)$) vibrations of the methylene groups, respectively . The band at 2959 cm^{-1} is associated with in-plane (ip) and out-of-plane (oop) asymmetric stretching vibrations of the methyl groups ($\nu_{as}(CH_3)$ip and $\nu_{as}(CH_3)$oop)). The position of the $\nu_{as}(CH_2)$ band is a strong metric for order in the alkyl chains [154], appearing at 2917 cm^{-1} for highly ordered SAMs and shifting to higher wavenumbers with increasing gauche conformations along the polymethylene chain. In our case, $\nu_{as}(CH_2)$ appears at 2922 cm^{-1}, thus indicating disorder in the anchor monolayer formed via silnization.

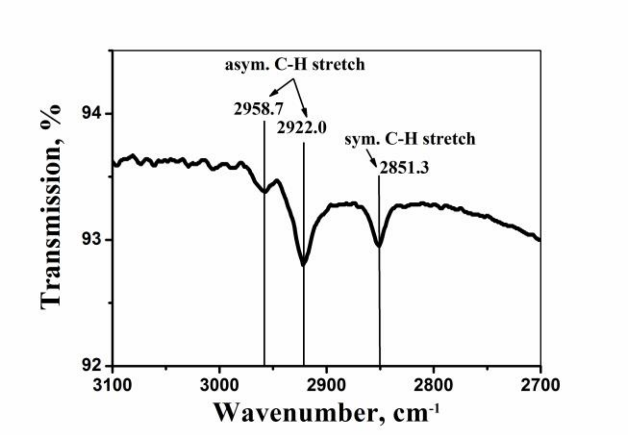

Fig. 20. FT-IR spectra of silanized (0.1% OTS solution) CTO electrode.

Nevertheless, because of relatively low wavenumbers of the $\nu_s(CH_2)$ as well as $\nu_{as}(CH_2)$ we conclude that silanization of the CTO films yielded partly ordered monolayer of alkyl chains on the surface. Such situation may be observed only in case of relatively high density of the anchor molecules.

The completeness of an anchor monolayer may be assessed by the electrochemical techniques. In particular, one may expect a significant differential capacitance decrease upon formation of an insulating organic film. Also, the electron transfer to and from the redox active species present in solution is blocked by the compact insulating films.

Fig. 21 displays cyclic voltammetry traces obtained on pristine and OTS functionalized CTO films in phosphate buffer solutions with and without redox species. In solutions with not redox species (Fig. 21 A) the current during the cyclic voltammetry scan arises due to a charging of the electric double layer.

The formation of a compact organic dielectric film should trigger the decrease of the charging current. Such an effect is clearly visible in the voltammetry scans plotted in Fig. 21 A. Another proof of the compactness of the anchor monolayer is the blockage of the redox current shown in Fig. 21 B. Together with FT-IR data (Fig. 20) the electrochemical experiments in Fig. 21 confirms the formation of a dense and compact hydrophobic monolayer which is further used for phospholipid hybrid bilayer formation.

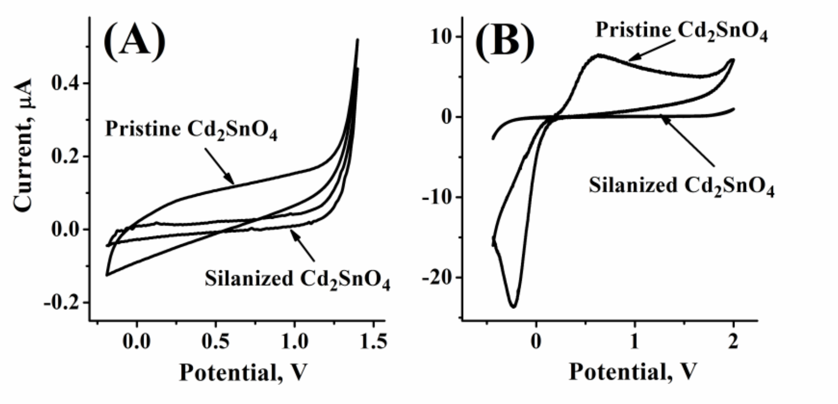

Fig. 21. Voltammetric curves of pristine and silanized CTO film electrodes recorded in A - phosphate buffer, pH 7.1, B – same phosphate buffer containing 1 mM of the potassium hexacyanoferrate. Scan rate 0.01 V s^{-1}. Surface area is 0.32 cm^2.

3.1.3. Formation of hybrid phospholipid bilayer on CTO surface

Formation of hybrid bilayer was accomplished by the vesicle fusion to a CTO surface functionalized with anchor OTS monolayer. Main force driving the vesicle fusion process is the hydrophobic interaction between the OTS octadecyl silane layer on CTO surface and phospholipid vesicles [10], specifically, the hydrophobic chains of a lipid. The vesicle fusion process was monitored by the EIS. Fig. 22 illustrates processes that take place during the sequence of surface functionalization events. Initially, pristine CTO film exhibits semicircular-shaped EIS features with the capacitance of 7-9 µF cm^{-2} (Fig. 22, open circles). Silanization in 0.1% OTS solution, leads to a 3-fold decrease (Fig. 22, filled circles) of the capacitive semicircle to approx. 2.5 µF cm^{-2}. The EIS measured capacitance decrease is consistent with the cyclic voltammetry data (Fig. 22 A). Even though the capacitance decrease is indicative of the formation of an octadecylalkane dielectric layer, the specific capacitance value 2.5 µF cm^{-2} is significantly higher compared to that (approximately 1.5 µF cm^{-2}) of similar chain-length octadecylthiolate (ODT) layers on noble metals such as gold [10]. This hints at significantly lesser density [10] and higher packing disorder in polymethylene chains, an effect leading to an increased capacitance in self-assembled monolayers.

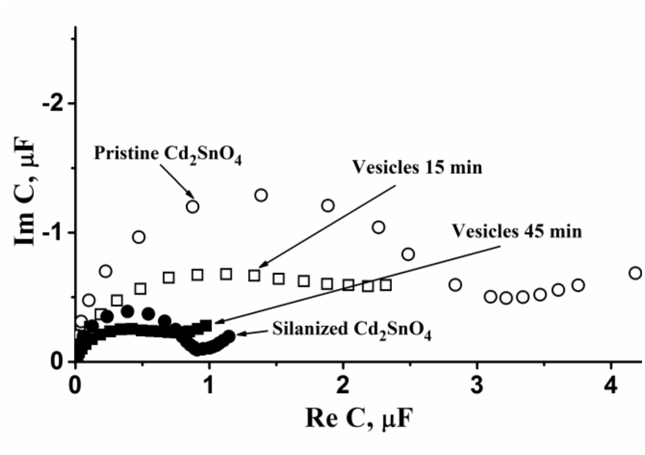

Fig. 22. Evolution of EIS spectra in Cole – Cole plot in the process of surface modifications: open circles – pristine CTO surface, filled circles – CTO modified with OTS, open squares – CTO/OTS surfaces treated with vesicles solution for 900 s, closed squares – CTO/OTS surfaces treated with vesicles solution for 2700 s. Surface area of the electrode 0.32 cm^2.

The interaction of OTS functionalized CTO surfaces with vesicle solutions proceeds via two stages. During first 15 min, a significant increase of the capacitance in the complex capacitance plot (Fig. 22, open squares) was observed. The semicircle was highly distorted (squeezed) indicating sharp increase of heterogeneity of the interphase during the initial stage of fusion. This effect was highly reproducible indicating the systemic alteration of the molecular architecture by vesicles. After the initial capacitance increase slow decrease followed. Eventually, the capacitance curve trended down towards the one showed in Fig. 22, filled squares with the final capacitance approaching value of approximately 0.8 µF cm^{-2} typical for hybrid bilayer on ODT modified gold surfaces [10]. The schematic representation of formed phospholipid bilayer on cadmium tin oxide surface functionalised with OTS can be seen in Fig. 23.

The initial increase of the capacitance seems counterintuitive. As vesicle material is transferred to a surface one would expect continuous capacitance decrease as it is typically observed on alkanethiolate monolayers on gold [10]. However, in this work, the opposite effect was observed. Such a non-monotonic complex capacitance trend (initial increase, and subsequent decrease) during vesicle fusion is observed, to our best knowledge, for the first time. This effect may be tentatively interpreted presuming certain structural

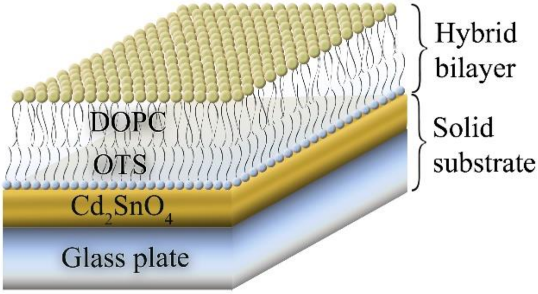

Fig. 23. Structure of hybrid phospholipid bilayer on cadmium tin oxide surface.

changes occurring in the anchor monolayer during the initial stages of the vesicle fusion. As demonstrated recently [155] sparsely populated lipid-likeanchor compounds form self-assembled monolayers on gold with predominantly horizontally oriented, disorderly piled polymethylene chains. Presumably, such a molecular arrangement, i.e., horizontal piling of molecules one over another corresponds to a minimum of an unfavourable hydrophobic interaction, in case when the surface density of alkane chains is not enough to form predominantly vertically oriented compact monolayers [155]. The significantly higher specific capacitance (approx. 2.5 µF cm^{-2}) of the OTS SAMs compared to the ODT monolayers (approx. 1 µF cm^{-2}) on gold points to the lack of density of organic material, to form perfect nearly vertically oriented SAM. RAIRS data obtained in the current work confirms moderately disordered state of polyethylene chains in the OTS SAM (vide supra). Interaction with vesicles triggers reorientation of anchor molecules from predominantly horizontal to predominantly vertical position. This leads to exposing to a solution vast areas of metal oxide surface that initially are not fully covered by the phospholipid overlayer. These events triggers an initial capacitance increase observed in Fig. 22 (open squares). As the vesicle interaction proceeds and the hybrid bilayer becomes more and more dense, the phospholipid overlayer insulates CTO areas exposed to the solution, so the capacitance variation reverses and it starts decreasing.

3.2. Formation of hybrid phospholipid bilayer on fluorine doped tin oxide

3.2.1. Formation and properties of octadecyl silane self-assembled monolayer on FTO

As a first step in bilayer formation a functionalization of tin oxide film was carried out in OTS solutions. A formation of an octadecylsilane monolayer should lead to a sharp change in surface hydrophilicity. Fig. 24 A illustrates anticipated increase of surface hydrophobicity with contact angle values changing from 44 to over 115 degrees upon silanization for 30 min. Such changes immediately confirm the formation of a hydrophobic layer atop of the FTO film. Variation of the silanization time does not show significant increase of the contact angle. It stays relatively constant in the vicinity of 120 degrees within measurement error as the silanization time increases from 30 to 60 min. We, however, noticed a consistently higher experimental error spread for shorter times of incubation: 30 and 45 min. Therefore, for further experiments we chose 60 min silanization time during which a reproducible hydrophobic layer can be formed in 0.25 – 2.5 mM solutions of OTS in heptane.

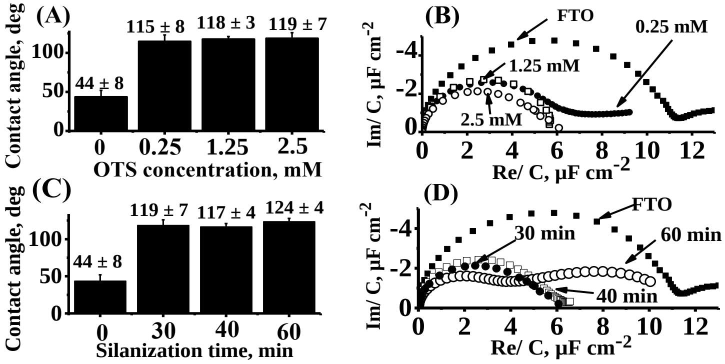

Fig. 24. Contact angles (A, C) and EI spectra in Cole - Cole plot (B, D): (A) and (B) – FTO silanized for 30 minutes in different OTS concentration; (C) and (D) – FTO silanized in 2.5 mM OTS for different periods of time.

In addition to a sharp jump of the contact angle values, the silanization significantly changes the EI spectra. In all cases, the capacitance of tin oxide electrode decreases attesting for the formation of a dielectric layer formed by the octadecyl chains of OTS on FTO. In Cole – Cole plot this effect can be easily tracked by the decrease of the diameter of the semicircular part (Fig. 24 B and D). At constant incubation time (30 min) the diameter of the semicircle decreased with OTS concentration during silanization (Fig. 24 B). An increase of incubation time leads not only to the quantitative but also to qualitative changes of the EI spectra. In particular, at incubation times of 60 min double semicircular features appear on the Cole – Cole plots. Such semicircular features are typical for the compact tethered bilayer systems [156] and may appear on FTO with OTS with the compact organization of the polyethylene chains in OTS monolayer. This was another argument that prompted us to choose OTS formation time of 60 min and 2.5 mM OTS concentration in incubation solution. As we will show further (Fig. 29), the presence of double semicircular features can be also used as a diagnostic tool for predicting the suitability of substrate for the complete vesicle fusion leading to a formation of the tethered bilayer.

Finally, the formation of an electrically insulating OTS monolayers may be also confirmed by testing electron transfer processes before and after silanization. Fig. 25 displays electrical double layer charging voltammograms (Fig. 25 A) and voltammograms (Fig. 25 B) of an electron transfer process on FTO before (continuous lines) and after the silanization (dashed lines). Upon silanization, consistent with the EIS data one should observe a decrease of the double layer charging current, as seen in Fig. 25 A. A compact layer of dielectric should also significantly slow down an electron transfer rate. Indeed, Fig. 25 B clearly confirms this supposition. Peak-shaped redox currents of ferro/ferri cyanide iron complexes are totally suppressed by the silanization confirming a formation of a compact OTS layer on FTO. Such large pin-hole-free, highly hydrophobic anchor monolayer must provide a perfect substrate for the vesicle fusion leading to a formation of the phospholipid bilayer.

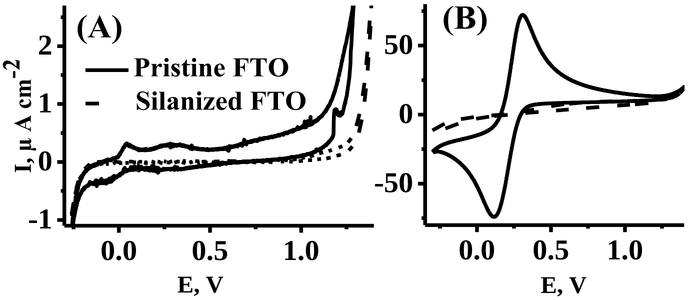

Fig. 25. Voltammetric curves of pristine (continuous line) and silanized FTO electrodes in 2.5 mM OTS solution for 1h (dashed lines), recorded in A – phosphate buffer, pH 7.1; B – same phosphate buffer with 1 mM $K_4[Fe(CN)_6]$ and 1 mM $K_3[Fe(CN)_6]$. Scan rate 0.01 V s^{-1}.

SECM technique was applied for the monitoring of FTO surface before and after the modification with OTS monolayer. According to expectations SECM data could provide information about surface properties on different spots of investigated sample. Therefore, approach curves were recorded towards FTO surface covered by OTS SAM (OTS/FTO) using UME approach step of 10 µm. Unexpectedly, no changes were observed in approach curves (Fig. 26), therefore, it was predicted that OTS/FTO still exhibits same conductivity (due to incomplete coverage of FTO surface by OTS). Therefore, approach curves towards OTS/FTO registered at larger scale (from 500 µm up to 0 µm) at high extent are similar to that, which are registered while UME is approaching bare FTO surface (Fig. 26). However, using slower UME pace with approach step of 1 µm, approach curves started to exhibit constant current region when UME distance from the surface reached by 10 µm (Fig. 27). This effect can be explained by the properties of SAM, which consists of dielectric OTS molecules and the monolayer of these aliphatic layers is considered to be dielectric. For this reason, when UME reaches OTS/FTO surface the diffusion of redox able compounds is being blocked and current of UME stabilizes.

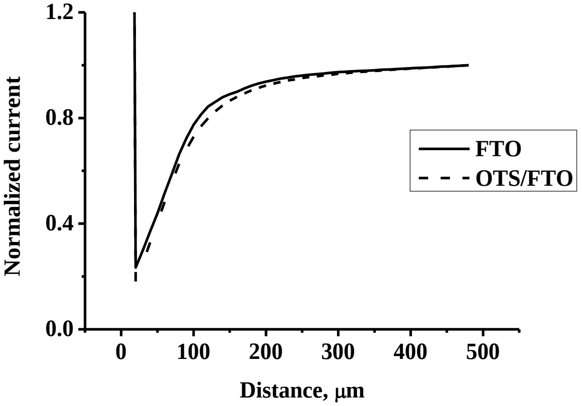

Fig. 26. Approach curves towards FTO (line) and FTO modified with OTS-based SAM (dashed line). Approach step 10 µm.

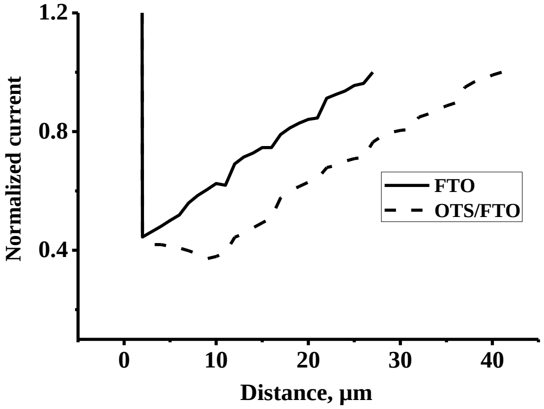

Fig. 27. Approach curves towards bare FTO (line) and FTO modified with OTS-based SAM (dashed line). Approach step 1 µm.

3.2.2. Formation of hybrid phospholipid bilayer on FTO

Once the formation of the anchor monolayer was accomplished, multilamellar vesicle fusion methodology was applied [43]. The vesicle fusion and formation of lipid overlayers was monitored in real time by the FFT EIS (Fig. 28). EI spectra in Fig. 28 A indicates that the completion of the vesicle fusion may be accomplished within approximately 2000 s. The Bode plot transforms in a manner similar to the one observed in gold/thiolipid anchor electrode systems [43]. In particular, the Bode impedance phase curve develops minimum at around f = 4 Hz. The negative of the impedance phase at f_{min} is 58 degrees, which is considerably higher, compared to the minimum observed on gold supported tBLMs.

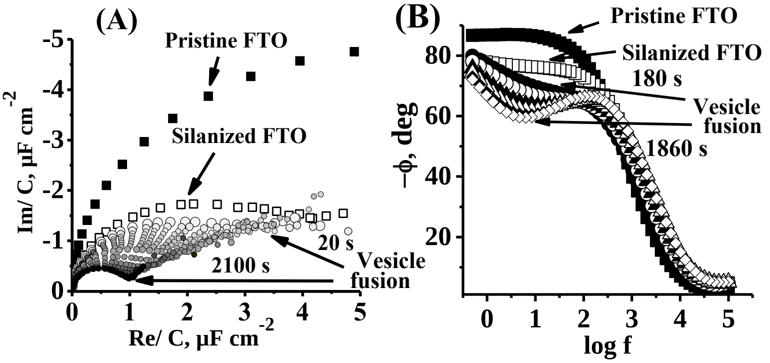

Fig. 28. EI spectra recorded using pristine, silanized and after vesicle fusion FTO electrodes, A – Cole – Cole plot, B – Bode plot.

While interaction of silanized FTO with vesicles always triggers EI spectral changes, however, the mode of the change strongly depends on the initial EI spectra of the substrate (Fig. 29). Generally, the EIS Cole – Cole plots of silanized FTO exhibits either single semicircular (Fig. 29 A and B) or double semicircular (Fig. 29 C) shape. According to the numerical analysis presented in ref [156], single semicirculars are observed for sparsely populated SAM anchors. hBLMs containing high number (per area) of defects should exhibit a single semicircular shape as it is seen in Fig. 29 A. Less defective hBLMs start developing a smaller semicircular feature in the high frequency end of the spectrum. Such development is observed in this work, too, (Fig. 29 B)[156]. Further decrease of the high frequency semicircular seen in Fig. 29 C attests for the formation a compact with low number of defects hBLMs [156]. Data in Fig. 29 provides diagnostic criteria for the formation of

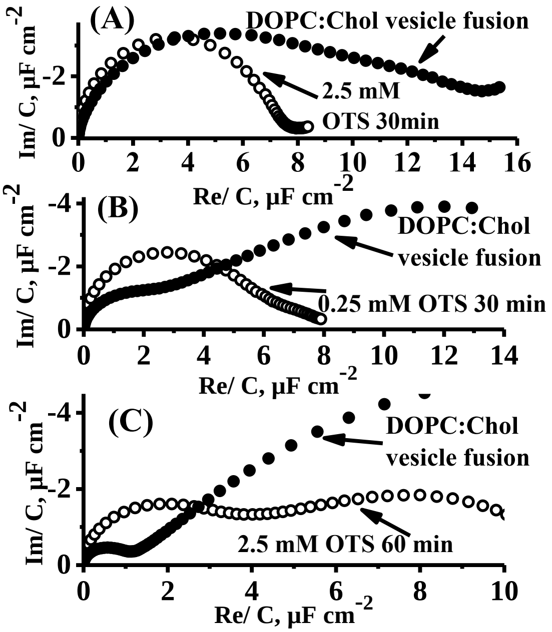

Fig. 29. Different shapes of EIS Cole - Cole spectra after vesicle fusion (filled circles) on differently silanized OTS SAMs (open circles).

the intact bilayers. In particular, double semicircular spectra of the anchor SAMs predict the formation of the intact lipid bilayer. Such spectra were consistently observed on FTO surfaces silanized for 60 min in 2.5 mM OTS solution. So, the silanization conditions are of upmost importance for the formation of intact hBLMs on silanized FTO.

Silanization of the FTO changes surface properties of the substrate. In particular, chemical bonds may alter surface electron distribution. Because FTO should exhibit n-type semiconductor properties [157], next experiment was carried out to see if silanization as well as the formation of the hBLMs affect the electronic properties of the electrode. First, the electric differential capacitance of the FTO at several bias potential values were recorded. The increase of the electrode potential causes gradual decrease of the diameter of semicircle (Fig. 30A). In the Mott – Schottky representation one observes almost linear line in the range from 0.1 to 1.1 V. The slope 0.027 cm^4 μF^{-2} V^{-1} of the Mott-Schottky plot (assuming $\varepsilon = 10$) yields charge density of $8.49 \cdot 10^{21}$ cm^{-3}.

Formation of the OTS monolayer and subsequent fusion of the vesicles results in sharp decrease of the capacitance semicircle (Fig. 30 B and C) as well as the increase of the slopes of the Mott – Schottki plots (Fig. 30 D) to

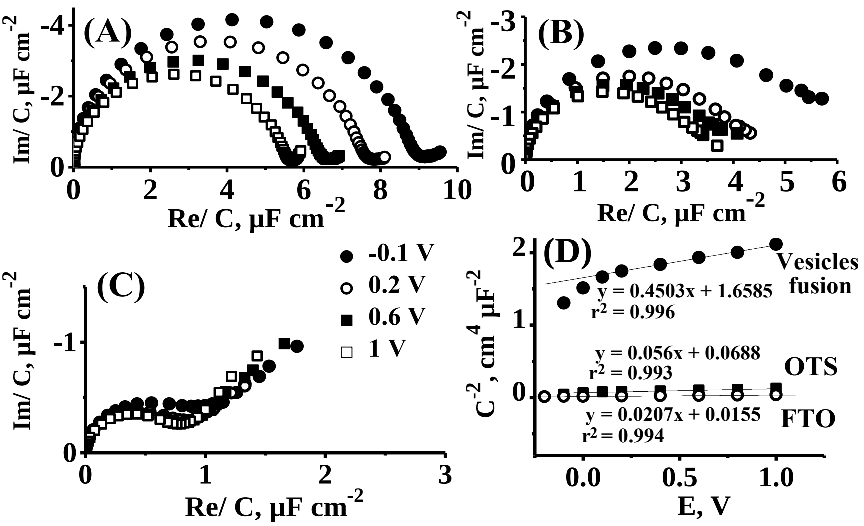

Fig. 30. EI spectra obtained at various potentials in Cole – Cole plot: A – using pristine FTO electrode, B – using FTO electrode after silanization with 2.5 mM OTS, C – using FTO electrode after vesicle fusion for 45 min, D – EI spectra in Mott – Schottky plot.

0.056 and 0.45 cm^4 μF^{-2} for OTS monolayer and hBLM correspondingly. Also, as follows from the data in Fig. 30 the apparent shift of the flat band potential (an extrapolated value of E at the limit $1/C^2 \rightarrow 0$) from ≈ - 0.75 V (pristine FTO) to - 1.23 V (silanized FTO) and to -3.69 V (silanized FTO with fused vesicles). These effects, however, are neither related to the change in the carrier concentration nor the change in the band structure of the FTO semiconductor. It is easy to demonstrate that both decrease of the Mott – Schottky slope and the apparent shift of the flat band potential is always expected when the surface of the semiconductor is covered by the layer of a dielectric with potential independent dielectric permittivity and thickness and correspondingly potential independent specific capacitance. The capacitance of these additional layers of dielectrics, in our case can be estimated using the following planar capacitor equations:

$$1/C_{FTO/OTS} = 1/C_{FTO} + 1/C_{OTS} \qquad (13)$$

$$1/C_{hBLM} = 1/C_{FTO/OTS} + 1/C_{PL} \qquad (14)$$

in which C_{FTO} is the capacitance of pristine FTO, C_{OTS} is the capacitance of the OTS monolayer and C_{PL} is the capacitance of the composite: OTS plus phospholipid layer atop of the FTO. From the experimental data (C_{FTO},

$C_{FTO/OTS}$ and C_{hBLM}) in Fig. 30, according to eqs. (13) and (14) we found the average values of C_{OTS} = 6.54 ± 0.15 µF cm^{-2} , while C_{PL} = 0.82 ± 0.10 µF cm^{-2}.

Calculated value of the C_{OTS} is significantly higher than the typical capacitance of the similar length octadecyl thiol monolayers on gold, ~1 µF cm^{-2} [158]. Quite likely, the capacitance C_{OTS} = 6.54 ± 0.15 µF cm^{-2} signals about a significant disorder in the OTS monolayer. Disorder affects both ε_{OTS} (typically increases due to a presence of polar molecules and trapped ions) and the dielectric thickness (typically decreases due to collapsed sites in monolayers). Both factors result in an increase of interfacial capacitance. Such effects are common in monolayers on gold, where higher than expected capacitances were frequently observed [155][159].

In contrast, the composite OTS/DOPC phospholipid bilayer exhibits C_{PL}, which is comparable to the capacitance of DOPC bilayers assembled on saturated alkane chain anchor compounds [155]. Assuming a relative dielectric constant 2.8 [160] for the bilayer one obtains from C_{PL} the effective thickness of the phospholipid bilayer to be 3.02 nm. This value is close to thickness of DOPC bilayers observed by the neutron reflectometry tBLMs on gold surfaces [43][155]. From these data, we conclude that the anchor monolayer of OTS is rather sparse, while near intact bilayer of DOPC is formed via vesicle fusion on FTO/OTS surface (Fig. 31).

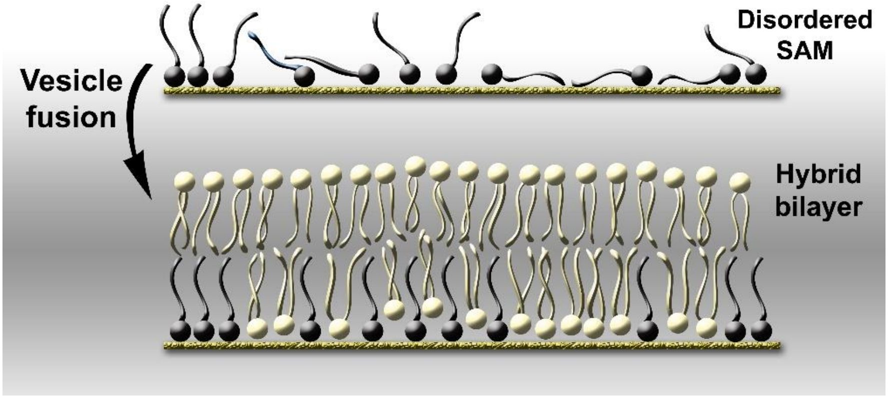

Fig. 31. Structure of hybrid phospholipid bilayer on FTO surface.

3.2.3. Hybrid phospholipid bilayer interaction with vaginolysin and phospholipase A_2

Biological relevance of hBLMs assembled on FTO was tested. As seen in Fig. 32, exposure of the DOPC/Chol hBLM to the solution containing pore-forming cholesterol-dependent protein, vaginolysin. This protein was shown [13] to trigger deterioration of the electrical insulation properties of tBLM.

The destruction of the tBLM manifested itself as a sharp increase of the semicircular part of the EI spectra and a significant shift of the ϕ_{min} characteristic point on the Bode phase vs frequency plot [50][161]. In the present study, any noticeable changes in the spectra were not observed (Fig. 32). This leads to a conclusion that the assembled bilayers on FTO/OTS exhibit limited biologically relevant fluidity, which prevents proper reconstitution of the membrane proteins. One of the main reasons, in our opinion, is the proximity of the inner phospholipid leaflet to a metal oxide surface. In this work, the membrane tethering anchor was OTS molecules which, in contrast to WH14, HC18 anchors [7][153], lack of hydrophilic spacer providing water filled 1-2 nm thick reservoir separating the bilayer from the surface.

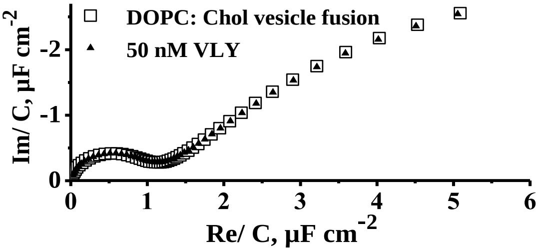

Fig. 32. Evolution of EI spectra in Cole – Cole plot in several surface modification steps: after vesicle fusion (rectangles) and immersion of 50 nM vaginolysin (triangles).

While not suitable for transmembrane protein reconstitution, the hBLMs on FTO/OTS may be used for studying membrane/protein interactions, when only distal leaflet of the phospholipid is involved. Proteins such as phospholipase A_2 interact with the outer leaflet of the bilayers, cleaving ester bond located at the second carbon atom in a glycerol backbone of the phospholipids. Fig. 33 summarizes the experiment in which cholesterol containing DOPC hBLMs on FTO/OTS anchor were exposed to a solution of the phospholipase A_2 (PLA2). Data in Fig. 33 clearly shows an effect of the PLA2 on the complex capacitance of the studied hBLMs. The semicircular part of the spectra starts increasing immediately after the PLA2 aliquot was added to the electrolyte bathing hBLMs. The effect occurs in a PLA2 concentration dependent manner, thus attesting interaction of the protein with the outer leaflet of the hBLM.

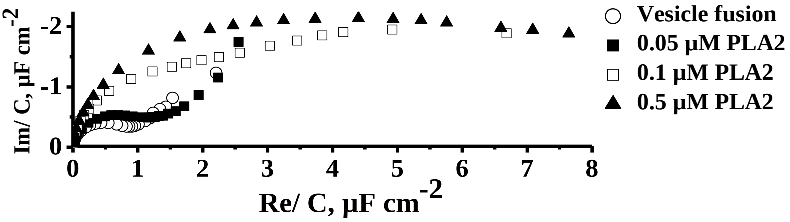

Fig. 33. EI spectra recorded using different concentration of phospholipase A_2 (PLA2) to disrupt DOPC/Chol (6:4) bilayer membrane.

3.2.4. Hybrid phospholipid bilayer regeneration on FTO

The regeneration of the hBLMs is a serious problem which impedes practical applications of hBLMs [155]. In particular, it was demonstrated that it is impossible to regenerate tBLMs assembled on gold achieving exactly the same EIS parameters [155]. In the current study, we show that FTO/OTS anchor monolayers retain their property to fuse vesicles after the repetitive washing of the self-assembled phospholipid bilayers. As we can see in Fig. 34, after several cycles of vesicle fusion Cole – Cole spectra semicircle radius restores to the same value in the course of vesicle fusion, thus indicating that bilayer was repetitively formed with the same electrical properties. Such effect, as mentioned, was not observed in gold/thiol systems [155]. The author demonstrated that the possible reason for the degradation of anchor monolayers maybe related to clustering of the anchor molecules in self-assembled SAM's due to their surface mobility. Most likely strong metal oxide silane bond in the OTS monolayer as well as the chemical/physical nature of the metal oxide surface precludes surface mobility thus ensuring long lasting structural and functional stability of the monolayers. Such property of the OTS anchors is quite beneficial in the context of the possibility to create phospholipid bilayer based biosensors [162].

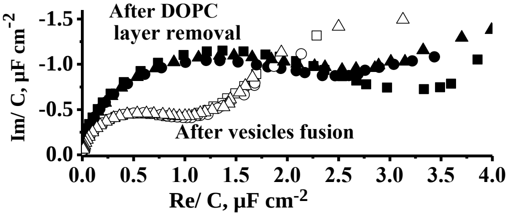

Fig. 34. EI spectra in Cole – Cole plot recorded over several cycles of vesicle fusion and washing off the phospholipid bilayer membrane.

3.3. Formation of mixed hybrid phospholipid bilayer on fluorine doped tin oxide

3.3.1. Formation of mixed self-assembled monolayer on FTO

In order to attest the hydrophobic properties and the effect of hydration of FTO surface, surface wetting characteristics – contact angles of non-hydrated and pre-hydrated FTO substrates (FTO-P1 and FTO-P2, respectively) were measured and compared to contact angles of FTO substrates silanized by the mixture of silanes (SAM-P1 and SAM-P2, respectively). Before silanization procedure pristine FTO-P1 surface exhibited hydrophilic properties reaching contact angle of 44° ± 8° (Fig. 35, white column-P1). However, overnight pre-incubation in water leads to formation of OH- groups on FTO-P2 surface increasing surface hydrophilic properties and decreasing CA values to 27° ± 6° (Fig. 35, white column-P2).

After silanization of FTO-P1 substrate with 100% OTS (SAM-P1), CA values increased to 124° ± 4° (Fig. 35, OTS:MTS 10:0). However, contact angles of silanized FTO-P1 surface decreased to 88° ± 2° (Fig. 35, OTS:MTS 0:10) with increasing concentration of short alkylchain MTS in silanization solution. Similar tendency in CA evolution was observed on gold electrodes when mixture of a spacer unit and long alkylchain thiols [10] was used. Taking into account that SAMs are hydrophobic enough for successful formation of phospholipid membrane when CA values are higher than 100° [10], we predict that FTO-P1 surfaces silanized with OTS:MTS 8:2 and 10:0 molar ratios are suitable for phospholipid membrane formation.

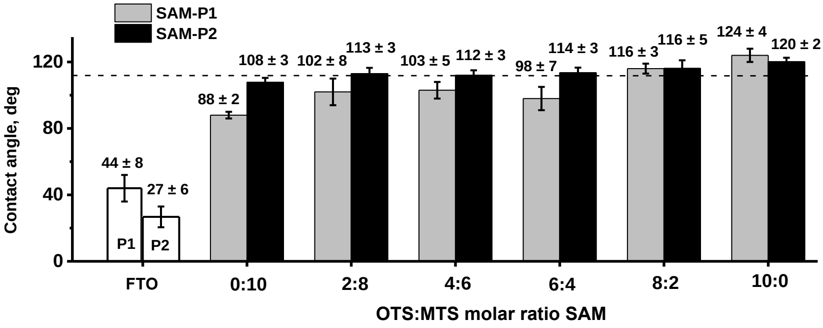

Fig. 35. Contact angle measurements of mixed OTS:MTS SAMs on FTO electrodes prepared accordingly to P1 and P2 protocols. Horizontal dashed line shows the threshold of contact angle value above which the vesicles fusion on SAMs would proceed until the formation.

Pre-incubation of FTO substrate in water prior to silanization significantly affects the contact angles of anchor SAMs. Similarly to P1 protocol, an increase in molar ratio of MTS results in decrease of contact angles of SAM-P2 from 120° ± 2° (Fig. 35, OTS:MTS 10:0) to 108° ± 3° (Fig. 35, OTS:MTS 0:10). These results indicate that more abundant hydroxylgroups on FTO-P2 substrate yields higher surface coverage with silane SAM because smaller and more active MTS spacer is available to react with OH- groups on FTO-P2 surface forming more homogeneous layers of mixed SAMs. Therefore, in contrast to FTO-P1 substrates, pre-incubated in water FTO-P2 substrates yielded higher than 100° values of CA (Fig. 35, SAM-P2) for all SAM-P2 samples. Further experiments showed that the contact angle at or above 113º ± 3º (Fig. 35, horizontal dashed line) is a convenient predictor of facile phospholipid membrane formation.

While CA measurements showed dependence of mixed self-assembled monolayers composition on surface hydrophobicity the electrochemical properties of mixed SAMs as well as phospholipid bilayers on FTO surfaces were evaluated by using the method of the electrochemical impedance spectroscopy. It is seen in Fig. 36 that the complex capacitance plots exhibit semicircular shape typical for ideally polarizable interphases exhibiting near ideal capacitive behaviour [163]. The capacitance of a bare FTO-P1 surface before silanization as established earlier is equal to 8.8 ± 0.3 μF cm^{-2}. It was observed that complex capacitance of bare FTO-P2 was the same as FTO-P1 (~9 μF cm^{-2}). It follows from data in Fig. 36, that silanization of the FTO surface leads to complex capacitance decrease for all OTS:MTS molar ratios SAMs-P1 and SAMs-P2. However, an increase of the molar ratio of MTS from 0 to 100% in OTS:MTS silanization solution (for SAM-P1 preparation) causes increase of complex capacitances from 3.4 ± 0.9 μF cm^{-2} (Fig. 36, F open circles) to 6.6 ± 0.7 μF cm^{-2} (Fig. 36, A open circles). This result

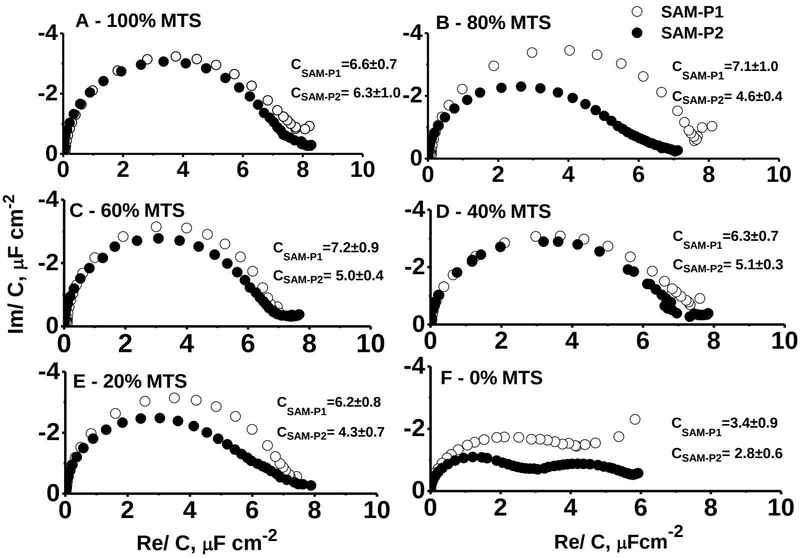

Fig. 36. EIS Cole – Cole plots of FTO electrodes after functionalization with mixed OTS:MTS SAMs prepared accordingly to P1 and P2 protocols. Molar ratios of OTS:MTS in silanization solutions: A – 0:10, B – 2:8, C – 4:6, D – 6:4, E – 8:2, F – 10:0. Insets – values of complex capacitances after SAM formation in μF cm^{-2} units. Bias potential 0 V vs Ag/AgCl, NaCl$_{sat}$ electrode.

indicates that the average thickness of a dielectric layer of mixed self-assembled monolayers can be regulated by simply adjusting molar ratios of OTS (anchors) and MTS (backfillers) in silanization solutions [7].

After silanization of pre-hydrated FTO-P2 surface with 100% MTS SAM-P2 complex capacitance reached the value of 6.3 ± 1 μF cm^{-2} (Fig. 36 A, filled circles) which is comparable to 6.6 ± 0.7 μF cm^{-2} obtained for 100% MTS SAM-P1 (Fig. 36 A, open circles). However, an increase of OTS amount in OTS:MTS silanization solution (SAM-P2) lead to more significant complex capacitance decrease reaching the lowest value of 2.8 ± 0.6 μF cm^{-2} for 100% OTS SAM-P2 (Fig. 36 E, filled circles).

The straightforward comparison between SAM-P1 and SAM-P2 could be observed in Fig. 37. It can be seen that complex capacitance for SAM-P2 (Fig. 37, black columns) is consistently lower than for SAM-P1 at every OTS:MTS SAM composition. Even though significant capacitance data scatter occurs, it was found that the complex capacitance below 6.2 μF cm^{-2} can provide suitable substrate for phospholipid membrane formation (Fig. 37, horizontal dashed line).

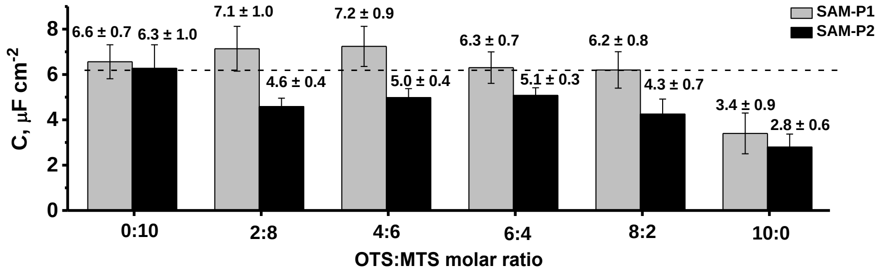

Fig. 37. Complex capacitance values derrived from EI spectra: after SAM-P1 and SAM-P2 formation. Horizontal dashed line indicates the threshold of the complex capacitance value below which vesicles fusion leads to a formation of intact mhBLMs.

3.3.2. Formation of mixed hybrid phospholipid bilayer on FTO

Lipid membrane formation by vesicle fusion on FTO surfaces modified with mixed OTS:MTS SAM-P1 and SAM-P2 leads to a complex capacitance changes dependent on anchor/backfiller molecular ratios (Fig. 38). EIS derived complex capacitance values for SAM-P1 substrates indicate that electrically insulating mhBLMs were formed only on SAMs obtained from depositions solutions containing 0 - 20% of MTS back-filler (Fig. 38 E and F, open circles). Further dilution of OTS by MTS causes significant increase in complex capacitances (Fig. 38 A-D, open circles) indicating a presence of a highly defective bilayer with significant portion of the surface free of phospholipids [156].

On the contrary, the pre-hydrated FTO substrates lead to a formation of mhBLMs on SAM-P2 substrates containing up to 80% of MTS back-filler (Fig. 38, filled circles). Complex capacitance values in the range from 1.1 ± 0.1 μF cm^{-2} to 0.8 ± 0.1 μF cm^{-2} (Fig. 38, filled circles) are comparable to those obtained on Au [155] or Ti [17][164] thus, indicate successful vesicle fusion and lipid layer formation. Fig. 39 clearly illustrates significant differences in properties of mhBLMs obtained on pre-hydrated and non-hydrated FTO substrates. After membrane formation on SAM-P2 (Fig. 39, black columns) major decrease in complex capacitance values was observed compared to the values for membranes formed on SAM-P1 substrates (Fig. 39, grey columns). Similar observation was made using cyclic voltammetry method, when CV data confirmed blockage of the direct electron transfer from the redox species to and from the electrode (Fig. 40,Fig. 41).

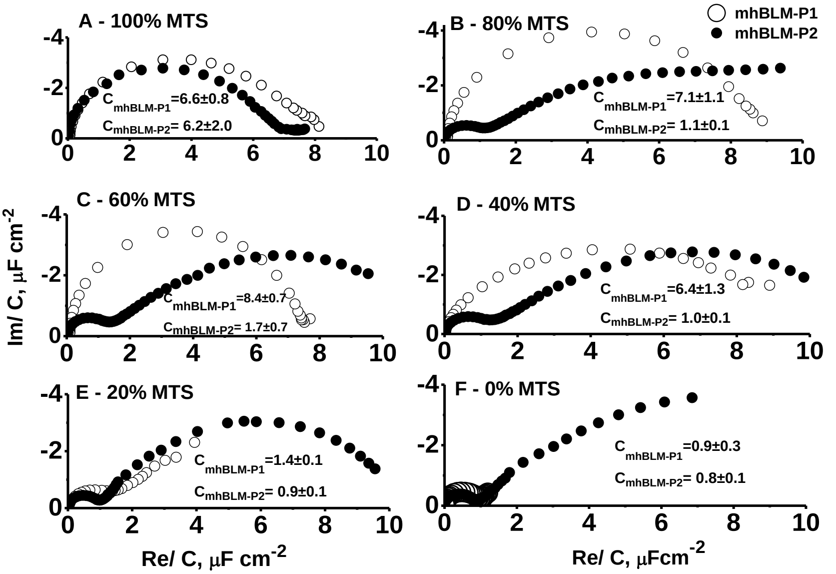

Fig. 38. EIS Cole – Cole plots of FTO electrodes after 1 h incubation of mixed OTS:MTS SAMs (prepared accordingly to P1 and P2 protocols) in DOPC/Chol 6:4 vesicle solution (open circles). Molar ratios of OTS:MTS in silanization solutions: A – 0:10, B – 2:8, C – 4:6, D – 6:4, E – 8:2, F – 10:0. Insets – values of complex capacitances after mhBLM formation in μF cm^{-2} units. Bias potential 0 V vs Ag/AgCl, $NaCl_{sat}$ electrode.

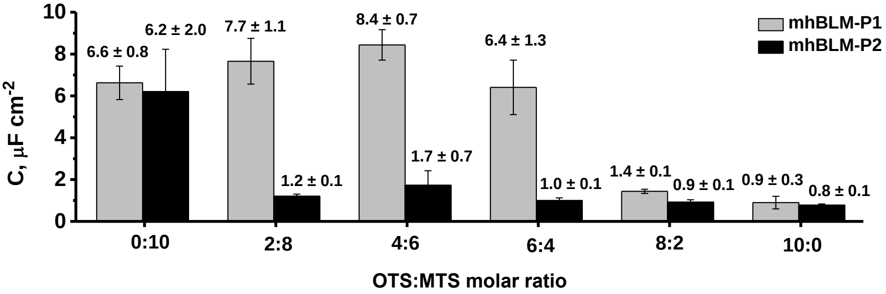

Fig. 39. Complex capacitance values derived from EI spectra after DOPC/Chol 6:4 vesicle fusion on pre-hydrated and non-hydrated FTO substrates (mhBLM-P2 and mhBLM-P1, respectively).

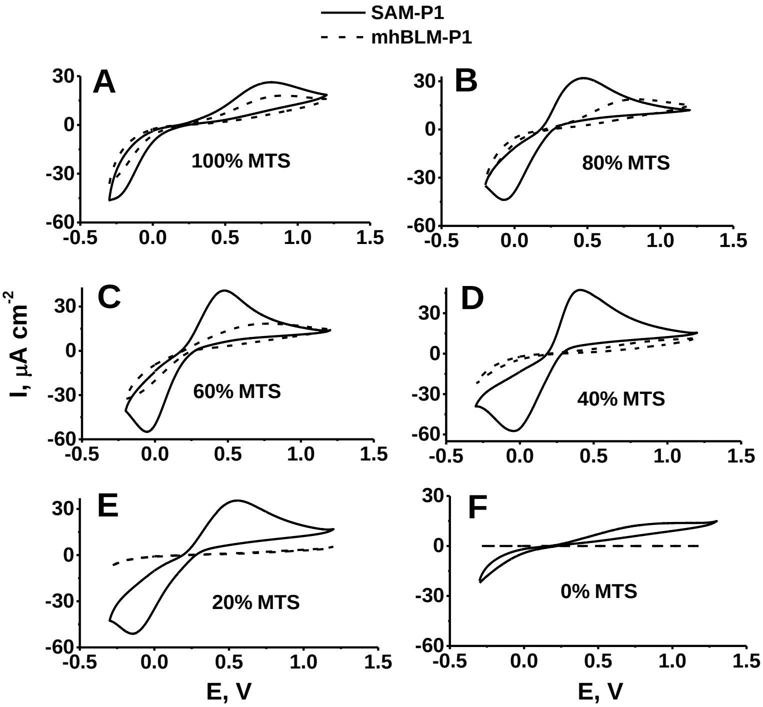

Fig. 40. Cyclic voltammograms recorded in 1 mM $K_4(Fe(CN)_6)$ and $K_3(Fe(CN)_6)$ solution (in PBS pH 7.1) using FTO electrode after mixed silane SAM-P1 formation (continuous line) in solution containing different OTS:MTS molar ratios: A – 0:10, B – 2:8, C – 4:6, D – 6:4, E – 8:2, F – 10:0 and after DOPC/Chol 6:4 vesicle fusion (dashed line). Potentials are in reference to Ag/AgCl, $NaCl_{sat}$ electrode.

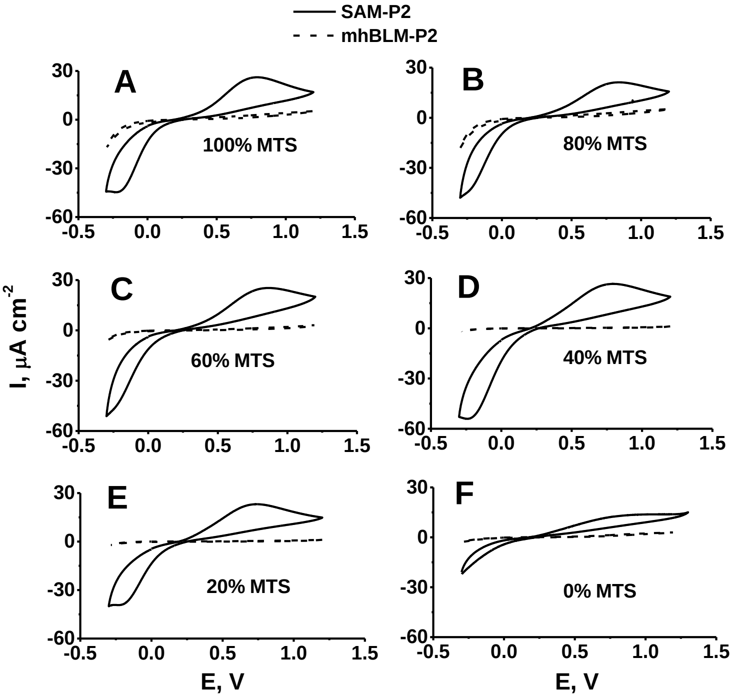

Fig. 41. Cyclic voltammograms recorded in 1 mM $K_4(Fe(CN)_6)$ and $K_3(Fe(CN)_6)$ solution (in PBS pH 7.1) using FTO electrode after mixed silane SAM-P2 formation (continuous line) in solution containing different OTS:MTS molar ratios: A – 0:10, B – 2:8, C – 4:6, , D – 6:4, E – 8:2, F – 10:0 and after DOPC/Chol 6:4 vesicle fusion (dashed line). Potentials are in reference to Ag/AgCl, $NaCl_{sat}$ electrode.

3.3.3. Mixed hybrid phospholipid bilayer interaction with melittin and α-hemolysin

As follows from the complex capacitance values of mhBLM-P1 and mhBLM-P2 (Fig. 38, Fig. 39), successful vesicle fusion process was observed for SAM-P1 containing 0 - 20% of MTS back-filler and for SAM-P2 containing up to 80% of MTS back-filler. Therefore, biological relevance of these mhBLMs was tested by their interaction with 100 nM of melittin first. Melittin is a cationic amphiphilic peptide that consists of 26 amino acids. It is found in honey bee (Apis mellifera) venom and it is the main pain producing ingredient [133]. Each peptide consists of two α-helixes that are connected at amino acid positions 10-12, which results in a bent conformation [165]. At the lipid-liquid interface melittin peptides act as surfactants because of their amphiphilic nature and lower surface tension [166]. Then peptides easily oligomerize into tetramer and form transmembrane channels inside plasma membrane which lead to lysis of the cell [167].

Fig. 42 shows the capacitance changes upon interaction of DOPC/Chol 6:4 mhBLMs on 20% MTS SAM-P1 with 100 nM melittin. After 90 min of exposure to the toxin, complex capacitance increased from 0.9 μF cm^{-2} to 1.6 μF cm^{-2} as observed in the Cole – Cole plot (Fig. 42 B), while the Bode plot (Fig. 42 B) shows noticeable shift of phase minimum towards higher frequencies. Similar changes are predicted by the theoretical model of impedance response of tethered bilayer membranes in the presence of a water filled pores [146]. On the contrary, 90 min interaction of mhBLM on 100% OTS SAM-P1 with 100 nM melittin did not reveal noticeable complex capacitance change (Fig. 42 A). In Bode plot (Fig. 42 A) phase shift is noticeable, although it is relatively small compared to the shift observed for mhBLMs formed on 20% MTS SAM-P1 (Fig. 42 B). Then, negative control experiments were carried out to see if membrane incubation in PBS pH 7.1 (without melittin) does not cause any instability of membrane. As it can be seen from Fig. 43, EIS spectra of mhBLMs remain unchanged over 1 h period suggesting that the observed in Fig. 42 membrane disruption is caused by the interaction with melittin.

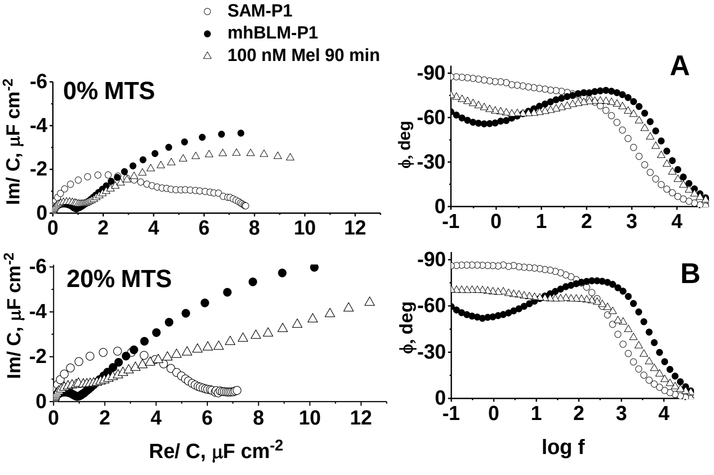

Fig. 42. EI spectra in Cole – Cole and Bode plot recorded after: SAM-P1 formation (open circles) in solution containing different OTS:MTS molar ratios: A – 0:10, B – 2:8; after DOPC/Chol 6:4 membrane formation (filled circles) and after 90 min interaction with with 100 nM melittin (open triangles). Bias potential 0 V vs Ag/AgCl, NaClsat electrode.

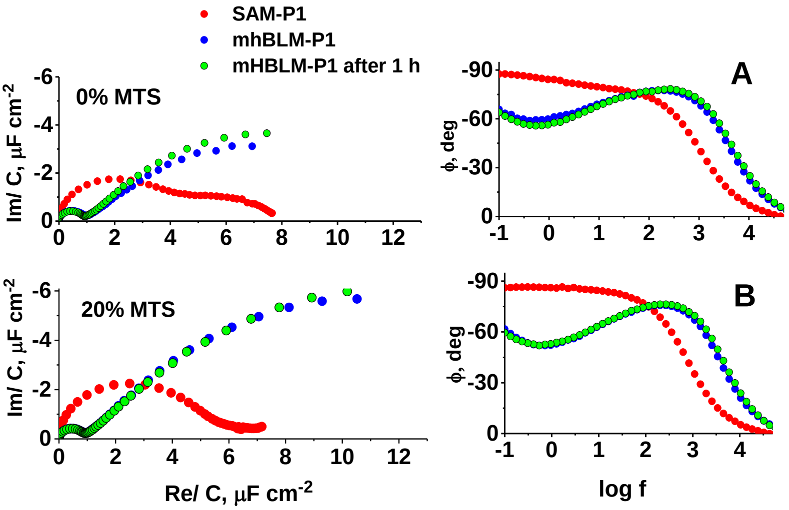

Fig. 43. EI spectra in Cole – Cole and Bode plot recorded after: SAM-P1 formation (red circles) in solution containing different OTS:MTS molar ratios: A – 0:10, B – 2:8, C – 4:6, D – 6:4, E – 8:2; after DOPC/Chol 6:4 membrane formation (blue circles) and after membrane was incubated in PBS pH 7.1 for 1 h (green circles). Bias potential 0 V *vs* Ag/AgCl, NaCl$_{sat}$ electrode.

Next, DOPC/Chol 6:4 mhBLM on 20% MTS SAM-P1 were probed with 500 α-hemolysin toxin (Fig. 44). In first 30 min the effext of α-hemolysin was not observed, however, after 24 hours a clear response was obtained, and complex capacitance value increased from 1.4 to 2 μF cm^{-2} (Fig. 44 A and B). Such long response time is unusual for phospholipid membranes systems. Frequently it is up to 30 min [168]. However, these moderate capacitive changes could not be attributed to membrane self-disruption, because formed BLM over long period of time (24 h) in PBS at atmospheric conditions does not change the properties of the bilayer (Fig. 44 C and D). In Fig. 44 presented membrane interaction with αhl indicates that the acquired membrane still does not possess enough ionic reservoir for protein to permeate the membrane.

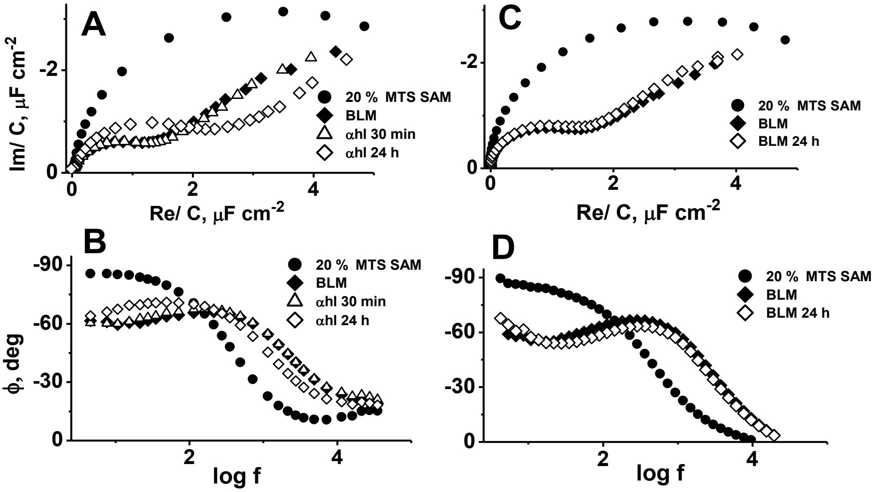

Fig. 44. EI spectra in Cole – Cole and Bode plot: bilayer membrane on OTS:MTS 8:2 molar ratio SAM after interaction with 500 nM α-hemolysin in Cole Cole plot (A), in Bode plot (B), bilayer on OTS:MTS 8:2 molar ratio SAM, recorded after 1 h of vesicle fusion and after 24 h in Cole – Cole plot (C), in Bode plot (D).

Fig. 45 shows interaction of vesicles DOPC/Chol 6:4 fused on 80%, 60%, 40%, 20% MTS and 100% OTS SAM-P2 with 100 nM melittin. DOPC/Chol 6:4 membranes on 100% OTS SAM-P2 (Fig. 45 A), similarly as membranes on 100% OTS SAM-P1 (Fig. 42 A), when challenged with 100 nM melittin exhibited relatively slight increase in capacitance in Cole – Cole plot (Fig. 45 A) and a relatively small shift of the phase minimum in Bode plot plots (Fig. 45 A). Dilution of molecular anchor with 20% - 80% MTS resulted in significantly more pronounced effects of 100 nM melittin on complex capacitance (Fig. 45 B-E) and phase shifts in Bode plot (Fig. 45 B-E). For 60% and 80% MTS SAM-P2 anchors (Fig. 45 D and E), the phase minimums became non-distinguishable, indicating significant number of defects produced upon incubation with 100 nM melittin. Control experiments (Fig. 46) showed that mixed hybrid membranes are stable for time period of 1 h and more, suggesting that observed membrane disruptions (Fig. 45) are caused by reconstitution of melittin. Hypothetical schemes representing melittin reconstitution into DOPC/Chol 6:4 membrane on SAM-P1 and SAM-P2 are shown in Fig. 47.

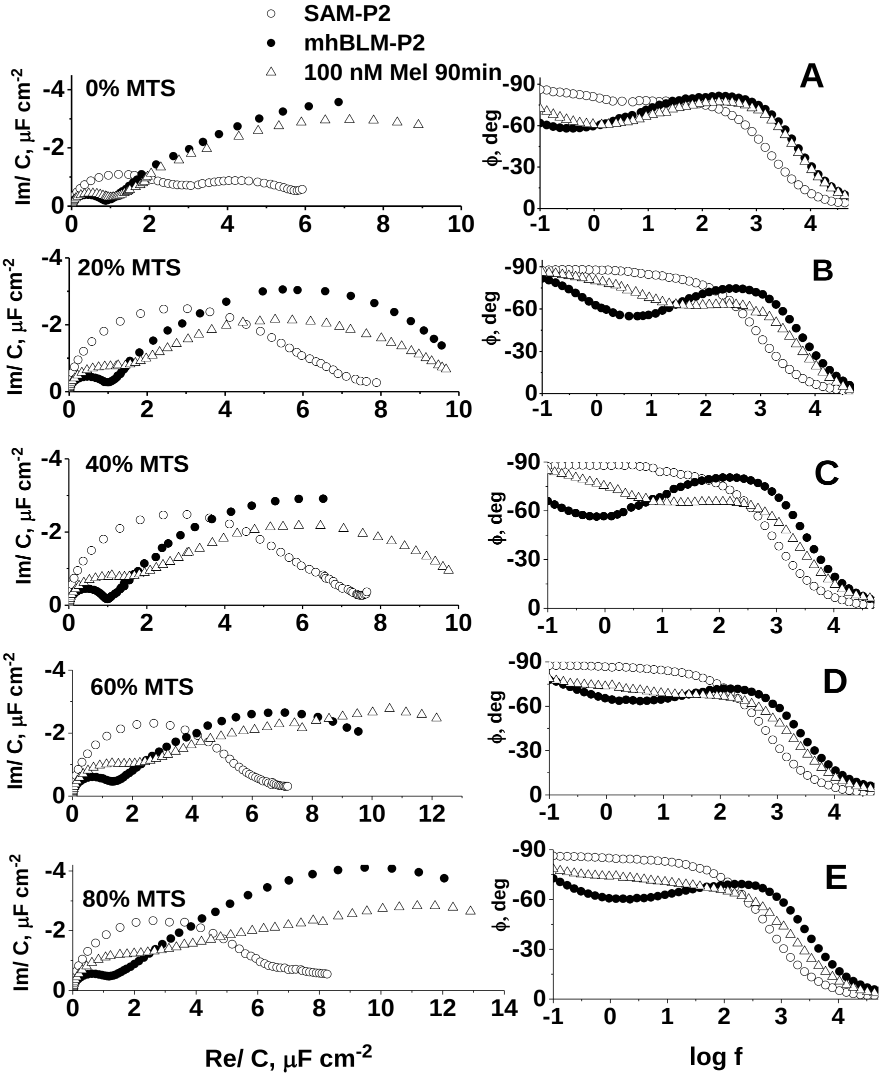

Fig. 45. EI spectra in Cole – Cole and Bode plot recorded after: SAM-P2 formation (open circles) in solution containing different OTS:MTS molar ratios: A – 0:10, B – 2:8, C – 4:6, D – 6:4, E – 8:2; after DOPC/Chol 6:4 membrane formation (filled circles) and after 90 min interaction with 100 nM melittin (open triangles). Bias potential 0 V *vs* Ag/AgCl, $NaCl_{sat}$ electrode.

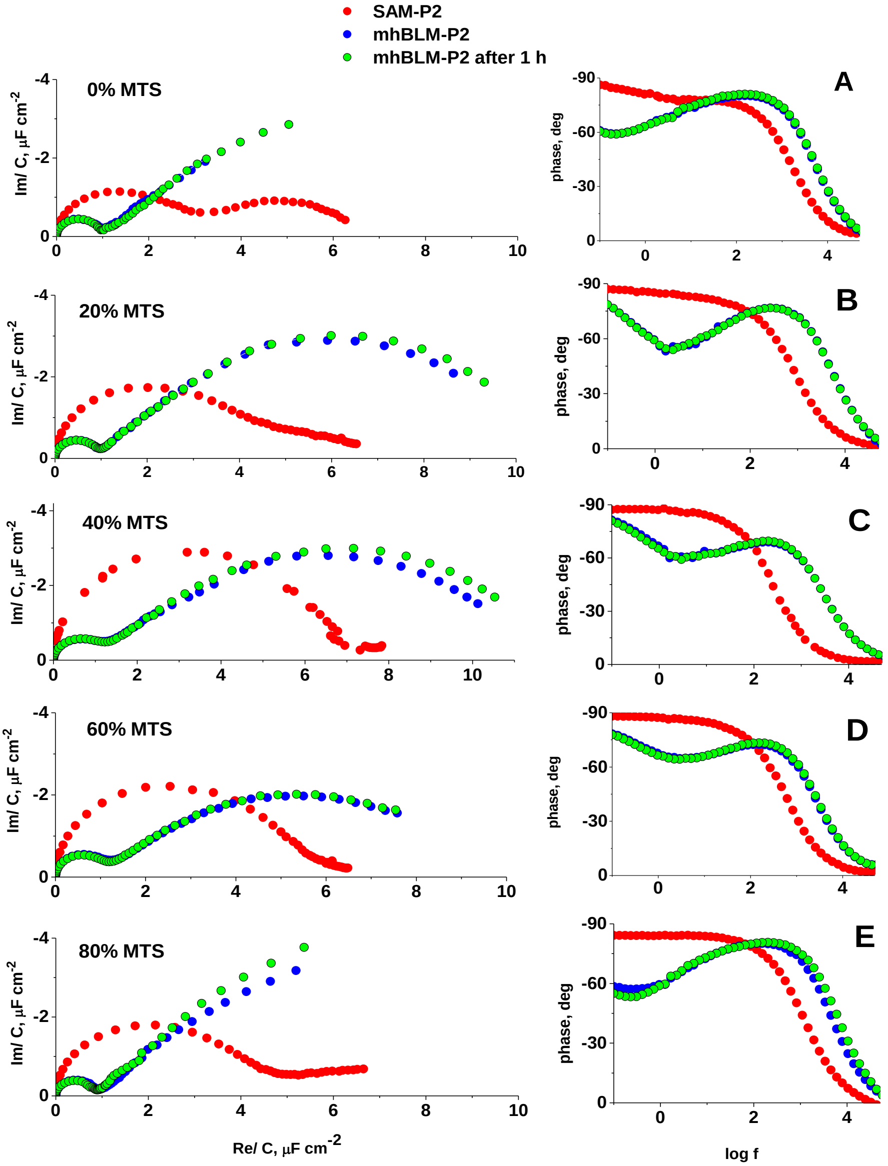

Fig. 46. EI spectra in Cole – Cole and Bode plot recorded after: SAM-P2 formation (red circles) in solution containing different OTS:MTS molar ratios: A – 0:10, B – 2:8, C – 4:6, D – 6:4, E – 8:2; after DOPC/Chol 6:4 membrane formation (blue circles) and after membrane was incubated in PBS pH 7.1 for 1 h (green circles). Bias potential 0 V *vs* Ag/AgCl, NaCl$_{sat}$ electrode.

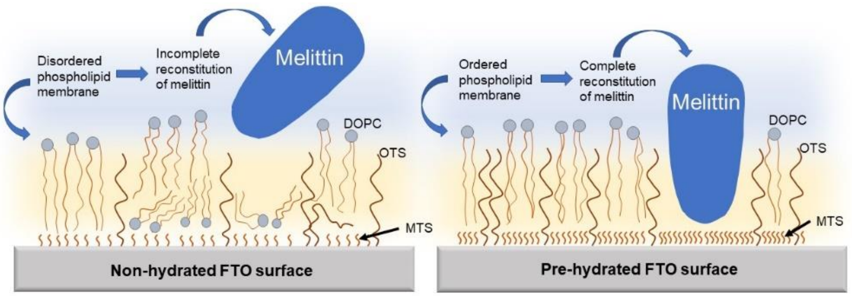

Fig. 47. Schematic representation of melittin interaction with phospholipid bilayer on OTS:MTS mixed SAM formed on non-hydrated and pre-hydrated FTO.

3.3.4. Regeneration of mixed hybrid phospholipid bilayer

Finally, the possibility of membrane regeneration was tested on OTS:MTS (8:2) SAM-P2. Vesicles were fused on mixed silane monolayer and then the lipid layer was rinsed off using deionized water and isopropanol 1:1 solution.

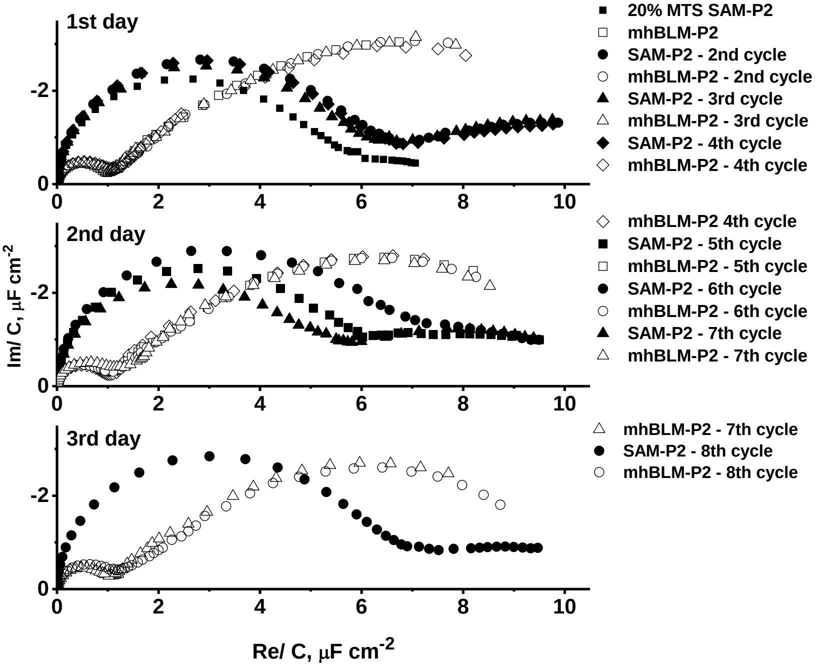

Fig. 48. EI spectra in Cole - Cole plot recorded over 3 days several cycles of vesicles fusion and washing off the phospholipid bilayer membrane on OTS:MTS (8:2) SAM-P2. Bias potential 0 V *vs* Ag/AgCl, $NaCl_{sat}$ electrode.

The cycles were repeated 8 times for the period of 3 days. After every membrane formation-washing off cycle EI spectra were recorded (Fig. 48). Each time the phospholipid membrane was formed, the capacitance decreased to values approximately of 1 μF cm^{-2}. After the removal of lipid layer, the complex capacitance restored to values slightly above the initial capacitance of the SAM. Nevertheless, membranes that were repeatedly formed over several cycles of fusion/rinsing exhibit similar electrical and functional properties, suggesting the same sample could be re-used for several experiments. This finding provides certain advantage over tethered phospholipid membranes on gold/thiol system, where functional properties of anchor SAMs were shown to degrade after similar formation/rinsing cycles [155].

3.4. Formation of tethered phospholipid bilayer on fluorine doped tin oxide

3.4.1. Synthesis of trichloro(3-(octadecylthio)propyl)silane

The molecular structure of TOPS and the presence of residual ATS in the reaction mixture were verified by ^1H and ^{13}C NMR spectroscopy (Fig. 49-43). The presence of ATS residue in synthesis product mixture TOPS:ATS is beneficial for the preparation of the molecular anchor SAM for the tethered phospholipid bilayers. In order to produce sparsely tethered tBLM, SAM should contain both long (at least C20 chain, in this study - TOPS) and short alkylchain (ATS) molecular anchors. While longer molecular anchors actually bind the phospholipid bilayer to solid support, short (1C – 3C chain) molecular anchors act as spacers to dilute the amount of long anchors on the surface and to provide space for the formation of the submembrane water reservoir. By adding ODT and ATS at molar ratio 1:2 during synthesis, theoretically, half of ATS should react with ODT and half of ATS should be left after the synthesis as residue (Fig. 14). Previous study [147] showed that click reaction under certain conditions can reach 98% conversion rate. This supports our anticipation, that synthesised TOPS and residue of ATS should be at molar ratio 1:1 after the synthesis. Remaining ATS would act as a spacer during lipid bilayer formation.

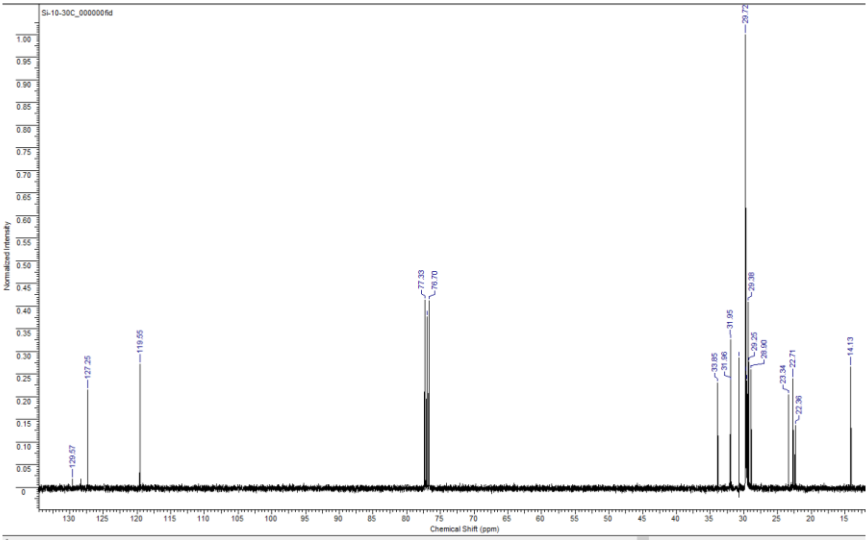

Fig. 49. ^{13}C NMR spectrum of reaction products (in $CDCl_3$). ^{13}C NMR spectrum (δ, ppm): 14.13 (CH_3); 22.36; 22.71; 23.34; 32.11; 28.90; 29.25; 29.38; 29.54; 29.62; 29.66; 29.68; 29.72; 30.71; 31,95; 31.96; 33.85; 119.55; 127.25; 128.33; 129.57.

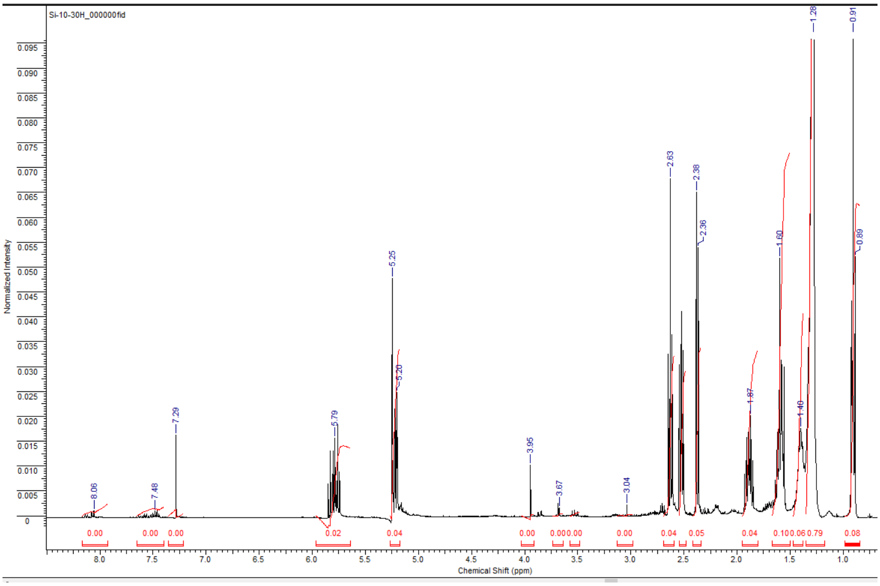

Fig. 50. ^{1}H NMR spectrum of reaction products (in $CDCl_3$). ^{1}H NMR spectrum (δ, ppm): 0.91 (3H, CH_3, t, J = 7 Hz), 1.23-1.34 (30 H, 15 CH_2 , m), 1.40 (2H, CH_2, t, J = 8 Hz), 1.53 (2H, CH_2, m), 1.60 (2H, CH_2, t, J = 8 Hz), 1.85-1.93 (2H, m), 2.37 (2H, d, J = 7, CH_2 signal from ATS residue), 2.53 (2H, CH_2, t, J = 8 Hz), 5.20-5.25 (2H, m, $H_2C=$ signal from ATS residue), 5.74-5.85 (1H, m, =CH- signal from ATS residue), 7.44-7.65 and 8.06-8.14 (trace aromatic protons signals from DMPA).

3.4.2. Formation of trichloro(3-(octadecylthio)propyl)silane self-assembled monolayer and tethered phospholipid bilayer on FTO electrode

Silanization of the FTO electrode by a mixture of TOPS and ATS resulted in contact angles at or above 113° ± 3°. Such high contact angles signal about the formation of hydrophobic layer on oxide surface, which now is expected to fuse of multilamellar vesicles [43] and form phospholipid bilayers as on FTO surface modified by OTS. Fig. 51 displays typical EIS curves of TOPS:ATS silane SAM and fused phospholipid bilayers of 100% DOPC and DOPC/Chol 6:4 (molar ratio), mixture of DOPC and cholesterol.

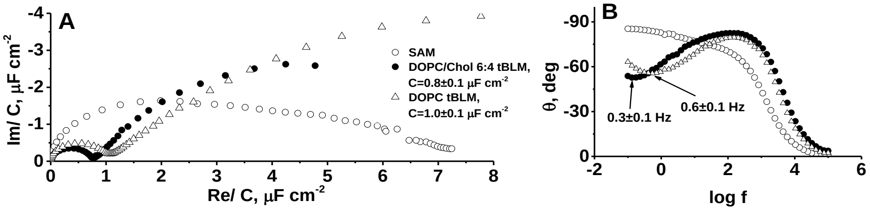

Fig. 51. EIS Cole – Cole (A) and Bode (B) plots of the FTO electrodes after formation of TOPS:ATS SAM (open circles), DOPC/Chol 6:4 tBLM (filled circles) and DOPC tBLM (open triangles). Arrows in Bode plot indicate average phase minimum frequency. Bias potential 0 V *vs* Ag/AgCl, $NaCl_{sat.}$ electrode.

EIS curves in Cole - Cole plot of TOPS:ATS silanized FTO surfaces exhibit shapes of highly depressed semicircles or a combination of several semicircles (Fig. 51 A, open circles) with the low frequency part of the line converging towards Re C → 8.8 ± 0.3 μF cm^{-2} , a value observed for bare FTO. Such shapes are typical for highly heterogeneous surfaces partly covered by an insulating layer separated from the electrode surface by a thin layer of an electrolyte [156]. Vesicle fusion produces additional layer of insulator – the phospholipid bilayer. This is reflected in the EIS spectra Cole – Cole plot as the appearance of a small semicircular feature in the high frequency range (Fig. 51). The schematic representation of formed tBLMS on FTO surface can be seen in Fig. 52. The diameter of the semicircle approximately equals to a capacitance of the bilayer, which in case of DOPC/Chol 6:4 and pure DOPC systems were 0.8 ± 0.1 μF cm^{-2} and 1.0 ± 0.1 μF cm^{-2} respectively. These values are in line with similar composition tBLMs observed on gold supported substrates [7]. The addition of cholesterol to DOPC bilayer consistently reduced the capacitance of tBLMs, which was previously observed [150].

The Cole-Cole plots of tBLMs exhibit quite significant low frequency "tails" which attest for the presence of defects in bilayers [156]. The length of the tail is proportional to the density of defects. As it is seen in Fig. 51 A, the cholesterol loaded bilayers indicated consistently shorter tails, and thus, signalling of destabilizing role of cholesterol on defects requiring high curvature bilayer edges. The cone-shaped cholesterol makes such edges unstable, and thus, decreasing density of defects in tBLMs [150]. Similar conclusion can be drawn from the Bode phase plots in Fig. 51 B. As it was shown in ref. [145], the position of the negative of impedance phase minima on the frequency scale is directly proportional to the defect density. The plots in Fig. 51 B clearly show that the minimum of the phase in the presence of cholesterol occurs at 0.3 Hz, while pure DOPC tBLMs showed consistently higher values, in this case 0.6 Hz. Importantly, the appearance of the phase minimum in Bode plots is consistent with the presence of ionic reservoir between the solid support and the lipid bilayer [145].

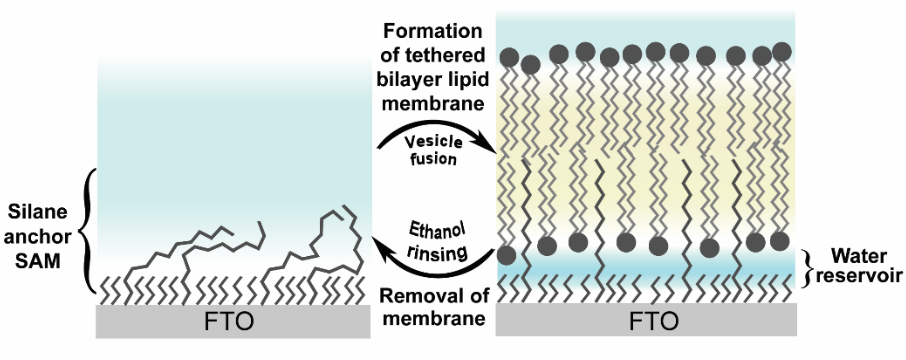

Fig. 52. Structure of tethered bilayer lipid membrane on FTO surface.

3.4.3. Tethered phospholipid bilayer interaction with melittin and α-hemolysin

DOPC/Chol 6:4 and DOPC tBLMs biological relevancy was tested using 50 nM and 100 nM melittin toxin (2,8 kDa) (Fig. 53). It is known that cholesterol inhibits melittin activity, therefore, two compositions of lipid membrane were tested: with cholesterol (DOPC/Chol 6:4) and without cholesterol (DOPC). As expected, increase of complex capacitance in Cole – Cole plot (Fig. 53 A) and the phase minimum shift towards higher frequencies

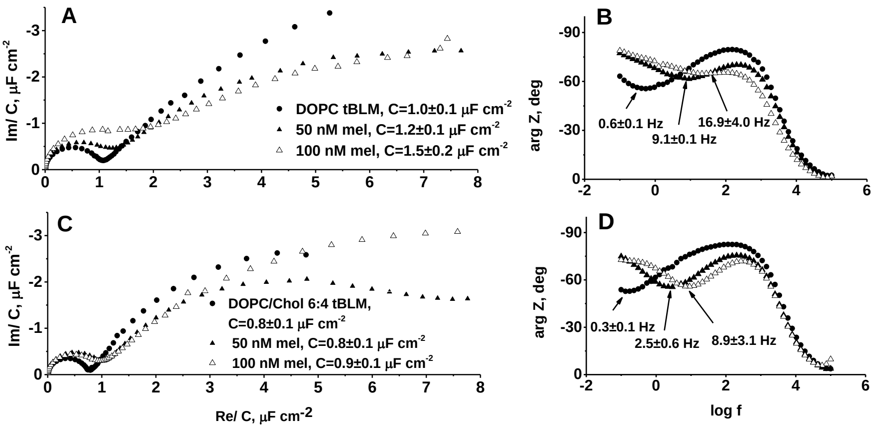

Fig. 53. EIS Cole – Cole (A, C) and Bode (B, D) plots obtained before and after 60 min interaction of 50 nM and 100 nM melittin with DOPC/Chol 6:4 (A, B) and with DOPC (C, D) tBLMs. Arrows in B and D indicate average phase minimum frequency. Bias potential 0 V *vs* Ag/AgCl, NaCl$_{sat.}$ electrode.

in Bode plot [145] (Fig. 53 B) were observed, indicating that melittin disrupted tBLMs without cholesterol (DOPC). However, the existence of cholesterol in tBLMs (DOPC/Chol 6:4) inhibited the activity of melittin because the increase of complex capacitance (Fig. 53 C) and the phase minimum shift towards higher frequencies in Bode plot (Fig. 53 D) was significantly reduced as compared to tBLMs without cholesterol.

To test if tBLMs are suitable for functional reconstitution of transmembrane proteins formed tBLMs were exposed to α-hemolysin (33 kDa) toxin from Staphylococcus aureus. Even though the toxin is not strictly dependent on cholesterol, the latter accelerates damage of cell membranes [141]. Therefore, two compositions of the phospholipid membranes were tested as in the previous case: with cholesterol (DOPC/Chol 6:4) and without cholesterol (DOPC). The data is presented in Fig. 54. Upon the exposure to 10 nM, 50 nM and 100 nM α-hemolysin solutions the complex capacitance, as witnessed by the diameter of the high frequency semicircular part of the EIS spectra, slightly increased from 0.8 to 0.9 µF cm^{-2} in case of DOPC/Chol 6:4 tBLM (Fig. 54 A). It remains almost constant in case of pure DOPC membrane (Fig. 54 C). Small alterations of capacitance in both cases are indicative of interaction between α-hemolysin and bilayers. However, these interactions result in relatively minor changes of the dielectric constant, which signals about relatively small amount of protein inserted into the membranes.

Quite different picture is revealed by the Bode plots (Fig. 54 B and D). Even though the dielectric properties of the membranes remain mostly unchanged, the negative of impedance phase minimum shifts considerably towards higher frequencies in case of DOPC/Chol 6:4 tBLM composition (Fig. 54 B). While in the absence of cholesterol no shift was observed (Fig. 54 D). Importantly, the phase minimum shift occurred in a concentration dependent manner, it showed signs of saturation at 100 nM concentration of α-hemolysin. Such phase minimum shifts are indicative of the formation of ion conducting pores in phospholipid bilayer [145], and can be used for quantitative estimate of the toxin-induced defect density. However, for such estimate the value of the specific resistance of the submembrane [146] and the type of defect density distribution [169] must be known. The specific resistance of the submembrane space of tBLMs on silane anchor SAMs at the moment is not known. However, some information about the distribution of density of α-hemolysin pores in membranes can be obtained from EIS Bode phase plot in Fig. 54 B.

It is known that α-hemolysin forms relatively small 1-1.5 nm diameter ion pores [170]. In such case, the value of the negative of the impedance phase minimum exhibits values of -arg Z $\approx 40^{o}$ if membrane defects are distributed randomly across the surface of tBLMs [171]. In case of formation of clusters of pores [169] in tBLMs -arg Z > 40^{o}. As seen from Fig. 54 B, at 10 nM α-hemolysin, -arg Z $\approx 45^{o}$, which indicates cluster formation. The increase of α-hemolysin concentration to 50 and 100 nM results in a sharp increase of the phase minimum to -arg Z $\approx 55^{o}$. Such significant increase can only be explained by the growth of cluster size and density of pores therein. Also, the upward shift of the negative of impedance phase can be expected in case of defect size increase [146][145][169][171]. Because α-hemolysin pores have a fixed size it is quite unlikely to expect α-hemolysin pore in tBLM with the diameter bigger than 1.5 nm. Nevertheless if clustered pore are close to each other like in a close-packed hexagonal array, the electrochemical response from such cluster is identical to a single pore of a considerably bigger diameter [146]. From the position of the phase minimum (1.9 Hz) and -arg Z $\approx 55^{o}$ (Fig. 54 B) we may hypothesize that the close-packed clusters of α-hemolysin may exhibit size significantly higher than 25 nm [169]. It can be claimed that exposure to α-hemolysin triggers EIS spectral changes typical for pore formation in tBLMs. The specific EIS features however, indicate significant heterogeneity in distribution of α-hemolysin pores in membranes with clear propensity of the formation of close-packed structures.

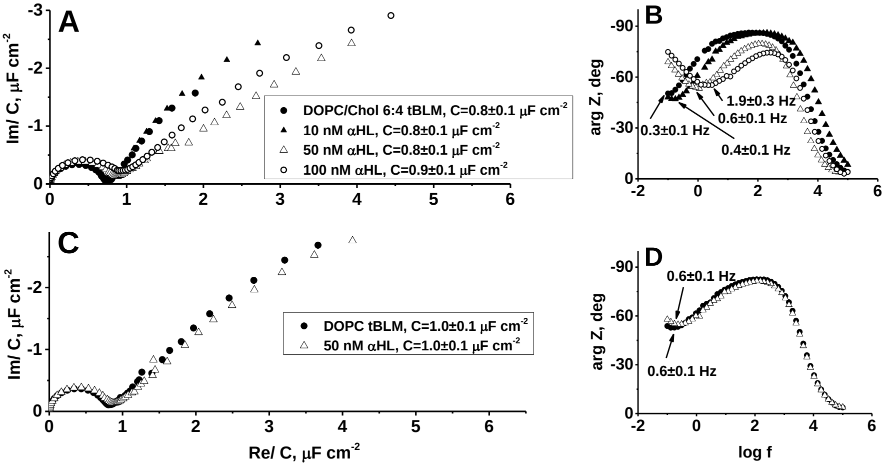

Fig. 54. EIS Cole – Cole (A, C) and Bode (B, D) plots of 10, 50 and 100 nM α-hemolysin 60 min interaction with DOPC/Chol 6:4 and DOPC tBLMs. Arrows in B and D indicate average phase minimum frequency. Bias potential 0 V *vs* Ag/AgCl, $NaCl_{sat.}$ electrode.

3.4.4. α-hemolysin channel penetration with polyethylene glycol

Functional reconstitution of α-hemolysin provides a tool which allows to prove/disapprove the presence of ionic/water reservoir between solid support and phospholipid bilayer membrane as it was demonstrated earlier on gold-supported tBLMs [172]. To prove the presence of reservoir we exposed tBLMs preloaded with α-hemolysin pores to a solution containing 30% of different size polyethylene glycols (PEG). The membrane conductance measured as EIS admittance Y_{fmin} at f_{min} (which is the frequency at which negative of impedance phase in Bode plots is observed) is assumed to be 1 (Fig. 55). By changing molar mass of PEG (M_{PEG}) variation of Y_{fmin} was measured. The plot of Y_{fmin} vs PEG size is presented in Fig. 55.

Small PEGs (200-2000 Da) are able to fully penetrate α-hemolysin pores and lower membrane conductance by approximately 40%, as it was the case in measurements using planar black lipid membranes [172]. However, in this research, the effect of lowering tBLMs conductivity is smaller because measured conductivity of tBLMs have a significant contribution from the submembrane reservoir. If the effective size of the submembrane space is smaller than the radius of the pore, then the reduction of conductivity is smaller than 40% as it was observed for gold supported tBLMs [172].

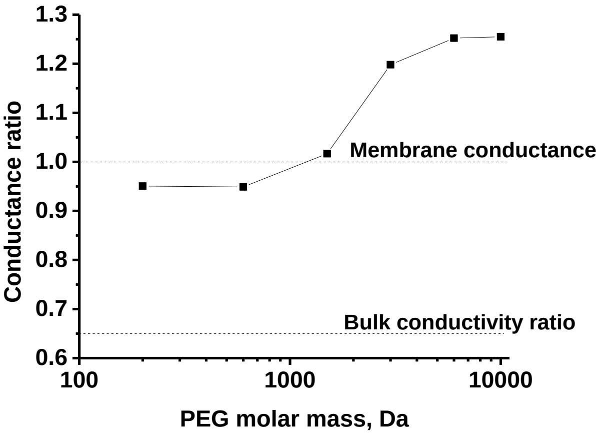

Fig. 55. Effect of size-selected PEGs on aHL channel conductance.

Below $M_{PEG} < 2000$ Da the curve decreases below 1 which is indicative of penetration of PEG polymers into α-hemolysin pores in tBLMs. If the pore conductance would dominate the measured conductance at f_{min}, then the conductance ratio would decrease to approximately 0.65 which is a ratio of conductance of PEG containing buffer over conductance of pristine (no PEG) buffer. However, as it was observed on gold supported tBLMs [172] this ratio is smaller than 1, though higher than 0.65, which indicates that the contribution from submembrane conductance is significant, and in our case it is dominating measured Y_{fmin}. The submembrane layer also is not allowing penetration of PEG even the smallest ones tested in the current study, M_{PEG} = 200 Da, which indicates highly constrained space between solid electrode and phospholipid bilayer. So, the question about the presence of water filled ionic reservoir can be addressed by interrogating response of Y_{fmin} in solution containing PEGs with $M_{PEG} > 2000$ Da.

As seen from Fig. 55, in solutions containing PEG with $M_{PEG} > 2000$ Da, the relative conductance increases by approximately 20%, to 1.2-1.25. Such effect, known as osmotic stress effect [172] is expected only if submembrane space contains exchangeable water. The effect arises because of the change of the water chemical potential in the bulk solution upon introduction of PEG. Increase of PEG concentration in the bulk solution causes the reduction of chemical potential of water. Due to size restrictions PEG cannot penetrate the submembrane space, the following inequality $\mu_{H_2O}^{sub} > \mu_{H_2O}^{bulk}$, where μ is the chemical potential of water in submembrane space and the bulk of solution, triggers water flow out of the submembrane space. This leads to a relative increase of the ion carriers (Na^+ and Cl^-, major ionic components of the buffer) in the submembrane space. Because submembrane space dominates measured conductance Y_{fmin}, the observer is recording relative increase of Y_{fmin}, which was also observed in case with gold-supported tBLMs [172] as well as in planar “black lipid membranes” [173].

Importantly, the observed curve in Fig. 55 proves two points. First, tBLMs on FTO contain reconstituted heptamers of α-hemolysin which start excluding PEG molecules at M_{PEG}>1500 Da, as observed on gold-supported tBLMs and black lipid membranes [172]. Second, the submembrane space separating solid support and phospholipid bilayer, which thickness is evidently smaller than the diameter of α-hemolysin, contains significant amount of water causing an osmotic stress effect and an increase of Y_{fmin} at M_{PEG}>1500 Da.

3.4.5. Tethered phospholipid bilayer regeneration

Lipid bilayer regeneration experiment was carried out to see, whether the same sample of TOPS:ATS silanized FTO could be used for several experiments. Fig. 56 shows that over 6th cycle of the tBLM formation, complex capacitance does exhibit relevant changes. However, after each removal of lipid bilayer, complex capacitance of the SAM increases slightly. This might happen due to long exposure of the SAM to aqueous environment that may cause hydration of the SAM. Nonetheless, formed tBLMs still exhibit the same complex capacitances confirming that the same TOPS:ATS silanized FTO sample can be used for multiple experiments.

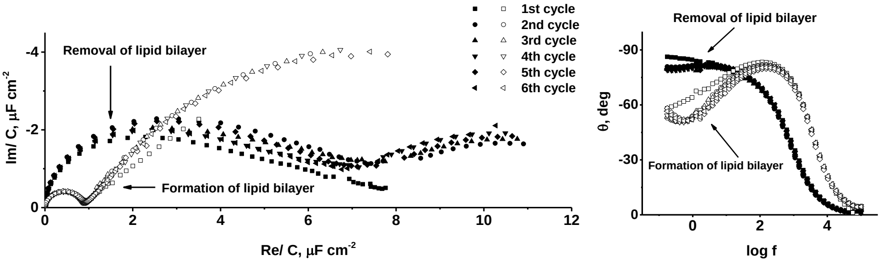

Fig. 56. EI spectra recorded during 6 consecutive cycles of phospholipid bilayer (DC 6:4) regeneration on the same FTO sample. Bias potential 0 V *vs* Ag/AgCl, $NaCl_{sat.}$ electrode.

CONCLUSIONS

1. It was determined that the optimal number of layers for cadmium tin oxide thin film deposition is 3 and annealing temperature is 520 °C. Prepared CTO films were suitable for OTS monolayer formation, the optimal concentration of OTS was determined to be 0.1% (or 2.5 mM). Complex capacitance values of OTS SAM was determined to be 2.5 µF cm^{-2} while similar gold-thiol system exhibits complex capacitance of 1.5 µF cm^{-2} [10]. This suggested sparse and defective packaging of OTS monolayer on CTO. Sparsely populated anchor SAM with numerous defects after DOPC/Chol (molar ratio 6:4) vesicle fusion resulted in bilayer membrane exhibiting complex capacitance value of 0.8 µF cm^{-2}, which was comparable to value obtained in gold-thiol system [10], showing that hybrid bilayer membrane formation was accomplished.

2. OTS self-assembled monolayer was formed on FTO surface. Optimal concentration of OTS was determined to be 0.1% (or 2.5 mM), incubation time – 60 min. Complex capacitance values of OTS SAM on FTO was determined to be similar to those obtained on CTO: 3.0 ± 0.8 µF cm^{-2}, suggesting sparse monolayer formation. Along with EIS, scanning electrochemical microscopy was used to characterise OTS SAM. Approach curves exhibited a distinctive feature – constant current region when UME distance from the surface reached 10 µm. Hybrid bilayer membrane of DOPC/Chol (molar ratio 6:4) was formed, exhibiting complex capacitance of 0.9 ± 0.1 µF cm^{-2} which was comparable to value obtained in gold-thiol systems [10]. Phospholipid membrane was not penetrated by vaginolysin however, phospholipase A_2 disrupted outer lipid layer in a concentration dependant manner displaying biosensing abilities.

3. Mixed hybrid bilayer membrane were formed on fluorine doped tin oxide surface silanized with a mix of OTS and MTS. It was determined that relatively small changes of SAM properties lead to large differences in properties of mhBLM obtained on pre-hydrated and non-hydrated substrates. It was found that mhBLM formed on SAM with even sparsely populated OTS molecular anchors (containing up to 80% of MTS back-filler) on pre-hydrated FTO surfaces exhibiting complex capacitance values of 1.1-0.8 ± 0.1 µF cm^{-2} similar to those obtained on gold-thiol systems [155]. Interaction of mhBLM with pore forming melittin confirmed the biological relevance of membrane formed on both types of SAMs (formed on pre-hydrated and non-hydrated FTO substrates).

4. Trichloro(3-(octadecylthio)propyl)silane molecular anchor was synthesised, confirmed by NMR measurements and used for the formation of

SAM on FTO surface. Tethered bilayer membrane formation was accomplished on TOPS SAM exhibiting complex capacitance of 0.8 ± 0.1 μF cm^{-2} which was comparable to value obtained for tBLMs on gold [7]. The biological relevance of investigated DOPC and DOPC/Chol membrane was confirmed with melittin and α-hemolysin toxins. The existence of ionic reservoir between the solid surface and the membrane was demonstrated by incorporating different size PEGs into α-hemolysin pores.

5. Hybrid bilayer, mixed hybrid bilayer and tethered bilayer membranes on silanized fluorine doped tin oxide surfaces can be used for multiple times of DOPC/Chol (molar ratio 6:4) membrane formation.

REFERENCES

[1] H.M. Keizer, B.R. Dorvel, M. Andersson, D. Fine, R.B. Price, J.R. Long, A. Dodabalapur, I. Köper, W. Knoll, P.A.V. Anderson, R.S. Duran, Functional ion channels in tethered bilayer membranes - Implications for biosensors, ChemBioChem. 8 (2007) 1246–1250. https://doi.org/10.1002/cbic.200700094.

[2] S. Pataraia, Y. Liu, R. Lipowsky, R. Dimova, Effect of cytochrome c on the phase behavior of charged multicomponent lipid membranes, Biochim. Biophys. Acta - Biomembr. 1838 (2014) 2036–2045. https://doi.org/10.1016/j.bbamem.2014.04.019.

[3] P. Mueller, D.O. Rudin, H.T. Tien, W.C. Wescott, Reconstitution of Cell Membrane Structure in vitro and its Transformation into an Excitable System, Nature. 194 (1962) 979–980. https://doi.org/10.1038/194979a0.

[4] P. Mueller, D.O. Rudin, H.T. Tien, W.C. Wescott, Methods for the formation of single bimolecular lipid membranes in aqueous solution, J. Phys. Chem. 67 (1963) 534–535. https://doi.org/10.1021/j100796a529.

[5] H.M. McConnell, T.H. Watts, R.M. Weis, A.A. Brian, Supported planar membranes in studies of cell-cell recognition in the immune system, BBA - Rev. Biomembr. 864 (1986) 95–106. https://doi.org/10.1016/0304-4157(86)90016-X.

[6] H. Lang, C. Duschl, H. Vogel, A New Class of Thiolipids for the Attachment of Lipid Bilayers on Gold Surfaces, 1994. https://doi.org/10.1021/la00013a029.

[7] D.J. McGillivray, G. Valincius, D.J. Vanderah, W. Febo-Ayala, J.T. Woodward, F. Heinrich, J.J. Kasianowicz, M. Lösche, Molecular-scale structural and functional characterization of sparsely tethered bilayer lipid membranes, Biointerphases. 2 (2007) 21–33. https://doi.org/10.1116/1.2709308.

[8] W. Knoll, K. Bender, R. Förch, C. Frank, H. Götz, C. Heibel, T. Jenkins, U. Jonas, A. Kibrom, R. Kügler, C. Naumann, R. Naumann, A. Reisinger, J. Rühe, S. Schiller, E.-K. Sinner, Polymer-Tethered Bimolecular Lipid Membranes, in: W.P. Meier, W. Knoll (Eds.), Polym. Membr., Springer Berlin Heidelberg, Berlin, Heidelberg, 2010: pp. 197–233. https://doi.org/10.1007/978-3-642-10479-4_27.

[9] B. Raguse, V. Braach-Maksvytis, B.A. Cornell, L.G. King, P.D.J. Osman, R.J. Pace, L. Wieczorek, Tethered lipid bilayer membranes: formation and ionic reservoir characterization, Langmuir. 14 (1998) 648–659. https://doi.org/10.1021/la9711239.

[10] V.I. Silin, H. Wieder, J.T. Woodward, G. Valincius, A. Offenhausser, A.L. Plant, The role of surface free energy on the formation of hybrid bilayer membranes, J. Am. Chem. Soc. 124 (2002) 14676–14683. https://doi.org/10.1021/ja026585+.

[11] A.L. Plant, Self-Assembled Phospholipid/Alkanethiol Biomimetic Bilayers on Gold, Langmuir. 9 (1993) 2764–2767. https://doi.org/10.1021/la00035a004.

[12] M.G. Friedrich, M.A. Plum, M.G. Santonicola, V.U. Kirste, W. Knoll, B. Ludwig, R.L.C. Naumann, In situ monitoring of the catalytic activity of cytochrome c oxidase in a biomimetic architecture, Biophys. J. 95 (2008) 1500–1510. https://doi.org/10.1529/biophysj.107.122747.

[13] R. Budvytyte, M. Pleckaityte, A. Zvirbliene, D.J. Vanderah, G. Valincius, Reconstitution of cholesterol-dependent vaginolysin into tethered phospholipid bilayers: Implications for bioanalysis, PLoS One. 8 (2013) 1–13. https://doi.org/10.1371/journal.pone.0082536.

[14] J.A. Jackman, W. Knoll, N.J. Cho, Biotechnology applications of tethered lipid bilayer membranes, Materials (Basel). 5 (2012) 2637–2657. https://doi.org/10.3390/ma5122637.

[15] L.W. Chong, Y.L. Lee, T.C. Wen, Surface modification of indium tin oxide anodes by self-assembly monolayers: Effects on interfacial morphology and charge injection in organic light-emitting diodes, Thin Solid Films. 515 (2007) 2833–2841. https://doi.org/10.1016/j.tsf.2006.05.010.

[16] A. Valiūnienė, T. Petrulionienė, I. Balevičiūtė, L. Mikoliūnaitė, G. Valinčius, Formation of hybrid bilayers on silanized thin-film Ti electrode, Chem. Phys. Lipids. 202 (2017) 62–68. https://doi.org/10.1016/j.chemphyslip.2016.12.001.

[17] T. Sabirovas, A. Valiūnienė, G. Valincius, Mechanically Polished Titanium Surface for Immobilization of Hybrid Bilayer Membrane, J. Electrochem. Soc. 165 (2018) G109–G115. https://doi.org/10.1149/2.0101810jes.

[18] T. Sabirovas, A. Valiūnienė, G. Valincius, Hybrid bilayer membranes on metallurgical polished aluminum, Sci. Rep. 11 (2021) 1–11. https://doi.org/10.1038/s41598-021-89150-2.

[19] T. Harayama, H. Riezman, Understanding the diversity of membrane lipid composition, Nat. Rev. Mol. Cell Biol. 19 (2018) 281–296. https://doi.org/10.1038/nrm.2017.138.

[20] H. Lodish, A. Berk, S.L. Zipursky, P. Matsudaira, D. Baltimore, J. Darnell, Membrane Proteins, 4th editio, W. H. Freeman, New York, 2000. https://www.ncbi.nlm.nih.gov/books/NBK21570/ (accessed July 12, 2021).

[21] S.J. Singer, G.L. Nicolson, The fluid mosaic model of the structure of cell membranes, Science (80-.). 175 (1972) 720–731. https://doi.org/10.1126/science.175.4023.720.

[22] T. Harayama, H. Riezman, Understanding the diversity of membrane lipid composition, (2018). https://doi.org/10.1038/nrm.2017.138.

[23] S. Leekumjorn, A.K. Sum, Molecular studies of the gel to liquid-crystalline phase transition for fully hydrated DPPC and DPPE

bilayers, Biochim. Biophys. Acta - Biomembr. 1768 (2007) 354–365. https://doi.org/https://doi.org/10.1016/j.bbamem.2006.11.003.

[24] X. Zhang, K.M. Barraza, J.L. Beauchamp, B.J. Finlayson-Pitts, R.N. Zare, Cholesterol provides nonsacrificial protection of membrane lipids from chemical damage at air-water interface, PNAS. 115 (2018). https://doi.org/10.1073/pnas.1722323115.

[25] B.A. Cornell, V.L.B. Braach-Maksvytis, L.G. King, P.D.J. Osman, B. Raguse, L. Wieczorek, R.J. Pace, A biosensor that uses ion-channel switches, Nature. 387 (1997) 580–583. https://doi.org/10.1038/42432.

[26] A.L. Plant, M. Brighamburke, E.C. Petrella, D.J. Oshannessy, Phospholipid/Alkanethiol Bilayers for Cell-Surface Receptor Studies by Surface Plasmon Resonance, Anal. Biochem. 226 (1995) 342–348. https://doi.org/https://doi.org/10.1006/abio.1995.1234.

[27] S. Terrettaz, M. Mayer, H. Vogel, Highly electrically insulating tethered lipid bilayers for probing the function of ion channel proteins, Eur. Cells Mater. 6 (2003) 107.

[28] Y. Shi, M. Cai, L. Zhou, H. Wang, Measurement of mechanical properties of naked cell membranes using atomic force microscope puncture test, Talanta. 210 (2020) 120637. https://doi.org/https://doi.org/10.1016/j.talanta.2019.120637.

[29] R. Naumann, E.K. Schmidt, A. Jonczyk, K. Fendler, B. Kadenbach, T. Liebermann, A. Offenhäusser, W. Knoll, The peptide-tethered lipid membrane as a biomimetic system to incorporate cytochrome c oxidase in a functionally active form, Biosens. Bioelectron. 14 (1999) 651–662. https://doi.org/https://doi.org/10.1016/S0956-5663(99)00036-6.

[30] L.J.C. Jeuken, S.D. Connell, P.J.F. Henderson, R.B. Gennis, S.D. Evans, R.J. Bushby, Redox Enzymes in Tethered Membranes, J. Am. Chem. Soc. 128 (2006) 1711–1716. https://doi.org/10.1021/ja056972u.

[31] B. Maier, J.O. Rädler, DNA on Fluid Membranes: A Model Polymer in Two Dimensions, Macromolecules. 33 (2000) 7185–7194. https://doi.org/10.1021/ma000075n.

[32] K.A. Kilian, T. Böcking, K. Gaus, J. King-Lacroix, M. Gal, J.J. Gooding, Hybrid lipid bilayers in nanostructured silicon: a biomimetic mesoporous scaffold for optical detection of cholera toxin, Chem. Commun. (2007) 1936–1938. https://doi.org/10.1039/B702762A.

[33] A.D. Bangham, R.W. Horne, Negative staining of phospholipids and their structural modification by surface-active agents as observed in the electron microscope, J. Mol. Biol. 8 (1964) 660–668. https://doi.org/10.1016/S0022-2836(64)80115-7.

[34] R.W. Horne, A.D. Bangham, V.P. Whittaker, Negatively stained lipoprotein membranes [43], Nature. 200 (1963) 1340. https://doi.org/10.1038/2001340a0.

[35] P.K. Deb, O. Al-Attraqchi, B. Chandrasekaran, A. Paradkar, R.K.

Tekade, Protein/peptide drug delivery systems: Practical considerations in pharmaceutical product development, in: Basic Fundam. Drug Deliv., Elsevier, 2018: pp. 651–684. https://doi.org/10.1016/B978-0-12-817909-3.00016-9.

[36] C.W. Meuse, S. Krueger, C.F. Majkrzak, J.A. Dura, J. Fu, J.T. Connor, A.L. Plant, Hybrid bilayer membranes in air and water: infrared spectroscopy and neutron reflectivity studies., Biophys. J. 74 (1998) 1388–1398. https://doi.org/10.1016/S0006-3495(98)77851-8.

[37] R. V Stahelin, Surface plasmon resonance: a useful technique for cell biologists to characterize biomolecular interactions, Mol. Biol. Cell. 24 (2013) 883–886. https://doi.org/10.1091/mbc.e12-10-0713.

[38] R. Naumann, S.M. Schiller, F. Giess, B. Grohe, K.B. Hartman, I. Kärcher, I. Köper, J. Lübben, K. Vasilev, W. Knoll, Tethered Lipid Bilayers on Ultraflat Gold Surfaces, Langmuir. 19 (2003) 5435–5443. https://doi.org/10.1021/la0342060.

[39] L.J.C. Jeuken, N.N. Daskalakis, X. Han, K. Sheikh, A. Erbe, R.J. Bushby, S.D. Evans, Phase separation in mixed self-assembled monolayers and its effect on biomimetic membranes, Sensors Actuators, B Chem. 124 (2007) 501–509. https://doi.org/10.1016/j.snb.2007.01.014.

[40] I.K. Vockenroth, C. Rossi, M.R. Shah, I. Köper, Formation of tethered bilayer lipid membranes probed by various surface sensitive techniques, Biointerphases. 4 (2009) 19–26. https://doi.org/10.1116/1.3122019.

[41] C. Miller, P. Cuendet, M. Grätzel, K+ sensitive bilayer supporting electrodes, J. Electroanal. Chem. Interfacial Electrochem. 278 (1990) 175–192. https://doi.org/https://doi.org/10.1016/0022-0728(90)85132-O.

[42] L.M. Williams, S.D. Evans, T.M. Flynn, A. Marsh, P.F. Knowles, R.J. Bushby, N. Boden, Kinetics of the Unrolling of Small Unilamellar Phospholipid Vesicles onto Self-Assembled Monolayers, Langmuir. 13 (1997) 751–757. https://doi.org/10.1021/la960805d.

[43] T. Ragaliauskas, M. Mickevicius, B. Rakovska, T. Penkauskas, D.J. Vanderah, F. Heinrich, G. Valincius, Fast formation of low-defect-density tethered bilayers by fusion of multilamellar vesicles, Biochim. Biophys. Acta - Biomembr. 1859 (2017) 669–678. https://doi.org/10.1016/j.bbamem.2017.01.015.

[44] A.L. Plant, Supported Hybrid Bilayer Membranes as Rugged Cell Membrane Mimics, Langmuir. 15 (1999) 5128–5135. https://doi.org/10.1021/la981662t.

[45] S. Mun, S.-J. Choi, Optimization of the hybrid bilayer membrane method for immobilization of avidin on quartz crystal microbalance, Biosens. & Bioelectron. 24 (2009) 2522—2527. https://doi.org/10.1016/j.bios.2009.01.006.

[46] A. Więckowska, E. Jabłonowska, E. Rogalska, R. Bilewicz,

Structuring of supported hybrid phospholipid bilayers on electrodes with phospholipase A2, Phys. Chem. Chem. Phys. 13 (2011) 9716–9724. https://doi.org/10.1039/C0CP02229B.

[47] K. E, F. S, T. LK, Formation of supported planar bilayers by fusion of vesicles to supported phospholipid monolayers, Biochim. Biophys. Acta. 1103 (1992) 307–316. https://doi.org/10.1016/0005-2736(92)90101-Q.

[48] E.T. Castellana, P.S. Cremer, Solid supported lipid bilayers: From biophysical studies to sensor design, Surf. Sci. Rep. 61 (2006) 429–444. https://doi.org/10.1016/j.surfrep.2006.06.001.

[49] S.A. Glazier, D.J. Vanderah, A.L. Plant, H. Bayley, G. Valincius, J.J. Kasianowicz, Reconstitution of the Pore-Forming Toxin α-Hemolysin in Phospholipid/18-Octadecyl-1-thiahexa(ethylene oxide) and Phospholipid/n-Octadecanethiol Supported Bilayer Membranes, Langmuir. 16 (2000) 10428–10435. https://doi.org/10.1021/la000690k.

[50] G. Valincius, D.J. McGillivray, W. Febo-Ayala, D.J. Vanderah, J.J. Kasianowicz, M. Lösche, Enzyme activity to augment the characterization of tethered bilayer membranes, J. Phys. Chem. B. 110 (2006) 10213–10216. https://doi.org/10.1021/jp0616516.

[51] R.G. Nuzzo, D.L. Allara, Adsorption of Bifunctional Organic Disulfides on Gold Surfaces, J. Am. Chem. Soc. 105 (1983) 4481–4483. https://doi.org/10.1021/ja00351a063.

[52] S.R. Wasserman, Y.T. Tao, G.M. Whitesides, Structure and Reactivity of Alkylsiloxane Monolayers Formed by Reaction of Alkyltrichlorosilanes on Silicon Substrates, Langmuir. 5 (1989) 1074–1087. https://doi.org/10.1021/la00088a035.

[53] A. Ulman, Formation and Structure of Self-Assembled Monolayers, (1996).

[54] J.C. Love, L.A. Estroff, J.K. Kriebel, R.G. Nuzzo, G.M. Whitesides, Self-Assembled Monolayers of Thiolates on Metals as a Form of Nanotechnology, Chem. Rev. 105 (2005) 1103–1170. https://doi.org/10.1021/cr0300789.

[55] H. Hillebrandt, M. Tanaka, Electrochemical characterization of self-assembled alkylsiloxane monolayers on Indium-Tin oxide (ITO) semiconductor electrodes, J. Phys. Chem. B. 105 (2001) 4270–4276. https://doi.org/10.1021/jp004062n.

[56] S.A. Kulinich, M. Farzaneh, Alkylsilane self-assembled monolayers: Modeling their wetting characteristics, Appl. Surf. Sci. 230 (2004) 232–240. https://doi.org/10.1016/j.apsusc.2004.02.031.

[57] M. Wang, K.M. Liechti, Q. Wang, J.M. White, Self-assembled silane monolayers: Fabrication with nanoscale uniformity, Langmuir. 21 (2005) 1848–1857. https://doi.org/10.1021/la048483y.

[58] A. Muthurasu, V. Ganesh, Electrochemical characterization of Self-assembled Monolayers (SAMs) of silanes on indium tin oxide (ITO)

electrodes - Tuning electron transfer behaviour across electrode-electrolyte interface, J. Colloid Interface Sci. 374 (2012) 241–249. https://doi.org/10.1016/j.jcis.2012.02.007.

[59] T. Ragaliauskas, M. Mickevicius, R. Budvytyte, G. Niaura, B. Carbonnier, G. Valincius, Adsorption of β-amyloid oligomers on octadecanethiol monolayers, J. Colloid Interface Sci. 425 (2014) 159–167. https://doi.org/10.1016/j.jcis.2014.03.042.

[60] A. Kolodziej, F. Fernandez-Trillo, P. Rodriguez, Determining the parameters governing the electrochemical stability of thiols and disulfides self-assembled monolayer on gold electrodes in physiological medium, J. Electroanal. Chem. 819 (2018) 51–57. https://doi.org/10.1016/j.jelechem.2017.07.039.

[61] F. Frederix, K. Bonroy, W. Laureyn, G. Reekmans, A. Campitelli, W. Dehaen, G. Maes, Enhanced performance of an affinity biosensor interface based on mixed self-assembled monolayers of thiols on gold, Langmuir. 19 (2003) 4351–4357. https://doi.org/10.1021/la026908f.

[62] I. Markovich, D. Mandler, Preparation and characterization of octadecylsilane monolayers on indium-tin oxide (ITO) surfaces, J. Electroanal. Chem. 500 (2001) 453–460. https://doi.org/10.1016/S0022-0728(00)00458-7.

[63] M. Baranowska, A.J. Slota, P.J. Eravuchira, M. Alba, P. Formentin, J. Pallarès, J. Ferré-Borrull, L.F. Marsal, Protein attachment to silane-functionalized porous silicon: A comparison of electrostatic and covalent attachment, J. Colloid Interface Sci. 452 (2015) 180–189. https://doi.org/https://doi.org/10.1016/j.jcis.2015.04.022.

[64] S.D. Alvarez, A.M. Derfus, M.P. Schwartz, S.N. Bhatia, M.J. Sailor, The compatibility of hepatocytes with chemically modified porous silicon with reference to in vitro biosensors, Biomaterials. 30 (2009) 26–34. https://doi.org/10.1016/j.biomaterials.2008.09.005.

[65] S.J. Schoell, A. Oliveros, M. Steenackers, S.E. Saddow, I.D. Sharp, Multifunctional SiC Surfaces: From Passivation to Biofunctionalization, Silicon Carbide Biotechnol. (2012) 63–117. https://doi.org/10.1016/B978-0-12-385906-8.00003-9.

[66] M. Baranowska, A.J. Slota, P.J. Eravuchira, M. Alba, P. Formentin, J. Pallarès, J. Ferré-Borrull, L.F. Marsal, Protein attachment to silane-functionalized porous silicon: A comparison of electrostatic and covalent attachment, J. Colloid Interface Sci. 452 (2015) 180–189. https://doi.org/10.1016/j.jcis.2015.04.022.

[67] C. Hoffmann, G.E.M. Tovar, Mixed self-assembled monolayers (SAMs) consisting of methoxy-tri(ethylene glycol)-terminated and alkyl-terminated dimethylchlorosilanes control the non-specific adsorption of proteins at oxidic surfaces, J. Colloid Interface Sci. 295 (2006) 427–435. https://doi.org/10.1016/j.jcis.2005.10.005.

[68] D.A. Offord, J.H. Griffin, Kinetic Control in the Formation of Self-Assembled Mixed Monolayers on Planar Silica Substrates, Langmuir.

9 (1993) 3015–3025. https://doi.org/10.1021/la00035a046.

[69] M.C. Howland, A.R. Sapuri-Butti, S.S. Dixit, A.M. Dattelbaum, A.P. Shreve, A.N. Parikh, Phospholipid morphologies on photochemically patterned silane monolayers, J. Am. Chem. Soc. 127 (2005) 6752–6765. https://doi.org/10.1021/ja043439q.

[70] T.N. Sut, J.A. Jackman, N.-J. Cho, Understanding How Membrane Surface Charge Influences Lipid Bicelle Adsorption onto Oxide Surfaces, Langmuir. 35 (2019) 8436–8444. https://doi.org/10.1021/ACS.LANGMUIR.9B00570.

[71] C. Renault, C.P. Andrieux, R.T. Tucker, M.J. Brett, V. Balland, B. Limoges, Unraveling the mechanism of catalytic reduction of O 2 by microperoxidase-11 adsorbed within a transparent 3D-nanoporous ITO film, J. Am. Chem. Soc. 134 (2012) 6834–6845. https://doi.org/10.1021/ja301193s.

[72] N. Rushe, M. Ball, W.M. Carroll, S. Healy, J. Mcmanus, D. Cunningham, Cytocompatibility of novel tin oxide thin films, J. Mater. Sci. Mater. Med. 16 (2005) 247–252. https://doi.org/10.1007/s10856-005-6686-z.

[73] M. Yasuyuki, K. Kunihiro, S. Kurissery, N. Kanavillil, Y. Sato, Y. Kikuchi, Antibacterial properties of nine pure metals: A laboratory study using Staphylococcus aureus and Escherichia coli, Biofouling. 26 (2010) 851–858. https://doi.org/10.1080/08927014.2010.527000.

[74] J. Feng, Y.X. Ci, C.Y. Zhang, A.L. Ottova, H.T. Tien, Photoelectric measurements of self-assembled and supported planar lipid bilayers: a new technique for studying apoptosis, Electrochem. Commun. 1 (1999) 145–147. https://doi.org/https://doi.org/10.1016/S1388-2481(99)00021-1.

[75] S. Gritsch, P. Nollert, F. Jähnig, E. Sackmann, Impedance spectroscopy of porin and gramicidin pores reconstituted into supported lipid bilayers on indium-tin-oxide electrodes, Langmuir. 14 (1998) 3118–3125. https://doi.org/10.1021/la9710381.

[76] G. Wiegand, N. Arribas-Layton, H. Hillebrandt, E. Sackmann, P. Wagner, Electrical Properties of Supported Lipid Bilayer Membranes, J. Phys. Chem. B. 106 (2002) 4245–4254. https://doi.org/10.1021/jp014337e.

[77] H.M. Lemire, K.A. Peterson, M.S. Breslau, K.D. Singer, I.T. Martin, R.H. French, Degradation of Transparent Conductive Oxides, and the Beneficial Role of Interfacial Layers, 2013.

[78] S. Jasiecki, J. Czupryniak, T. Ossowski, G. Schroeder, FTO coated glass electrode functionalization with transition metal cations receptors via electrostatic self-assembly, Int. J. Electrochem. Sci. 8 (2013) 12543–12556.

[79] L. Rojas, L. Molero, R.A. Tapia, R. Del Rio, M.A. Del Valle, M. Antilén, F. Armijo, Electrochemistry behavior of endogenous thiols on fluorine doped tin oxide electrodes, Electrochim. Acta. 56 (2011)

8711–8717. https://doi.org/10.1016/j.electacta.2011.07.074.

[80] B. Pandit, T. Luitel, D.R. Cummins, A.K. Thapa, T. Druffel, F. Zamborini, J. Liu, Spectroscopic Investigation of Photoinduced Charge-Transfer Processes in FTO/TiO2/N719 Photoanodes with and without Covalent Attachment through Silane-Based Linkers, J. Phys. Chem. A. 117 (2013) 13513–13523. https://doi.org/10.1021/jp407270j.

[81] P. Topolovsek, F. Lamberti, T. Gatti, A. Cito, J.M. Ball, E. Menna, C. Gadermaier, A. Petrozza, Functionalization of transparent conductive oxide electrode for TiO 2-free perovskite solar cells †, (2017). https://doi.org/10.1039/c7ta02405c.

[82] M.J. Song, S. Kim, N. Ki Min, J.H. Jin, Electrochemical serotonin monitoring of poly(ethylenedioxythiophene): Poly(sodium 4-styrenesulfonate)-modified fluorine-doped tin oxide by predeposition of self-assembled 4-pyridylporphyrin, Biosens. Bioelectron. 52 (2014) 411–416. https://doi.org/10.1016/j.bios.2013.08.040.

[83] R.R. Mehta, S.F. Vogel, Sputtered Cadmium Oxide and Indium Oxide/Tin Oxide Films as Transparent Electrodes to Cadmium Sulfide, J. Electrochem. Soc. 119 (1972) 752. https://doi.org/10.1149/1.2404320.

[84] J.C.C. Fan, F.J. Bachner, Transparent heat mirrors for solar-energy applications, Appl. Opt. 15 (1976) 1012. https://doi.org/10.1364/ao.15.001012.

[85] J.C. Manifacier, L. Szepessy, J.F. Bresse, M. Perotin, R. Stuck, In2O3 : (Sn) and SnO2 : (F) films - application to solar energy conversion part II - Electrical and optical properties, Mater. Res. Bull. 14 (1979) 163–175. https://doi.org/10.1016/0025-5408(79)90115-6.

[86] A.J. Nozik, Optical and electrical properties of Cd2 SnO4: A defect semiconductor, Phys. Rev. B. 6 (1972) 453–459. https://doi.org/10.1103/PhysRevB.6.453.

[87] R. Kumaravel, V. Krishnakumar, V. Gokulakrishnan, K. Ramamurthi, K. Jeganathan, Effect of annealing on the electrical, optical and structural properties of cadmium stannate thin films prepared by spray pyrolysis technique, Thin Solid Films. 518 (2010) 2271–2274. https://doi.org/10.1016/j.tsf.2009.08.049.

[88] A. Abrutis, G. Valincius, G. Baltrunas, L. Parafionovic, A. Valiuniene, Z. Saltyte, Spray-pyrolysis Cd2SnO4 films for electrochemical applications, Thin Solid Films. 515 (2007) 6817–6823. https://doi.org/10.1016/j.tsf.2007.02.075.

[89] J.A. Stoke, J.D. Beach, W.C. Bradford, T.R. Ohno, Electrical and optical properties of magnetron sputtered Cd 2SnO4 transparent conducting oxide thin films for use in CdTe solar devices, Thin Solid Films. 562 (2014) 254–259. https://doi.org/10.1016/j.tsf.2014.04.076.

[90] T. Meng, B. McCandless, W. Buchanan, E. Kimberly, R. Birkmire, Cadmium tin oxide thin films deposited by RF magnetron sputtering

for photovoltaic applications, J. Alloys Compd. 556 (2013) 39–44. https://doi.org/10.1016/j.jallcom.2012.12.146.

[91] K. Jeyadheepan, M. Thamilselvan, K. Kim, J. Yi, C. Sanjeeviraja, Optoelectronic properties of R-F magnetron sputtered Cadmium Tin Oxide (Cd2SnO4) thin films for CdS/CdTe thin film solar cell applications, J. Alloys Compd. 620 (2015) 185–191. https://doi.org/10.1016/j.jallcom.2014.09.056.

[92] B.J. Zheng, J.S. Lian, L. Zhao, Q. Jiang, Optical and electrical properties of Sn-doped CdO thin films obtained by pulse laser deposition, Vacuum. 85 (2011) 861–865. https://doi.org/10.1016/j.vacuum.2011.01.002.

[93] R.A. Ismail, S.A. Tawfiq, R. Hababa, R.S. Sabry, O.A. Abdulrazaq, Pulsed laser deposition of crystalline Cd2SnO4 thin film, E-Journal Surf. Sci. Nanotechnol. 5 (2007) 152–154. https://doi.org/10.1380/ejssnt.2007.152.

[94] C.J. Diliegros-Godines, F.J. Flores-Ruiz, R. Castanedo-Pérez, G. Torres-Delgado, F.J. Espinoza-Beltrán, E. Broitman, Mechanical and tribological properties of CdO + SnO2 thin films prepared by sol–gel, J. Sol-Gel Sci. Technol. 74 (2015) 114–120. https://doi.org/10.1007/s10971-014-3584-1.

[95] C.J. Diliegros Godines, C.G. Torres Castanedo, R. Castanedo Pérez, G. Torres Delgado, O. Zelaya Ángel, Transparent conductive thin films of Cd2SnO4 obtained by the sol-gel technique and their use in a solar cell made with CdTe, Sol. Energy Mater. Sol. Cells. 128 (2014) 150–155. https://doi.org/10.1016/j.solmat.2014.05.023.

[96] R. Bel-Hadj-Tahar, N. Bel-Hadj-Tahar, A.B. Mohamed, Sol-gel processing of highly transparent conducting Cd2SnO4 thin films, EPJ Appl. Phys. 69 (2015) 30302. https://doi.org/10.1051/epjap/2015140464.

[97] R. Bel Hadj Tahar, T. Ban, Y. Ohya, Y. Takahashi, Effect of Processing Parameters on Physical Properties of Cadmium Stannate Thin Films Prepared by a Dip-Coating Technique, J. Am. Ceram. Soc. 84 (2001) 85–91. https://doi.org/10.1111/j.1151-2916.2001.tb00612.x.

[98] H. Khallaf, C.T. Chen, L.B. Chang, O. Lupan, A. Dutta, H. Heinrich, F. Haque, E. Del Barco, L. Chow, Chemical bath deposition of SnO 2 and Cd 2 SnO 4 thin films, Appl. Surf. Sci. 258 (2012) 6069–6074. https://doi.org/10.1016/j.apsusc.2012.03.004.

[99] H. Dislich, P. Hinz, History and principles of the sol-gel process, and some new multicomponent oxide coatings, J. Non. Cryst. Solids. 48 (1982) 11–16. https://doi.org/10.1016/0022-3093(82)90242-3.

[100] G. Valincius, V. Reipa, V. Vilker, J.T. Woodward, M. Vaudin, Electrochemical Properties of Nanocrystalline Cadmium Stannate Films, J. Electrochem. Soc. 148 (2001) E341. https://doi.org/10.1149/1.1379742.

[101] United States Patent Application: 0090272437, (n.d.). https://appft.uspto.gov/netacgi/nph-Parser?Sect1=PTO2&Sect2=HITOFF&p=1&u=%2Fnetahtml%2FPTO%2Fsearch-adv.html&r=1&f=G&l=50&d=PG01&S1=4229491&OS=4229491&RS=4229491 (accessed June 1, 2021).

[102] D. Hall, Properties of Cadmium Stannate Thin Film Electrodes and Their Use in Photogalvanic Cells, J. Electrochem. Soc. 124 (1977) 804–807. https://doi.org/10.1149/1.2133411.

[103] C.S. Ferekides, R. Mamazza, U. Balasubramanian, D.L. Morel, Transparent conductors and buffer layers for CdTe solar cells, Thin Solid Films. 480–481 (2005) 224–229. https://doi.org/10.1016/j.tsf.2004.11.094.

[104] S. Schiller, G. Beister, E. Buedke, H.J. Becker, H. Schicht, Properties of cadmium stannate thin films produced by reactive high rate d.c. magnetron-plasmatron sputtering, Thin Solid Films. 96 (1982) 113–120. https://doi.org/10.1016/0040-6090(82)90609-5.

[105] G. Haacke, Evaluation of cadmium stannate films for solar heat collectors, Appl. Phys. Lett. 30 (1977) 380–381. https://doi.org/10.1063/1.89439.

[106] S.M. Al-Sofiany, H.E. Hassan, Radiation treatment of Cd2SnO4 thin films prepared by RF sputtering with different preparation conditions, J. Alloys Compd. 651 (2015) 149–156. https://doi.org/10.1016/j.jallcom.2015.08.042.

[107] W. Ke, G. Fang, Q. Liu, L. Xiong, P. Qin, H. Tao, J. Wang, H. Lei, B. Li, J. Wan, G. Yang, Y. Yan, Low-temperature solution-processed tin oxide as an alternative electron transporting layer for efficient perovskite solar cells, J. Am. Chem. Soc. 137 (2015) 6730–6733. https://doi.org/10.1021/jacs.5b01994.

[108] P.H. Chen, T.C. Chang, K.C. Chang, T.M. Tsai, C.H. Pan, C.C. Shih, C.H. Wu, C.C. Yang, Y.T. Su, C.Y. Lin, Y.T. Tseng, M.C. Chen, R.C. Wang, C.C. Leu, K.H. Chen, I. Lo, J.C. Zheng, S.M. Sze, Obtaining Lower Forming Voltage and Self-Compliance Current by Using a Nitride Gas/Indium-Tin Oxide Insulator in Resistive Random Access Memory, IEEE Trans. Electron Devices. 63 (2016) 4769–4775. https://doi.org/10.1109/TED.2016.2619704.

[109] B.C. Yadav, K. Agrahari, S. Singh, T.P. Yadav, Fabrication and characterization of nanostructured indium tin oxide film and its application as humidity and gas sensors, J. Mater. Sci. Mater. Electron. 27 (2016) 4172–4179. https://doi.org/10.1007/s10854-016-4279-x.

[110] A.N. Banerjee, S. Kundoo, P. Saha, K.K. Chattopadhyay, Synthesis and Characterization of Nano-Crystalline Fluorine-Doped Tin Oxide Thin Films by Sol-Gel Method, 2003.

[111] B. Zhang, Y. Tian, J.X. Zhang, W. Cai, Structural, optical, electrical properties and FTIR studies of fluorine doped SnO2 films deposited

by spray pyrolysis, J. Mater. Sci. 46 (2011) 1884–1889. https://doi.org/10.1007/s10853-010-5021-3.

[112] H. Kim, C.M. Gilmore, A. Piqué, J.S. Horwitz, H. Mattoussi, H. Murata, Z.H. Kafafi, D.B. Chrisey, Electrical, optical, and structural properties of indium-tin-oxide thin films for organic light-emitting devices, J. Appl. Phys. 86 (1999) 6451–6461. https://doi.org/10.1063/1.371708.

[113] N. Noor, I.P. Parkin, Enhanced transparent-conducting fluorine-doped tin oxide films formed by Aerosol-Assisted Chemical Vapour Deposition, J. Mater. Chem. C. 1 (2013) 984–996. https://doi.org/10.1039/c2tc00400c.

[114] S.D. Lounis, E.L. Runnerstrom, A. Bergerud, D. Nordlund, D.J. Milliron, Influence of dopant distribution on the plasmonic properties of indium tin oxide nanocrystals, J. Am. Chem. Soc. 136 (2014) 7110–7116. https://doi.org/10.1021/ja502541z.

[115] E. Elangovan, K. Ramamurthi, A study on low cost-high conducting fluorine and antimony-doped tin oxide thin films, Appl. Surf. Sci. 249 (2005) 183–196. https://doi.org/10.1016/j.apsusc.2004.11.074.

[116] K. Subba Ramaiah, V. Sundara Raja, Structural and electrical properties of fluorine doped tin oxide films prepared by spray-pyrolysis technique, Appl. Surf. Sci. 253 (2006) 1451–1458. https://doi.org/10.1016/j.apsusc.2006.02.019.

[117] S.N. Sujatha Lekshmy, V.S.N. Anitha, P.V. Thomas, K. Joy, Magnetic Properties of Mn-doped SnO 2 Thin Films Prepared by the Sol-Gel Dip Coating Method for Dilute Magnetic Semiconductors , J. Am. Ceram. Soc. 97 (2014) 3184–3191. https://doi.org/10.1111/jace.13084.

[118] E. Elangovan, K. Ramamurthi, Studies on micro-structural and electrical properties of spray-deposited fluorine-doped tin oxide thin films from low-cost precursor, Thin Solid Films. 476 (2005) 231–236. https://doi.org/10.1016/j.tsf.2004.09.022.

[119] S. Shanthi, C. Subramanian, P. Ramasamy, Growth and characterization of antimony doped tin oxide thin films, J. Cryst. Growth. 197 (1999) 858–864. https://doi.org/10.1016/S0022-0248(98)01066-5.

[120] V. Reipa, M.P. Mayhew, V.L. Vilker, A direct electrode-driven P450 cycle for biocatalysis, Proc. Natl. Acad. Sci. U. S. A. 94 (1997) 13554–13558. https://doi.org/10.1073/pnas.94.25.13554.

[121] P.J. Hotchkiss, S.C. Jones, S.A. Paniagua, A. Sharma, B. Kippelen, N.R. Armstrong, S.R. Marder, The modification of indium tin oxide with phosphonic acids: Mechanism of binding, tuning of surface properties, and potential for use in organic electronic applications, Acc. Chem. Res. 45 (2012) 337–346. https://doi.org/10.1021/ar200119g.

[122] L. Barraud, Z.C. Holman, N. Badel, P. Reiss, A. Descoeudres, C.

Battaglia, S. De Wolf, C. Ballif, Hydrogen-doped indium oxide/indium tin oxide bilayers for high-efficiency silicon heterojunction solar cells, Sol. Energy Mater. Sol. Cells. 115 (2013) 151–156. https://doi.org/10.1016/j.solmat.2013.03.024.

[123] J.A. Jeong, J. Lee, H. Kim, H.K. Kim, S.I. Na, Ink-jet printed transparent electrode using nano-size indium tin oxide particles for organic photovoltaics, Sol. Energy Mater. Sol. Cells. 94 (2010) 1840–1844. https://doi.org/10.1016/j.solmat.2010.05.052.

[124] V. Arivazhagan, S. Rajesh, Preparation of nanocrystalline SnO2 thin films for micro gas sensors, J. Ovonic Res. 6 (2010) 221–226.

[125] M. Pleckaityte, Cholesterol-Dependent Cytolysins Produced by Vaginal Bacteria: Certainties and Controversies, Front. Cell. Infect. Microbiol. 9 (2020) 1–14. https://doi.org/10.3389/fcimb.2019.00452.

[126] T. Ragaliauskas, M. Plečkaitytė, M. Jankunec, L. Labanauskas, L. Baranauskiene, G. Valincius, Inerolysin and vaginolysin, the cytolysins implicated in vaginal dysbiosis, differently impair molecular integrity of phospholipid membranes, Sci. Rep. 9 (2019). https://doi.org/10.1038/s41598-019-47043-5.

[127] R.K. Tweten, Cholesterol-dependent cytolysins, a family of versatile pore-forming toxins, Infect. Immun. 73 (2005) 6199–6209. https://doi.org/10.1128/IAI.73.10.6199-6209.2005.

[128] B. Geny, M.R. Popoff, Bacterial protein toxins and lipids: pore formation or toxin entry into cells, Biol. Cell. 98 (2006) 667–678. https://doi.org/10.1042/bc20050082.

[129] D.C. Wilton, Phospholipases A2: Structure and function, Eur. J. Lipid Sci. Technol. 107 (2005) 193–205. https://doi.org/10.1002/EJLT.200401089.

[130] W.L. Smith, The eicosanoids and their biochemical mechanisms of action, Biochem. J. 259 (1989) 315–324. https://doi.org/10.1042/BJ2590315.

[131] J.E. Burke, E.A. Dennis, Phospholipase A2 structure/function, mechanism, and signaling., J. Lipid Res. 50 Suppl (2009) S237-42. https://doi.org/10.1194/jlr.R800033-JLR200.

[132] D.A. Six, E.A. Dennis, The expanding superfamily of phospholipase A(2) enzymes: classification and characterization., Biochim. Biophys. Acta. 1488 (2000) 1–19. https://doi.org/10.1016/s1388-1981(00)00105-0.

[133] J. Chen, S.M. Guan, W. Sun, H. Fu, Melittin, the Major Pain-Producing Substance of Bee Venom, Neurosci. Bull. 32 (2016) 265–272. https://doi.org/10.1007/s12264-016-0024-y.

[134] B. Bechinger, Structure and functions of channel-forming peptides: Magainins, cecropins, melittin and alamethicin, J. Membr. Biol. 156 (1997) 197–211. https://doi.org/10.1007/s002329900201.

[135] D. Mudhakir, H. Harashima, Learning from the Viral Journey: How to Enter Cells and How to Overcome Intracellular Barriers to Reach the

Nucleus, (n.d.). https://doi.org/10.1208/s12248-009-9080-9.

[136] G. Sessa, J.H. Freer, G. Weissmann, MACROMOLECULES : with Lipid Membrane Systems Interaction of a Lytic Polypeptide , Lipid Membrane Systems *, 244 (1969).

[137] M.T. Tosteson, D.C. Tosteson, The sting. Melittin forms channels in lipid bilayers, Biophys. J. 36 (1981) 109–116. https://doi.org/10.1016/S0006-3495(81)84719-4.

[138] Y. Shai, Mechanism of the binding, insertion and destabilization of phospholipid bilayer membranes by α-helical antimicrobial and cell non-selective membrane-lytic peptides, Biochim. Biophys. Acta - Biomembr. 1462 (1999) 55–70. https://doi.org/10.1016/S0005-2736(99)00200-X.

[139] S. Pandidan, A. Mechler, Nano-viscosimetry analysis of the membrane disrupting action of the bee venom peptide melittin, Sci. Reports 2019 91. 9 (2019) 1–12. https://doi.org/10.1038/s41598-019-47325-y.

[140] L. Song, M.R. Hobaugh, C. Shustak, S. Cheley, H. Bayley, J.E. Gouaux, Structure of staphylococcal alpha-hemolysin, a heptameric transmembrane pore., Science. 274 (1996) 1859–1866. https://doi.org/10.1126/science.274.5294.1859.

[141] T. Tomita, M. Watanabe, T. Yasuda, Influence of membrane fluidity on the assembly of Staphylococcus aureus alpha-toxin, a channel-forming protein, in liposome membrane., J. Biol. Chem. 267 (1992) 13391–13397.

[142] Y. Du, L. Liu, C. Zhang, Y. Zhang, Two residues in Staphylococcus aureus α-hemolysin related to hemolysis and self-assembly, Infect. Drug Resist. 11 (2018) 1271–1274. https://doi.org/10.2147/IDR.S167779.

[143] Electrochemical Methods: Fundamentals and Applications, 2nd Edition | Wiley, 2001.

[144] M. Aliofkhazraei, Modern Electrochemical Methods in Nano, Surface and Corrosion Science, Mod. Electrochem. Methods Nano, Surf. Corros. Sci. (2014). https://doi.org/10.5772/57202.

[145] G. Valincius, T. Meškauskas, F. Ivanauskas, Electrochemical impedance spectroscopy of tethered bilayer membranes, Langmuir. 28 (2012) 977–990. https://doi.org/10.1021/la204054g.

[146] G. Valincius, M. Mickevicius, Tethered Phospholipid Bilayer Membranes. An Interpretation of the Electrochemical Impedance Response, in: Adv. Planar Lipid Bilayers Liposomes, Elsevier B.V., 2015: pp. 27–61. https://doi.org/10.1016/bs.adplan.2015.01.003.

[147] A.K. Tucker-Schwartz, R.A. Farrell, R.L. Garrell, Thiol - Ene click reaction as a general route to functional trialkoxysilanes for surface coating applications, J. Am. Chem. Soc. 133 (2011) 11026–11029. https://doi.org/10.1021/ja202292q.

[148] G.S. Popkirov, R.N. Schindler, A new impedance spectrometer for the investigation of electrochemical systems, Rev. Sci. Instrum. 63 (1992)

5366–5372. https://doi.org/10.1063/1.1143404.

[149] G.S. Popkirov, R.N. Schindler, Validation of experimental data in electrochemical impedance spectroscopy, Electrochim. Acta. 38 (1993) 861–867. https://doi.org/10.1016/0013-4686(93)87002-U.

[150] R. Budvytyte, M. Mickevicius, D.J. Vanderah, F. Heinrich, G. Valincius, Modification of tethered bilayers by phospholipid exchange with vesicles, Langmuir. 29 (2013) 4320–4327. https://doi.org/10.1021/la304613a.

[151] X. Wu, T.J. Coutts, W.P. Mulligan, Properties of transparent conducting oxides formed from CdO and ZnO alloyed with SnO2 and In2O3, J. Vac. Sci. Technol. A Vacuum, Surfaces, Film. 15 (1997) 1057–1062. https://doi.org/10.1116/1.580429.

[152] R. Mamazza, D.L. Morel, C.S. Ferekides, Transparent conducting oxide thin films of Cd2SnO4 prepared by RF magnetron co-sputtering of the constituent binary oxides, Thin Solid Films. 484 (2005) 26–33. https://doi.org/10.1016/j.tsf.2005.01.097.

[153] R. Budvytyte, G. Valincius, G. Niaura, V. Voiciuk, M. Mickevicius, H. Chapman, H.Z. Goh, P. Shekhar, F. Heinrich, S. Shenoy, M. Lösche, D.J. Vanderah, Structure and properties of tethered bilayer lipid membranes with unsaturated anchor molecules, Langmuir. 29 (2013) 8645–8656. https://doi.org/10.1021/la401132c.

[154] P.E. Laibinis, G.M. Whitesides, D.L. Aliara, Y.T. Tao, A.N. Parikh, R.G. Nuzzo, Comparison of the Structures and Wetting Properties of Self-Assembled Monolayers of n-Alkanethiols on the Coinage Metal Surfaces, Cu, Ag, Au, J. Am. Chem. Soc. 113 (1991) 7152–7167. https://doi.org/10.1021/ja00019a011.

[155] B. Rakovska, T. Ragaliauskas, M. Mickevicius, M. Jankunec, G. Niaura, D.J. Vanderah, G. Valincius, Structure and function of the membrane anchoring self-assembled monolayers, Langmuir. 31 (2015) 846–857. https://doi.org/10.1021/la503715b.

[156] K.J. Kwak, G. Valincius, W.C. Liao, X. Hu, X. Wen, A. Lee, B. Yu, D.J. Vanderah, W. Lu, L.J. Lee, Formation and finite element analysis of tethered bilayer lipid structures, Langmuir. 26 (2010) 18199–18208. https://doi.org/10.1021/la1021802.

[157] Z.Y. Banyamin, P.J. Kelly, G. West, J. Boardman, Electrical and Optical Properties of Fluorine Doped Tin Oxide Thin Films Prepared by Magnetron Sputtering, Coatings. 4 (2014) 732–746. https://doi.org/10.3390/coatings4040732.

[158] D.J. Vanderah, R.S. Gates, V. Silin, D.N. Zeiger, J.T. Woodward, C.W. Meuse, G. Valincius, B. Nickel, Isostructural self-assembled monolayers. 1. Octadecyl 1-thiaoligo(ethylene oxides), Langmuir. 19 (2003) 2612–2620. https://doi.org/10.1021/la026990e.

[159] * David J. Vanderah, † Jennifer Arsenault, Hongly La, ‡ Richard S. Gates, and Vitalii Silin, C.W. Meuse, G. Valincius§, Structural Variations and Ordering Conditions for the Self-Assembled

Monolayers of HS(CH2CH2O)3-6CH3, Langmuir. 19 (2003) 3752–3756. https://doi.org/10.1021/LA026580Q.

[160] G. Valincius, F. Heinrich, R. Budvytyte, D.J. Vanderah, D.J. McGillivray, Y. Sokolov, J.E. Hall, M. Lösche, Soluble amyloid β-oligomers affect dielectric membrane properties by bilayer insertion and domain formation: Implications for cell toxicity, Biophys. J. 95 (2008) 4845–4861. https://doi.org/10.1529/biophysj.108.130997.

[161] G. Preta, M. Jankunec, F. Heinrich, S. Griffin, I.M. Sheldon, G. Valincius, Tethered bilayer membranes as a complementary tool for functional and structural studies: The pyolysin case, Biochim. Biophys. Acta - Biomembr. 1858 (2016) 2070–2080. https://doi.org/10.1016/j.bbamem.2016.05.016.

[162] T.N. Tun, A.T.A. Jenkins, An electrochemical impedance study of the effect of pathogenic bacterial toxins on tethered bilayer lipid membrane, Electrochem. Commun. 12 (2010) 1411–1415. https://doi.org/10.1016/j.elecom.2010.07.034.

[163] M. Itagaki, S. Suzuki, I. Shitanda, K. Watanabe, Electrochemical impedance and complex capacitance to interpret electrochemical capacitor, Electrochemistry. 75 (2007) 649–655. https://doi.org/10.5796/electrochemistry.75.649.

[164] T. Sabirovas, A. Valiūnienė, I. Gabriunaite, G. Valincius, Mixed hybrid bilayer lipid membranes on mechanically polished titanium surface, Biochim. Biophys. Acta - Biomembr. 1862 (2020). https://doi.org/10.1016/j.bbamem.2020.183232.

[165] B. Bechinger, Structure and functions of channel-forming peptides: Magainins, cecropins, melittin and alamethicin, J. Membr. Biol. 156 (1997) 197–211. https://doi.org/10.1007/s002329900201.

[166] G. Sessa, J.H. Freer, G. Colacicco, G. Weissmann, Interaction of alytic polypeptide, melittin, with lipid membrane systems., J. Biol. Chem. 244 (1969) 3575–3582. https://doi.org/10.1016/s0021-9258(18)83408-1.

[167] M.T. Tosteson, D.C. Tosteson, The sting. Melittin forms channels in lipid bilayers, Biophys. J. 36 (1981) 109–116. https://doi.org/10.1016/S0006-3495(81)84719-4.

[168] G. Valincius, M. Mickevicius, T. Penkauskas, M. Jankunec, Electrochemical Impedance Spectroscopy of Tethered Bilayer Membranes: An Effect of Heterogeneous Distribution of Defects in Membranes, Electrochim. Acta. 222 (2016) 904–913. https://doi.org/10.1016/j.electacta.2016.11.056.

[169] T. Raila, F. Ambrulevičius, T. Penkauskas, M. Jankunec, T. Meškauskas, D.J. Vanderah, G. Valincius, Clusters of protein pores in phospholipid bilayer membranes can be identified and characterized by electrochemical impedance spectroscopy, Electrochim. Acta. 364 (2020) 137179. https://doi.org/https://doi.org/10.1016/j.electacta.2020.137179.

[170] L. Song, M.R. Hobaugh, C. Shustak, S. Cheley, H. Bayley, J.E. Gouaux, Structure of staphylococcal α-hemolysin, a heptameric transmembrane pore, Science (80-.). 274 (1996) 1859–1866. https://doi.org/10.1126/science.274.5294.1859.

[171] T. Raila, T. Penkauskas, M. Jankunec, G. Dreižas, T. Meškauskas, G. Valincius, Electrochemical impedance of randomly distributed defects in tethered phospholipid bilayers: Finite element analysis, Electrochim. Acta. 299 (2019) 863–874. https://doi.org/https://doi.org/10.1016/j.electacta.2018.12.148.

[172] D.J. McGillivray, G. Valincius, F. Heinrich, J.W.F. Robertson, D.J. Vanderah, W. Febo-Ayala, I. Ignatjev, M. Lösche, J.J. Kasianowicz, Structure of functional Staphylococcus aureus α-hemolysin channels in tethered bilayer lipid membranes, Biophys. J. 96 (2009) 1547–1553. https://doi.org/10.1016/j.bpj.2008.11.020.

[173] S.M. Bezrukov, I. Vodyanoy, R.A. Brutyan, J.J. Kasianowicz, Dynamics and free energy of polymers partitioning into a nanoscale pore, Macromolecules. 29 (1996) 8517–8522. https://doi.org/10.1021/ma960841j.

SANTRAUKA

ĮVADAS

Plazminė membrana apsupa kiekvieną gyvą ląstelę. Membrana apsaugo ir atskiria ląstelės vidų nuo išorės. Jos pagrindinė sudedamoji dalis yra fosfolipidai išsidėstę dviem sluoksniais, kur hidrofobinės uodegos išsidėsčiusios dvisluoksnio viduryje, o hidrofilinės galvos – dvisluoksnio išorėje. Dėl elektrostatinių ir hidrofilinių – hidrofobinių sąveikų, skirtingi baltymai gali prikibti prie plazminės membranos: integraliniai (pvz., jonų kanalai) ir periferiniai membranos baltymai (elektronų pernešėjai, fermentai, peptidai). Dėl to buvo sukurti membraniniai modeliai, kurie būtų pritaikomi kaip platforma baltymų tyrimams.

Pirmasis membranos modelis buvo juodoji lipidinė membrana. Membrana buvo pakabinta dešimties mikrometrų apertūroje iš hidrofobinės medžiagos. Kadangi šis membranos modelis pasižymėjo nepakankamu stabilumu, todėl buvo pasiūlyta membranas formuoti ant kietų paviršių arba imobilizuoti paviršiuje naudojant inkarinius junginius. Suformavus membranos modelius ant kietų paviršių, galima pritaikyti paviršių tyrimų metodus, tokius kaip atominių jėgų mikroskopija, paviršiaus plazmonų rezonansas arba elektrocheminio impedanso spektroskopija.

Siekiant membranos modelį pritaikyti baltymų tyrimams, jis turi turėti ploną 1-3 nm vandeninį rezervuarą, tarp kieto paviršiaus ir lipidinės membranos. Šis vandens sluoksnis imituoja ląstelės citoplazmą ir užtikrina integralinių baltymų įsiterpimą į membraną, neprarandant biologinio aktyvumo. Dėl to buvo sukurtos paviršiuje prikabintos membranos, kur susiformuoja plonas vandens sluoksnis tarp membranos ir kieto paviršiaus. Daugiausia tyrimų yra atlikta aukso paviršius padengiant tiolių savitvarkiais monosluoksniais. Stiprus kovalentinis tarp auksinio paviršiaus ir tiolio (Au-SR) ryšys užtikrina sistemos stabilumą ir todėl paviršiuje prikabintos membranos yra tinkamos baltymų tyrimams, arba biologinių jutiklių kūrimui. Kadangi auksiniai paviršiai ir jų paruošimas yra gana brangūs, todėl kiti paviršiai yra siūlomi membranų formavimui, pavyzdžiui, metalų oksidai. Skirtingi metalų oksidai gali būti funkcionalizuojami silanų savitvarkiais monosluoksniais: indžio alavo oksidas (angl. ITO), garintas Ti/TiO_2, metalurginis Ti ir Al. Metalų oksidai yra pranašesni už auksinius paviršius dėl to, kad jie yra lengvai paruošiami ir komerciškai prieinami. Dėl šių savybių, metalų oksidai gali būti sėkmingai pritaikomi paviršiuje prikabintų membranų formavimui. Tačiau membranų modelių formavimas su plonu vandens rezervuaru ant metalo oksidinių paviršių yra sudėtingas dėl komerciškai prieinamų silanų trūkumo. Nepaisant to, metalo oksidiniai paviršiai būtų pranašesni už auksinius paviršius paviršiuje prikabintų membranų formavimui ir biologinių jutiklių kūrimui.

Šio darbo tikslas yra suformuoti fosfolipidines bisluoksnes membranas ant kadmio alavo oksido ir fluoru legiruoto alavo oksido paviršių bei ištirti membranų tinkamumą biologinių jutiklių, skirtų membranas ardančių/poras formuojančių toksinų kiekybiniam nustatymui, kūrimui.

Darbo uždaviniai:

1. Nustatyti optimalias sąlygas kadmio alavo oksido plonų plėvelių padengimui; suformuoti oktadeciltrichlorosilano (OTS) savitvarkį monosluoksnį (SAM) ir fosfolipidinę bisluoksnę membraną. Ištirti SAM ir bisluoksnio savybes kontaktinio kampo, CV ir EIS metodais.

2. Nustatyti optimalias sąlygas OTS SAM formavimui ant fluoru legiruoto alavo oksido (FTO) paviršiaus. Ištirti bisluoksnės membranos formavimąsi ir sąveiką su vaginolizinu ir fosfolipaze A_2. Modifikuotą FTO paviršių ištirti kontaktinio kampo, SECM, CV ir EIS metodais.

3. Ištirti fosfolipidinės membranos formavimąsi ant mišraus OTS/MTS SAM‘o ir membranos sąveiką su melitinu. Ištirti paviršiaus drėkinimo įtaką SAM ir membranos sąvybėms. Modifikuotą FTO paviršių ištirti kontaktinio kampo, CV ir EIS metodais.

4. Funkcionalizuoti FTO paviršių sintetintu trichloro(3-(octadeciltio)propil)silanu (TOPS) molekuliniu inkaru ir pritaikyti paviršiuje prikabintos fosfolipidinės membranos formavimui, kuri turėtų ploną vandens sluoksnį tarp kieto paviršiaus ir membranos. Ištirti membranos sąveiką su α-hemolizinu. Modifikuotą FTO paviršių ištirti kontaktinio kampo ir EIS metodais.

5. Ištirti, ar ant FTO paviršiaus suformuotas silano savitvarkis monosluoksnis gali būti tinkamas daugkartiniam fosfolipidinio bisluoksnio formavimui.

Mokslinis naujumas

Dirbtinių membranų modeliai buvo sukurti kaip platforma biologinių jutiklių kūrimui. Pagrindiniai dirbtinių membranų tyrimai buvo atlikti formuojant membranas ant alkiltioliais modifikuotų auksinių paviršių. Tačiau aukso-tiolatų sistema pasižymi keliais trūkumais. Pirma, ant aukso prikibusios alkiltiolių inkarinės molekulės pasižymi paviršiniu mobilumu vandeninėje terpėje, dėl to susiformuoja SAM klasteriai ant paviršiaus ir tokiomis pačiomis savybėmis pasižyminti membrana gali būti suformuota tik vieną kartą ant auksinių paviršių. Tačiau, silanų savitvarkiai monosluoksniai sudaro stiprius kovalentinius ryšius su metalų oksidiniais paviršiais, dėl to suformuotos lipidinės membranos gali būti regeneruojamos ant to paties paviršiaus. Antra, atomiškai lygus auksinis paviršius paprastai yra paruošiamas naudojantis magnetroninio dulkinimo prietaisu kas padidina biologinio jutiklio paruošimo kaštus, tuo tarpu metalų oksidiniai paviršiai yra pigesni ir jų paruošimas yra paprastesnis. Tačiau alkilsilanų molekulinių inkarų panaudojimas fosfolipidinių dvisluoksnių formavimui nėra pakankamai ištirtas. Atsižvelgiant į minėtas problemas, šio darbo metu buvo atlikti eksperimentiniai tyrimai, iš kurių analizės galima išskirti keletą šios disertacijos naujumo elementų:

1. Plonų plėvelių kadmio alavo oksidas ir fluoru legiruotas alavo oksido paviršius funkcionalizuotas su OTS SAM-u gali būti naudojamas DOPC/Chol fosfolipidinių bisluoksnių formavimui

2. Fosfolipidiniai bisluoksniai ant silanizuoto FTO paviršiaus (priešingai nei ant aukso) gali būti lengvai regeneruojami kelis kartus, neprarandant savo funkcionalumo.

3. Priklausomai nuo FTO paviršiaus drėkinimo, fosfolipidiniai bisluoksniai gali būti suformuoti net ant retai išsidėsčiusio OTS inkaro (mišriame SAM gali būti iki 80% trumpagrandžio MTS).

4. Pasiūlyta paviršiuje prikabintų bisluoksnių membranų formavimo ant FTO paviršiaus procedūra, kur oksidinis paviršius yra funkcionalizuojamas sintetintu silano molekuliniu inakaru.

Apibendrinant, tokie metalų oksidai kaip kadmio alavo oksidas ir fluoru legiruotas alavo oksidas gali būti naudojami fosfolipidinių bisluoksnių membranų formavimui; tai galėtų sumažinti biologinių jutiklių toksinų nustatymui kūrimo kaštus bei praplėstų membranų tyrimo ir pritaikymo galimybes dėl metalų oksidinių paviršių komercinio prieinamumo, žemos savikainos ir optinio skaidrumo.

Ginamieji teiginiai

1. Kadmio alavo oksidas ir fluoru legiruotas alavo oksidas funkcionalizuoti OTS savitvarkiu monosluoksniu gali būti pritaikomi hibridinės bisluoksnės membranos formavimui.

2. Skenuojančios elektrocheminės mikroskopijos metodas gali būti pritaikytas savitvarkių monosluoksnių tyrimui, kartu su kontaktinio kampo, CV ir EIS metodais.

3. Fluoru legiruotas alavo oksidas modifikuotas mišriu ilgagrandžiu OTS ir trumpagrandžiu MTS savitvarkiu monosluoksniu gali būti naudojamas mišrios hibridinės bisluoksnės membranos formavimui, kuri būtų tinkama toksino melitino įterpimui.

4. Susintetintas trichloro(3-(octadeciltio)propil)silano molekulinis inkaras gali būti naudojamas fluoru legiruoto alavo oksido funkcionalizavimui

SAM-u, kuris yra tinkamas formuojant paviršiuje prikabintą fosfolipidinę membraną, pasižyminčią plonu vandens rezervuaru tarp kieto paviršiaus ir membranos, reikalingu toksino alfa-hemolizino įsiterpimui.

5. Fluoru legiruotas alavo oksidas funkcionalizuotas silanų savitvarkiais monosluoksniais gali būti pritaikomas daugkartiniam fosfolipidinių membranų, pasižyminčių tomis pačiomis savybėmis, formavimui.

EKSPERIMENTŲ METODIKA

Kadmio alavo oksido (CTO) plonų plėvelių formavimas. Oksido plėvelės buvo paruoštos zolių-gelių metodu. Nusodinimo tirpalas buvo paruoštas ištirpinant 1 ml alavo (IV) tret-butoksido ir 1,06 g bevandenio kadmio acetato 13 ml metanolyje. Ištirpus druskoms buvo pridėta 0,2 ml acetilacetono. Paruoštas tirpalas paliktas per naktį nusistovėti pusiausvyrai eksikatoriuje. CTO plėvelės buvo dengiamos ant mikroskopinių stiklo plokštelių, kurios buvo nuplautos “Micro 90” plovikliu, dejonizuotu vandeniu ir 2-propanoliu ultragarsinėje vonelėje bei išdžiovintos azoto dujomis. Sukamojo dengimo metodu buvo dengiami 2-4 CTO sluoksniai. Kiekvienas sluoksnis buvo dengiamas taip: 200 μl tirpalo užpilama ant švaraus substrato ir 3000 apsisukimų per minutę greičiu sukamas substratas kol pasiskirsto tirpalas ant paviršiaus. Substratas yra džiovinamas ant kaitlentės 200 °C temperatūroje 20 min. Padengus norimą skaičių sluoksnių, plokštelės vėl kaitinamos 400 ° ir 520 °C temperatūroje po 20 min.

Fluoru legiruoto alavo oksido (FTO) paruošimas. Visų pirma, FTO stikliukai (10 x 25 mm) plaunami “Micro 90” plovikliu ir dejonizuotu vandeniu ultragarsinėje vonelėje. Po to FTO laikomas koncentruotoje sieros rūgštyje 1 val., plaunamas dejonizuotu vandeniu ir 2-propanoliu ultragarsinėje vonelėje. Paviršiai išdžiovinami azoto dujomis ir iškarto naudojami tolimesniems eksperimentams.

Savitvarkio monosluoksnio (SAM) formavimas. Šiame darbe SAM buvo formuojami iš skirtingų medžiagų: oktadeciltrichlorosilano (OTS), metiltrichlorosilano (MTS) bei trichloro(3-(octadecyltio)propil)silano (TOPS) ir aliltrichlorosilano (ATS) mišinio. Silanizavimo tirpalas buvo paruošiamas taip: 50 ml heptano pašildoma iki 60 °C temperatūros, įpilama atitinkamo silano arba jų mišinio kad bendra koncentracija būtų 0,1% (v/v; 2,5 mM). Paruoštas CTO arba FTO stikliukas įstatomas į tirpalą vertikalioje pozicijoje ir laikoma 60 min. maišant 60 °C temperatūroje. Po to stikliukas ištraukiamas, nuplaunamas heptanu ir išdžiovinamas azoto dujomis.

Fosfolipidinės bisluoksnės membranos formavimas. Šiame darbe membrana buvo formuojama vezikulių liejimo metodu, iš 1,2-dioleoyl-sn-glicero-3-fosfocholino (DOPC) ir cholesterolio (Chol) moliniu santykiu 6:4 arba 100% DOPC. Bendra lipidų koncentracija buvo 1 mM fosfatiniame buferiniame tirpale pH 4,6.

Kontaktinių kampų matavimas. Paviršiaus drėkinimas buvo nustatomas Theta Lite optiniu tensiometru. 5 µl tūrio dejonizuoto vandens lašai užlašinami ant FTO arba CTO paviršių 6 skirtingose vietose, išmatuojami kontaktiniai kampai ir apskaičiuojamas vidurkis.

Elektrocheminiai matavimai. Visi elektrocheminiai matavimai buvo atlikti fosfatiniame buferiniame tirpale pH 7,1. Elektrocheminio impedanso spektroskopijos (EIS) matavimai buvo atlikti 0,1 Hz – 100 kHz dažnių ribose naudojantis µAutolab (Type III) arba Zahner Zennium potenciostatais. Dinaminiai greitosios Furjė transformacijos (FFT) EIS matavimai buvo atlikti EIS-128/16 impedanso spektrometru. Standartinė trijų elektrodų celė buvo naudojama tyrimų metu, kur palyginamasis elektrodas – Ag/AgCl, $NaCl_{sot.}$, pagalbinis – platinos viela ir darbinis – CTO arba FTO elektrodai. EIS matavimai atlikti esant 0 V *vs* Ag/AgCl, $NaCl_{sot.}$ potencialui.

Priartėjimo kreivės prie FTO paviršiaus buvo nustatytos Sensolytics SECM – 030 skenuojančiu elektrocheminiu mikroskopu (SECM). Darbinis elektrodas – ultramikroelektrodas (UME), kurio skersmuo 20 µm, palyginamasis - Ag/AgCl, $NaCl_{sot.}$, pagalbinis – platinos viela. SECM matavimai atlikti esant -0,75 V *vs* Ag/AgCl, $NaCl_{sot.}$ potencialui.

REZULTATŲ APTARIMAS

Kadmio alavo oksido ir savitvarkio monosluoksnio formavimas

Siekiant suformuoti CTO plėveles, kurios pasižymėtų kuo aukštesniu laidumu, buvo dengiamas skirtingas sluoksnių skaičius (2-4) ir keičiama kaitinimo temperatūra (500-530 °C). Paviršių laidumas buvo nustatomas matuojant varžą, dvejais elektrodais 1 cm atstumu vienas nuo kito, priliečiant paviršių. Žemiausia varža (0,3 kΩ) buvo nustatyta CTO plėveles dengiant 3 sluoksniais ir kaitinant 520 °C temperatūroje (Fig. 15, 31 p.), todėl tolimesniems tyrimams ir buvo parinktos šios CTO dengimo sąlygos.

Toliau CTO paviršius buvo funkcionalizuojamas OTS savitvarkiu monosluoksniu. SAM formavimo (silanizavimo) metu buvo naudojama skirtinga OTS koncentracija (0,01 – 5 %). Kontaktinio kampo metodas buvo naudojamas nustatyti paviršiaus hidrofobiškumą. Naudojant 0,1 % OTS koncentracijos tirpalą CTO silanizavimui, buvo pasiektas aukščiausias kontaktinis kampas – 103 °, palyginus su švariu CTO – 40 ° (Fig. 19, 35 p.), kas parodė, kad modifikuotas paviršius yra hidrofobinis. Atlikus EIS matavimus, kompleksinė talpa sumažėjo nuo ~8 µF cm^{-2} (švaraus CTO) iki 2,5 µF cm^{-2} (0,1 % OTS silanizuotu CTO). Kompleksinės talpos sumažėjimas parodo apie CTO padengimą SAM.

Hibridinio fosfolipidinio bisluoksnio formavimas ant CTO paviršiaus

Vezikulių liejimas ant OTS SAM funkcionalizuoto CTO vyksta dvejais etapais. Pirmas 15 min stebimas kompleksinės talpos padidėjimas. Tačiau toliau liejantis vezikulėms stebimas kompleksinės talpos sumažėjimas iki 0,8 µF cm^{-2} (Fig. 22, 38 p.). Netipiškas vezikulių liejimasis dviem etapais parodo apie heterogeniško SAM susiformavimą ant CTO paviršiaus. Sąveika su vezikulėmis prisideda prie SAM molekulių persitvarkymo iš horizontalios į vertikalią padėtį. Dėl to, CTO paviršius turi kontaktą su buferiniu tirpalu ir EI spektruose registruojamas kompleksinės talpos padidėjimas. Toliau liejantis vezikulėms formuojasi hibridinis bisluoksnis, kur fosfolipidai izoliuoja CTO, todėl kompleksinė talpa pradeda mažėti.

Savitvarkio monosluoksnio formavimas ant FTO paviršiaus

FTO paviršius buvo modifikuojamas OTS SAM ir parenkama optimali OTS koncentracija ir silanizavimo trukmė naudojantis kontaktinio kampo ir EIS metodais. Keičiant OTS koncentracijas nuo 0,01% (0,25 mM) iki 0,1% (2,5 mM) ir silanizavimo trukmę nuo 30 min iki 60 min buvo nustatyta, kad žemiausia kompleksinė talpa ir aukščiausi kontaktiniai kampai pasiekiami silanizavimą atliekant 60 min 0,1% (2,5 mM) OTS koncentracijos tirpale (Fig. 24, 40p.), todėl tolimesniems tyrimams buvo parinktos šios silanizavimo sąlygos.

Papildomai, OTS SAM ant FTO paviršiaus buvo ištirtas skenuojančios elektrocheminės mikroskopijos metodu. Buvo nustatyta, kad registruojant priartėjimo kreives prie OTS SAM, 10 µm atstumu nuo paviršiaus yra stebimas srovės nusistovėjimas prieš ultramikroelektrodui paliečiant paviršių (Fig. 27, 42 p.). Šis rezultatas buvo stebimas dėl to, kad OTS SAM yra dielektrikas ir UME artėjant prie paviršiaus yra blokuojamas redokso aktyvių medžiagų patekimas prie darbinio elektrodo ir registruojama srovė nebedidėja.

Hibridinio fosfolipidinio bisluoksnio formavimas ant FTO paviršiaus

Suformavus OTS SAM ant FTO paviršiaus, buvo liejamos DOPC/Chol vezikulės. FFT EIS metodu buvo užregistruoti impedanso spektrai fosfolipidinio bisluoksnio formavimosi metu (Fig. 28, 43 p.) ir nustatyta, kad pilnai bisluoksnis susiformuoja per ~2000 s (30 min). Nustačius kompleksinės talpos vertes, galima nustatyti kiekvieno sluoksnio talpą ir storį naudojantis plokščiojo kondensatoriaus lygtimis:

$$1/C_{FTO/OTS} = 1/C_{FTO} + 1/C_{OTS} \quad (1)$$

$$1/C_{tBLM} = 1/C_{FTO/OTS} + 1/C_{PL} \quad (2)$$

Kur C_{FTO}, $C_{FTO/OTS}$ ir C_{tBLM} yra atitinkamai eksperimentinės FTO, OTS SAM ir fosfolipidinio bisluoksnio kompleksinės talpos vertės; C_{OTS} – OTS monosluoksnio talpa; C_{PL} – OTS SAM ir fosfolipidinio bisluoksnio kompozito talpa.

Remiantis eksperimentiniais duomenimis ir (1) bei (2) lygtimis apskaičiuotos C_{OTS} ir C_{PL} talpos yra lygios atitinkamai 6,54 ± 0,15 µF cm^{-2} ir 0,82 ± 0,10 µF cm^{-2}. Apskaičiuota C_{OTS} vertė yra keletą kartų didesnė nei palyginus su panašaus ilgio alkil tiolių SAM kompleksine talpa. Apskaičiuotas OTS SAM efektyvus storis d_{OTS} = 0,29 nm (dielektrinė konstanta 2,1). Tačiau remiantis literatūros duomenimis jis turėtų būti apytikriai 10 kartų didesnis, todėl šiame darbe suformuotas SAM dengia tik ~11% FTO paviršiaus.

Apskaičiavus OTS ir DOPC kompozito C_{PL} sluoksnio storį, buvo gautas 3,02 nm storis (dielektrinė konstanta 2,8). Ši apskaičiuota vertė sutampa su fosfolipidinio bisluoksnio ant alkiltiolių SAM storiu. Todėl remiantis šiais duomenimis, buvo padaryta išvada, kad buvo suformuotas retai išsidėstęs OTS monosluoksnis, tačiau vezikulių liejimo metu susidarė beveik tvarkingas bisluoksnis (Fig. 31, 46 p.).

Suformuoto bisluoksnio biologinis suderinamumas buvo ištirtas su toksinais vaginolizinu (VLY) ir fosfolipaze A_2 (PLA2). Remiantis EI spektrų duomenimis (Fig. 32, 47 p.), nepastebėta esminių pokyčių po VLY įterpimo į bisluoksnį, dėl to, kad prie paviršiaus esantis SAM yra nepakankamai judrus, kad galėtų įsiterpti oligomerinė VLY pora į bisluoksnį. Todėl sekantys tyrimai buvo atlikti su fosfolipaze A_2. Šis toksinas suardo tik išorinį fosfolipididų sluoksnį, todėl nejudrus monosluoksnis neturėtų įtakoti PLA2 poveikio. EI spektruose (Fig. 33, 48p.) galima matyti kompleksinės talpos pokytį nuo skirtingos PLA2 koncentracijos poveikio bisluoksniui. Tai patvirtina suformuoto hibridinio fosfolipidinio bisluoksnio biologinį suderinamumą.

Mišraus savitvarkio monosluoksnio formavimas ant FTO paviršiaus

Siekiant suformuoti fluidiškesnį fosfolipidinį bisluoksnį, į kurį galėtų įsiterpti poras formuojantys toksinai, SAM formavimo metu buvo naudojamas mišinys ilgagrandžių ir trumpagrandžių alkilsilanų skirtingais santykiais, konkrečiai MTS ir OTS. Šio tyrimo metu taip pat buvo ištirta FTO paviršiaus hidratacijos įtaka silanizavimo metu susidarančio monosluoksnio savybėms (monosluoksnis suformuotas ant nehidratuoto FTO paviršiaus - SAM-P1; ant hidratuoto paviršiaus – SAM-P2). FTO hidratavimas buvo atliekamas paviršių pamerkiant į dejonizuotą vandenį ir paliekant per naktį, po to nudžiovinama azoto dujomis. Atlikus matavimus kontaktinio kampo metodu, buvo palyginti gauti rezultatai ant hidratuotų ir nehidratuotų paviršių: formuojant SAM-P2 su skirtingu OTS:MTS santykiu, buvo gauti aukštesni kontaktiniai kampai, nei palyginus su SAM-P1 tų pačių OTS:MTS santykių (Fig. 35, 49 p.). Aukštesni kontaktiniai kampai parodo didesnį paviršiaus hidrofobiškumą, o tai, remiantis literatūros duomenimis, turėtų palengvinti vezikulių liejimąsi ir bisluoksnio formavimąsi.

Elektrocheminės paviršių savybės buvo ištirtos EIS metodu, kur buvo nustatytos ir palygintos skirtingų OTS:MTS santykių SAM kompleksinės talpos hidratuoto FTO paviršiaus su nehidratuoto FTO. Didinant OTS kiekį silanizavimo mišinyje, EI spektruose kompleksinė talpa mažėja (Fig. 36, 51 p.). Toks kompleksinės talpos pokytis parodo apie storesnio ir homogeniškesnio SAM susidarymą. Įvertinus paviršiaus drėkinimo efektą, buvo pastebėta, kad susiformuoja monosluoksniai, kurie pasižymi žemesnėmis kompleksinėmis talpomis (palyginus su tais pačiais OTS:MTS santykiais ant nehidratuotų FTO paviršių). Tai parodo kompaktiškesnių sluoksnių susidarymą.

Mišraus hibridinio fosfolipidinio bisluoksnio formavimas ant FTO paviršiaus

Suformavus mišrų savitvarkį monosluoksnį, buvo liejamos DOPC/Chol vezikulės ir formuojamas mišrus hibridinis fosfolipidinis bisluoksnis. Atlikus vezikulių liejimą ant SAM-P1, bisluoksnis (mhBLM-P1) susiformavo tik ant tų monosluoksnių, kuriuose buvo 0-20% MTS, o ant SAM-P2 bisluoksnis (mhBLM-P2) formavosi ant tų monosluoksnių, kuriuose buvo 0-80% MTS (Fig. 38, Fig. 39, 53 p.). Šis rezultatas parodo FTO paviršiaus drėkinimo įtaką ne tik SAM, bet ir bisluoksnio formavimuisi ir jo savybėms, nes vezikulės liejosi ant daugiau skirtingų OTS:MTS santykių SAM-P2, nei ant SAM-P1.

Siekiant nustatyti ar suformuoti bisluoksniai ant skirtingų SAM pasižymi biologiniu suderinamumu, buvo ištirta sąveika su toksinais melitinu (Mel) ir α-hemolizinu (αHL). Impedanso spektruose stebėta mhBLM-P1 sąveika su αHL (Fig. 44, 58 p.) buvo netipinė, nes kompleksinė talpa pakito tik po 24 val. Remiantis literatūros duomenimis, jau per pirmas 30 min turėtų būti aiškiai matomas toksino poveikis. Todėl buvo padaryta išvada, kad suformuotas mhBLM-P1 bisluoksnis neturėjo vandeninio rezervuaro tarp bisluoksnio ir kieto paviršiaus, todėl toksinas negalėjo pilnai įsiterpti. Tačiau, atlikus tyrimus su mhBLM-P2 ir melitinu (Fig. 45, 59 p.) nustatyta, kad toksinas suardė bisluoksnį, kuris buvo suformuotas ant hidratuoto FTO paviršiaus. Remiantis šiais duomenimis, galima teigti, kad buvo suformuotas mišrus hibridinis bisluoksnis, kuris yra biologiškai suderinamas su bisluoksnius ardančiais toksinais, tačiau poras formuojantys toksinai negalėjo įsiterpti. Todėl tolimesni tyrimai buvo atliekami siekiant suformuoti bisluoksnį, kuris turėtų joninį vandens rezervuarą tarp kieto paviršiaus ir bisluoksnio.

Trichloro(3-(octadecyltio)propil)silano savitvarkio monosluoksnio ir paviršiuje prikabinto fosfolipidinio bisluoksnio formavimas ant FTO paviršiaus

Kadangi komerciškai prieinami silanai turi tik vieną hidrofobinę anglies atomų grandinę, kas nėra tinkama paviršiuje prikabinto bisluoksnio formavimui, todėl šiame darbe buvo susintetintas naujas silanas - trichloro(3-(octadecyltio)propil)silanas. Sintezės metu buvo paruošiamas silanų mišinys iš TOPS ir ATS. Aliltrchlorosilanas veikė kaip skiediklis, kad sumažintų TOPS inkarų kiekį ant FTO paviršiaus. Suformavus TOPS:ATS SAM kontaktinis kampas siekė 113 ° ± 3 ° , palyginus su švariu FTO – 27 °. Toks kontaktinio kampo pokytis parodo apie hidrofobinio sluoksnio susiformavimą. Atlikus EIS matavimus stebimas kompleksinės talpos sumažėjimas nuo 3,2 ± 0,6 µF cm^{-2} iki 0,8 ± 0.1 µF cm^{-2} ir 1.0 ± 0.1 µF cm^{-2} skirtingos sudėties bisluoksniams, atitinkamai DOPC/Chol ir DOPC (Fig. 51, 64 p.).

Suformuotų bisluoksnių DOPC/Chol ir DOPC biologinis suderinamumas buvo ištirtas 50 ir 100 nM koncentracijos melitinu. Kadangi, cholesterolis inhibuoja melitino veiklą, tai buvo stebimas mažesnis DOPC/Chol bisluoksnio suardymas melitinu nei membranos, kurioje yra tik DOPC (Fig. 53, 66 p.).

Toliau buvo ištirta, ar į paviršiuje prikabintą bisluoksnį gali įsiterpti poras formuojantys toksinai, konkrečiai α-hemolizinas. DOPC/Chol membrana buvo suardyta priklausomai nuo naudoto toksino koncentracijos 10, 50 arba 100 nM (Fig. 54, 68 p.). Jeigu bisluoksnį sudarė vien DOPC, tai αHL neįsiterpė į membraną, nes šio toksino aktyvumas priklauso nuo cholesterolio buvimo bisluoksnyje.

Siekiant įrodyti, kad susiformavo paviršiuje prikabintas bisluoksnis su vandeniniu rezervuaru tarp bisluoksnio ir kieto paviršiaus, į α-hemolizino poras buvo įterpiamas skirtingos molekulinės masės polietilenglikolis (PEG). Nedideli PEG‘ai (200-2000 Da) turėtų pilnai įsiterpti į heptamerinę αHL porą ir sumažinti membranos laidumą apie 40%, tačiau šiame darbe laidumas sumažėjo tik 5-10% (Fig. 55, 69 p.). Tai parodo, kad polimeras įsiterpė į toksino poras, tačiau pomembraninio joninio rezervuaro laidumas dominavo išmatuotą laidumą, todėl jo sumažėjimas buvo nežymus. Norint detaliau išsiaiškinti apie plono vandeninio rezervuaro egzistavimą, didesnės molekulinės masės PEG (>2000 Da) buvo įterpiami į αHL poras. Kaip stebima Fig. 55 (69 p.), membranos laidumas padidėja ~20%. Tai atsitinka dėl osmosinio streso, kurį sukelia vandens cheminio potencialo pokytis dėl PEG koncentracijos padidėjimo tiriamajame tirpale. Didesnis PEG negali įsiterpti į pomembraninį vandens rezervuarą dėl dydžio apribojimų, todėl pasikeitus vandens cheminiam potencialui, vanduo išteka iš pomembraninio rezervuaro ir ten padidėja jonų koncentracija. Dėl to stebimas membranos laidumo padidėjimas.

Hibridinio, mišraus hibridinio ir paviršiuje imobilizuoto fosfolipidinio bisluoksnio regeneracija ant FTO paviršiaus

Silanų savitvarkiai monosluoksniai suformuoti ant metalų oksidinių paviršių pasižymi labai stipriu kovalentiniu Si-O-metalas ryšiu, kuris yra atsparus drėgmei. Norint įrodyti suformuotų bisluoksnių ant FTO pranašumą prieš bisluoksnius ant auksinių paviršių, buvo atlikta membranos regeneracija, fosfolipidų sluoksnį nuplaunant alkoholiniais tirpikliais ir vėl iš naujo liejant vezikules ant to paties SAM. Buvo nustatyta, kad skirtingi bisluoksniai (hibridinis, mišrus hibridinis ir paviršiuje imobilizuotas) ant FTO paviršiaus yra pilnai regeneruojami iki 6-8 kartų ant to paties SAM. Šis rezultatas įrodo metalo oksidinių paviršių pranašumą prieš auksinius paviršius, nes aukso paviršiuje esantys judrūs atomai sustumia monosluoksnio inkarus į „saleles“ po ilgesnio kontakto su vandenine terpe, todėl nebegali susiformuoti homogeniškas bisluoksnis, į kurį galėtų funkcionaliai įsiterpti membraną pažeidžiantys ar poras formuojantys toksinai.

IŠVADOS

1. Buvo nustatyta, kad optimalus sluoksnių skaičius kadmio alavo oksido plonų plėvelių dengimo metu yra 3, kaitinimo temperatūra – 520 °C. Paruoštos CTO plėvelės buvo tinkamos OTS monosluoksnio formavimui, nustatyta optimali OTS koncentracija yra 0,1% (arba 2,5 mM). Suformuota hibridinė bisluoksnė membrana, kurios kompleksinė talpa buvo lygi 0,8 μF cm^{-2}.

2. Buvo suformuotas OTS monosluoksnis ant FTO paviršiaus, nustatyta optimali OTS koncentracija yra 0,1% (arba 2,5 mM), monosluoksnio formavimo trukmė – 60 min. Skenuojančios elektrocheminės mikroskopijos būdu priartėjimo kreivėse buvo nustatyta specifinė savybė – pastovios srovės sritis. UME artėjant prie paviršiaus buvo stebimas srovės nusistovėjimas likus

10 μm iki paviršiaus. Suformuota hibridinė bisluoksnė membrana, kurios kompleksinė talpa buvo lygi 0,9 μF cm^{-2}. Hibridinė membrana gali būti panaudojama fosfolipazės A_2 kiekybiniam nustatymui.

3. Suformuota mišri hibridinė membrana ant mišriu OTS/MTS monosluoksniu funkcionalizuoto FTO paviršiaus. Nustatyta, kad mhBLM gali susiformuoti ant OTS:MTS monosluoksnio, kurime MTS sudaro iki 80% molinės dalies. Mišri hibridinė membrana gali būti pritaikoma melitino detekcijai.

4. Sintetintas trichloro(3-(octadeciltio)propil)silanas (TOPS) molekulinis inkaras gali būti panaudojamas paviršiuje prikabintos fosfolipidinės membranos formavimui ant FTO paviršiaus. Suformuota membrana gali būti pritaikoma melitino ir alfa-hemolizino detekcijai. Plono vandens sluoksnio buvimas tarp membranos ir kieto paviršiaus buvo įrodytas įterpiant skrtingos molekulinės masės PEG į α-hemolizino poras.

5. Silanizuotas FTO paviršius gali būti pritaikomas daugkartiniam panaudojimui hibridinės, mišrios hibridinės ir paviršiuje prikabintos bisluoksnės membranos formavimui.

ACKNOWLEDGEMENT

I would like to express my gratitude to my supervisors assoc. prof. dr. Aušra Valiūnienė and prof. dr. Gintaras Valinčius for leading me through this challenging yet fascinating path, showing support and believing in me.

Also, I would like to acknowledge prof. habil. dr. Arūnas Ramanavičius for providing me with scientific and academic career opportunities. The trust that I was given immensely supported me.

I would like to thank all the members in Department of Physical Chemistry and everyone who contributed to this thesis, especially Aura, Modestas, Ramūnas and Tomas for all the good times spent in laboratory.

Most importantly I would like to thank my family for all the patience and support for my curiosity in science.

CURRICULUM VITAE

PERSONAL INFORMATION

Name, Surname	Inga Gabriūnaitė
Date of birth	1992-01-18
Address	Naugarduko str. 24, Vilnius
Phone number	+370 65364897
E-mail	inga.gabriunaite@chf.vu.lt

ACADEMIC EDUCATION

2011 – 2015	B.Sc in Chemistry, Vilnius University
2015 – 2017	M.Sc in Chemistry, Vilnius University

ACADEMIC/SCIENTIFIC AFFILIATIONS

2017-09 – now	Faculty of Chemistry and Geosciences, Vilnius University	Junior assistant
2018-03 – now	Center for Physical Sciences and Technologies, Department of Material Science and Electrical Engineering	Junior researcher

TRAINING

2017-10-08 – 2017-10-15	Secondment to Canakkale Onsekiz Mart University, Turkey
2018-05-23 – 2018-07-30	Internship in University of Montpellier, European Institute of Membranes, France

PROJECTS

2018-03 – now	“Smart Membranes for Electrochemical Devices”, Lithuania. Project is funded by Research Council of Lithuania (DOTSUT-11), under the program – the European Regional Development Fund according to the supported activity ‘Research Projects Implemented by World-Class Researcher Groups’ under Measure no. 01.2.2-LMT-K-718.

PATENTS

Regenerable Phospholipid Biosensor and Method of its Preparation on Silanized Oxide Surfaces. Lithuanian patent LT2021 533

PUBLISHED CONTRIBUTIONS TO ACADEMIC CONFERENCES

1. Inga Gabriūnaitė, Aušra Valiūnienė, Gintaras Valinčius. Detection of SAM heterogenity for lipid membrane formation on FTO electrode. 10-oji nanokonferencija "Current Trends in Electrochemistry and Material Sciences", Vilnius, spalio 24-25 d. 2017
2. Inga Gabriūnaitė, Aušra Valiūnienė, Gintaras Valinčius. Tin oxide based conducting oxide as solid substrate for hybrid bilayer membrane formation. 23rd topical meeting of International Society of the Electrochemistry. "Electrochemistry for Investigation of Biological objects: from Functional Nanomaterials to micro/nano-electrodes" gegužės 8-11 d. 2018, Vilnius, Lietuva
3. Tomas Sabirovas, Aušra Valiūnienė, Inga Gabriūnaitė. Electrochemical study of hybrid bilayer formation on polished titanium surface. 23rd topical meeting of International Society of the Electrochemistry. "Electrochemistry for Investigation of Biological Objects: from Functional Nanomaterials to micro/nano-electrodes" gegužės 8-11 d. 2018, Vilnius, Lietuva
4. S. Raišytė, I. Gabriūnaitė, A. Valiūnienė. Fosfolipidinių bisluoksnių formavimas ir jų tyrimas ant plonasluoksnių Au dangų paviršiaus. Chemija ir cheminė technologija. Klaipėda, Lietuva, gegužės 18 d. 2018. p. 157 – 160. 2018. ISBN 978-9955-18-989-3
5. Inga Gabriunaite, Aušra Valiūnienė. Functionalization of Fluorine Doped Tin Oxide with Mixed Self – Assembled Monolayer for Phospholipid Bilayer Membrane Formation. “Advanced Materials and Technologies” 20th International Conference – School, August 27-31, 2018 Palanga, Lithuania. ISSN 1822-7759
6. I. Gabriunaite, A. Valiūnienė. Silane Based Mixed Self – Assembled Monolayer Formation on Thin Film Semiconducting Oxide for Phospholipid Membrane Development. “Electrochemistry 2018” Ulm, Germany, September 24-26 2018.
7. Inga Gabriunaite, Aušra Valiūnienė. Thin Film Metal Oxide Application for Phospholipid Membrane Immobilization. “Oxygenalia 2018”. Vilnius, Lithuania. October 11-13. 2018. Page 84. ISBN 978-83-7597-348-8
8. I. Gabriunaite, A. Valiūnienė. Phospholipid Bilayer Formation on Fluorine Doped Tin Oxide. “Ecobalt 2018” Vilnius, Lithuania. October 25-27. 2018. Page 48
9. Inga Gabriunaite, Aušra Valiūnienė, Electrochemical Study of Phospholipid Bilayer Formation on Mixed Silane Self-assembled Monolayer on Oxide Surface. The 77th International Scientific conference of the

University of Latvia, Ryga, Latvia, February 8, 2019. Page 11. ISBN 978-9934-18-399-7.

10. Inga Gabriunaite, Aušra Valiūnienė, Phospholipid Bilayer Formation on Metal Oxides and Application for Biosensing Toxins, 1st International Congress on Analytical and Bioanalytical Chemistry, p. 128, Antalya, 27-30 March 2019

11. Margarita Poderytė, Aušra Valiūnienė, Inga Gabriūnaitė, Hybrid Phospholipid Bilayer surface properties investigation and modification using Scanning Electrochemical Microscopy, Lithuanian chemists conference „Chemistry and Chemical Technology“,Vilnius, 2019, May 16. p.106, ISBN 978-609-07-0167-6

12. Inga Gabriunaite, Aušra Valiūnienė, Phospholipid membrane formation on thin film tin oxide, 4th Vita Scientia conference, January 3rd, 2020, Vilnius, Lithuania

13. Inga Gabriunaite, Aušra Valiūnienė, Electrochemical Characterisation of Mixed Silane Based Self-Assembled Monolayers for Phospholipid Membrane Bilayer Formation, 63rd International Conference for Students of Physics and Natural Science „OpenReadings 2020“, Vilnius.

14. Inga Gabriūnaitė, Margarita Poderyte, Aušra Valiūnienė, SECM and EIS Characterization of Fluorine Doped Tin Oxide Glass Application for Phospholipid Membrane Formation, “Advanced Materials and Technologies” 22th International Conference – School, p. 41, August 24-28, 2020 Palanga, Lithuania, ISSN 1822-7759

15. I. Gabriunaite, M. Poderyte, A. Valiūnienė, Phospholipid Membrane Formation on Fluorine Doped Tin Oxide for Biosensing of Toxins, International Conference “Nanostructured Bioceramic Materials 2020”, Vilnius University, 1 - 3 of December, 2020, Vilnius.

Vilniaus universiteto leidykla
Saulėtekio al. 9, III rūmai, LT-10222 Vilnius
El. p. info@leidykla.vu.lt, www.leidykla.vu.lt
Tiražas 16 egz.